AN ABSTRACT OF THE THESIS OF

Allyson C. Mathis for the degree of Masters in Science in Geology presented on March 10, 1993.
Title: Geology and Petrology of a 26-Ma Trachybasalt to Peralkaline Rhyolite Suite Exposed at Hart Mountain, Southern Oregon

Abstract Approved: Redacted for privacy
Anita L. Grunder

Rocks older than the Steens Basalt in southeastern Oregon are mainly exposed in prominent fault scarps such as Steens Mountain, Hart Mountain, and Abert Rim. At Hart Mountain, the section consists of a suite of trachybasalt to trachyte to peralkaline rhyolite lava flows and tuffs. The Hart Mountain volcanic complex contains the only known pantellerites and the oldest peralkaline rhyolites (26.3 Ma) in the Basin and Range province.

^{40}Ar-^{39}Ar age determinations from feldspar separates from a basaltic trachyandesite near the base (26.48±0.13 Ma; one sigma error) and a peralkaline rhyolite near the top (26.33±0.04 Ma) of the exposed suite are analytically indistinguishable. The ages and the paucity of sedimentary rocks within the conformable section, indicate that the volcanic rocks erupted during a short time interval and that they probably represent a single magmatic system. The Hart Mountain trachyandesite suite, with a thickness of as much as 450 m, makes up the lower portion of the section and consists predominantly of basaltic trachyandesite to trachyte lava flows and tuffs. The upper portion of the sequence, the Warner Peak rhyolite, is at least 150 m thick and includes most of the exposed near-vent rocks of the Hart Mountain volcanic complex east of the field area, and is mostly

pantellerites and comendites with a few interlayered trachytes.

Major and trace element models demonstrate that crystal fractionation of plagioclase > olivine ≈ clinopyroxene > Fe-Ti oxides > apatite from a range of alkali basaltic to trachybasaltic parents can account for the Hart Mountain trachyandesite suite. Textural evidence indicates that some mixing also occurred in the trachyandesitic composition range. Approximately 90% crystal fractionation is required to produce trachyte from trachybasalt. Approximately 40-50% crystal fractionation of trachytic parents is needed to generate the range of peralkaline rhyolites in the Warner Peak rhyolite. Modeling of the petrogenesis of the Warner Peak rhyolite, however, is qualitative because of compositional changes these peralkaline rocks have undergone with crystallization and or devitrification.

The Hart Mountain volcanic complex is similar to strongly peralkaline volcanic systems, such as Pantelleria, rather than weakly peralkaline centers (e.g. McDermitt Caldera, Kane Spring Wash Caldera, etc.) exposed elsewhere in the Basin and Range. As in strongly peralkaline centers, the Hart Mountain volcanic complex contains pantellerites and comendites, does not include subalkaline rhyolites or high silica rhyolites, and consists predominantly of silicic rocks (~85 volume %). Unlike strongly peralkaline centers, the Hart Mountain volcanic complex does not have a silica gap between the mafic and silicic endmembers. Also, rhyolite of the Hart Mountain volcanic complex do not have the extreme enrichment of incompatible elements (Rb, Zr, REE) that are characteristic of pantellerites found elsewhere.

The well-documented association of peralkaline rhyolites with extensional environments suggests that south-central Oregon was at least an area of local extension in the late Oligocene. Volcanism elsewhere in the Great Basin at that time consisted of calc-alkaline intermediate to silicic magmatism.

APPROVED:

Redacted for privacy

Associate Professor of Geology in charge of major

Redacted for privacy

Head of Department of Geosciences

Redacted for privacy

Dean of Graduate School

Date thesis is presented March 10, 1993

Prepared by Allyson C. Mathis

Geology and Petrology of a 26-Ma Trachybasalt to Peralkaline Rhyolite Suite Exposed at Hart Mountain, Southern Oregon

by

Allyson C. Mathis

A THESIS

submitted to

Oregon State University

in partial fulfillment of
the requirements of the
degree of

Master of Science

Completed March 10, 1993

Commencement June 1993

Acknowledgements

I need to thank many people for their assistance during my five year journey to this degree. First of all, I thank my major professor Anita Grunder for guidance and patience. Her direction greatly improved my thesis from beginning to end. Committee members John Dilles and Ed Taylor provided thorough reviews of my thesis. I also thank John Dilles for his excellent review of my map.

Financial support was provided by the Chevron USA Scholarship Fund, Sigma Xi, and the Mazamas. The OSU Radiation Center generously provided INA analyses. Electron microprobe analyses were financed by the OSU Department of Geosciences. Age determinations were provided by Alan Deino, Institute of Human Origins, Berkeley, California. Thanks to the US Fish and Wildlife Service and the field staff at Hart Mountain National Antelope Refuge for permission to collect samples and for logistical support during field work.

Able assistance in the field was provided by Derck-Jan Graffelman, Eric Wilson, Nick Enos, Snort, Fred, and Betsy. Britt Hill was always available for petrologic advice. John Curless was a great officemate for four years.

Housemates-past Todd Feeley, Kimie Fukuda, Ken Bevis, Cam Carstarphen, Andrika Kuhle, Nick Enos, and Jim MacLean remain friends and provided many enjoyable moments during my years in Corvallis. Andy Nettell is acknowledged for his wise decision to play Hank on his radio show "Kokopelli Coffeehouse," and is encouraged to do so again. Special thanks to Dan McRoberts, Tom Cox, and the rest of the ISKY crew for their wonderful care during June 1991. My deepest thanks to Cara Wilson for support and friendship, and for encouraging me to be not only who I am, but also who I want to be.

TABLE OF CONTENTS

CHAPTER ONE: INTRODUCTION 1
Location 5
Structural Setting 7
Regional Stratigraphy 8
  Early Volcanic Rocks 9
  Steens Basalt 10
  High-Alumina Olivine Tholeiite (HAOT) 13
Previous work at Hart Mountain 14

CHAPTER TWO: STRATIGRAPHY AND STRUCTURE 15
Stratigraphy 15
  Hart Mountain volcanic complex 19
    Hart Mountain trachyandesite suite 19
      North Mountain section 22
        Base of North Mountain section 22
        North Mountain lava flows 25
        North Mountain ignimbrites 27
      Hart Lake section 32
    Warner Peak rhyolite 32
      Warner Peak tuff 33
      Warner Peak lava flows and tuffs undivided 34
      Warner Peak trachyte and rhyolite lava flows 35
      Warner Peak rhyolite intrusions 35
  Steens Basalt 36
  Plush tuff 36
  Upper Basalt (HAOT) 37
  Rattlesnake Ignimbrite 38
  Quaternary Deposits (Qal and Qls) 38
Structure 38

CHAPTER THREE: GEOCHEMISTRY 42
Age Determinations 42
Mineral Chemistry 44
  Feldspar 44
  Pyroxene 54
  Olivine 60
  Amphibole 60
  Discussion 63
Whole Rock Composition 65
  Methods 65
  Results 65
  Discussion 79

CHAPTER FOUR: PETROGENESIS OF THE HART MOUNTAIN VOLCANIC COMPLEX 86
Methods 86
Partition Coefficients 87
Hart Mountain trachyandesite suite 89
  Trachybasalt and basaltic trachyandesites 89
  Evolution of the trachyandesites 97

Magma mixing 97
Crystal fractionation 100
Fractionation of trachyandesite to trachyte 103
Warner Peak rhyolite 105
Choice of parent and daughter 106
Major element models 107
Trace element models 109
AM-89-90 as parent 110
AM-90-26 as parent 113
Discussion 116

CHAPTER FIVE: SUMMARY 119

BIBLIOGRAPHY 122

APPENDIX I: PETROGRAPHIC DESCRIPTIONS AND SAMPLE LOCATIONS 132

APPENDIX II: GLOSSARY OF PETROLOGIC TERMS 141

LIST OF FIGURES

Figure Page

1. Location map for Hart Mountain in southeastern Oregon 2

2. Generalized geology of Hart Mountain and vicinity 4

3. Schematic sections for rocks older than Steens Basalts in southern Oregon and adjacent parts of California and Nevada 6

4. Plot of weight percent Na_2O+K_2O versus weight percent SiO_2 for volcanic rocks older than the Steens Basalt in eastern Oregon 11

5. Generalized stratigraphy at Hart Mountain 16

6. Weight percent SiO_2 versus weight percent Na_2O+K_2O for samples analyzed from the Hart Mountain volcanic complex 18

7. Detailed composite stratigraphic columns of the North Mountain and Hart Lake sections 21

8. View of North Mountain section showing one of the buried vent complexes exposed at the base of the section 24

9. Photomicrograph of sample AM-89-42 showing mingled texture and anhedral plagioclase crystals 28

10. Schmidt equal area projection of poles to eutaxitic foliation in ignimbrites and platy jointing in lava flows in the Hart Mountain volcanic complex 39

11. Ternary projections of feldspar compositions from the Hart Mountain trachyandesite. 50

12. Ternary projections of feldspar compositions from the Warner Peak rhyolite. 51

13. Compositions of pyroxenes from the Hart Mountain volcanic complex 58

14. Minimum temperature of formation for pyroxenes from selected samples of the Hart Mountain trachyandesite 59

15. Major element variation diagrams for the Hart Mountain volcanic complex 70

16. Trace element variation diagrams for the Hart Mountain volcanic complex. 71

17. Range of REE concentration found in samples of the Hart Mountain volcanic complex 75

18. Concentrations of REEs found in selected samples of the Hart Mountain trachyandesite suite 76

19. The range of concentrations of REEs found in samples of the Warner Peak rhyolite 77

20. Map of the western United States showing the locations and ages of peralkaline rhyolites found in the Basin and Range 80

21. Selected variation diagrams demonstrating the compositional differences between rocks of the Hart Mountain volcanic complex, Kane Springs Wash caldera (weakly peralkaline), and Pantelleria (strongly peralkaline) 83

22. Compositional differences between the peralkaline rhyolites of the Hart Mountain volcanic complex, Kane Springs caldera, and Pantelleria 84

23. Summary of proposed evolution of the Hart Mountain trachyandesite suite 93

24. Plot of Rb versus Zr with fields of similar major element composition for trachytes and trachyandesites indicated 94

25. P_2O_5 versus Rb showing that the basaltic trachyandesites cannot be modeled by crystal fractionation of trachybasalt AM-90-23 96

26. Calculated versus observed trace element composition for trachyandesite AM-89-42 normalized to the mafic endmember of the mixing model (AM-89-61) 99

27. Calculated versus observed trace element composition of trachyandesite AM-89-65 normalized to the modeled parental trachybasalt (AM-90-23) 101

28. Calculated versus observed trace element composition of trachyandesite AM-89-74 normalized to the modeled parental trachybasalt (AM-90-23) 102

29. Calculated versus observed trace element composition of trachyte AM-89-90 normalized to the modeled parental trachyandesite (AM-89-74) 104

30. Calculated versus observed trace element compositions of the peralkaline rhyolites normalized to the modeled parent (AM-89-90) 111

31. Calculated versus observed trace element compositions of the peralkaline rhyolites normalized to the modeled parent (AM-90-26) 114

LIST OF TABLES

Table		Page
1.	Microprobe analysis of glass in ignimbrite AM-89-83 (Tia)	31
2.	^{40}Ar-^{39}Ar analytical data, Hart Mountain, southeastern Oregon	43
3.	Mineralogy of selected samples from the Hart Mountain trachyandesite suite	45
4.	Mineralogy of the peralkaline rhyolites	46
5.	Representative analyses of feldspar crystals from the Hart Mountain trachyandesite	47
6.	Representative analyses of feldspar crystals from the Warner Peak rhyolite	49
7.	Representative analyses of pyroxene crystals from the Hart Mountain trachyandesite	55
8.	Representative analyses of pyroxene crystals from the Warner Peak rhyolite	57
9.	Representative analyses of olivine phenocrysts in sample AM-89-70	61
10.	Representative analyses of amphibole crystals in sample AM-89-93	62
11.	Compositions of samples from the Hart Mountain volcanic complex	66
12.	Characteristics of strongly peralkaline and weakly peralkaline volcanic systems	82
13.	Partition coefficients between mineral and listed silicate melt used in fractionation models	88
14.	Summary of crystal fractionation models of the petrogenesis of samples of the Hart Mountain trachyandesite suite	90
15.	Fractionation models for the Hart Mountain trachyandesite suite	91
16.	Mixing models for the trachyandesites of the Hart Mountain trachyandesite suite	98

LIST OF PLATES

Plate

1. Bedrock geology of Hart Mountain, southern Oregon
2. Sample locations
3. Stratigraphy of the west side of Hart Mountain
4. Geologic cross section A-A'-A''

Geology and Petrology of a 26-Ma Trachybasalt to Peralkaline Rhyolite Suite Exposed at Hart Mountain, Southern Oregon

Chapter One: Introduction

Basin and Range block faulting in southeastern Oregon has exposed Oligocene and early Miocene volcanic rocks in prominent fault scarps including those at Steens Mountain, Hart Mountain, and Abert Rim (Figures 1 and 3). The older volcanic rocks exposed along these fault scarps are predominantly intermediate composition volcanic and volcaniclastic rocks. At Hart Mountain, the older section consists of a suite of 26.4-Ma trachybasalt to trachyte to peralkaline rhyolite lava flows and tuffs of the Hart Mountain volcanic complex.

The section is capped by the Steens Basalt. The Steens Basalt is composed of moderately fractionated olivine tholeiites erupted from NNE-trending feeder dikes at Steens Mountain and other localities in the northern Great Basin between 12-18 Ma. The onset of Steens Basalt volcanism in southeastern Oregon may mark a change from predominantly calc-alkaline volcanism attributed to the subduction of the Farallon Plate underneath North America (Hart and Carlson, 1987) to bimodal basalt-rhyolite volcanism in a back arc environment (Hart et al., 1984).

The rock suites exposed beneath the Steens Basalt in these fault scarps are important because little is known about the timing and composition of early Basin and Range volcanism in Oregon. By comparison, early Basin and Range volcanism is well understood in parts of Nevada, Utah, California, and Arizona (e.g., Feeley and Grunder, 1991; Best and Christiansen, 1991; Glazner and Bartley, 1990; Eaton, 1982). The Hart Mountain volcanic complex is especially significant because it is among the most lithologically diverse suites in southeastern Oregon (Larson, 1965), the rocks have undergone little alteration, and they erupted over

Figure 1: Location map for Hart Mountain in southeastern Oregon. The inset with physiographic provinces is modified after Hart and Carlson (1987). BM = Blue Mountain; OW = Owyhee Upland. Location of northwest trending fault zones is from Lawrence (1976). Location of calderas and of the Orevada rift from Rytuba et al. (1981). Isochrons (dotted lines) for silicic centers from MacLeod et al. (1976). Extent of Steens Basalts from Mankinen et al. (1987). PH = Paisley Hills; CH = Coyote Hills; PM = Pueblo Mountains.

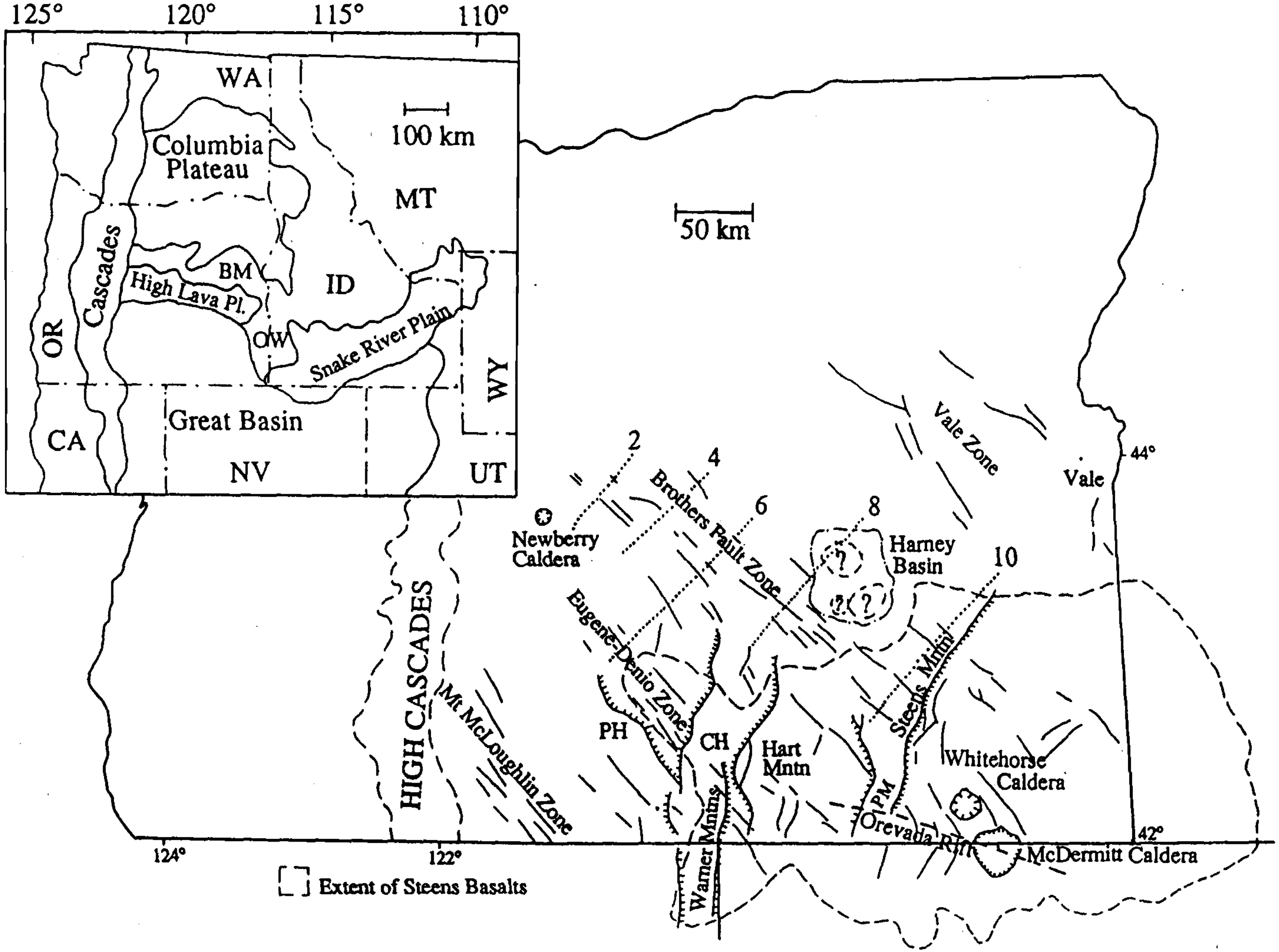
125°
120°
115°
110°
WA
100 km
Columbia Plateau
MT
Cascades
BM
High Lava Pl.
ID
OR
OW
Snake River Plain
WY
CA
Great Basin
NV
UT
50 km
Vale Zone
Vale
44°
2
4
6
8
10
Brothers Fault Zone
Newberry Caldera
Harney Basin
?
?
?
Eugene-Denio Zone
Steens Mntn
HIGH CASCADES
Mt McLoughlin Zone
PH
CH
Hart Mntn
PM
Whitehorse Caldera
Warner Mntns
Orevada Rift
McDermitt Caldera
42°
124°
122°
Extent of Steens Basalts

Figure 1

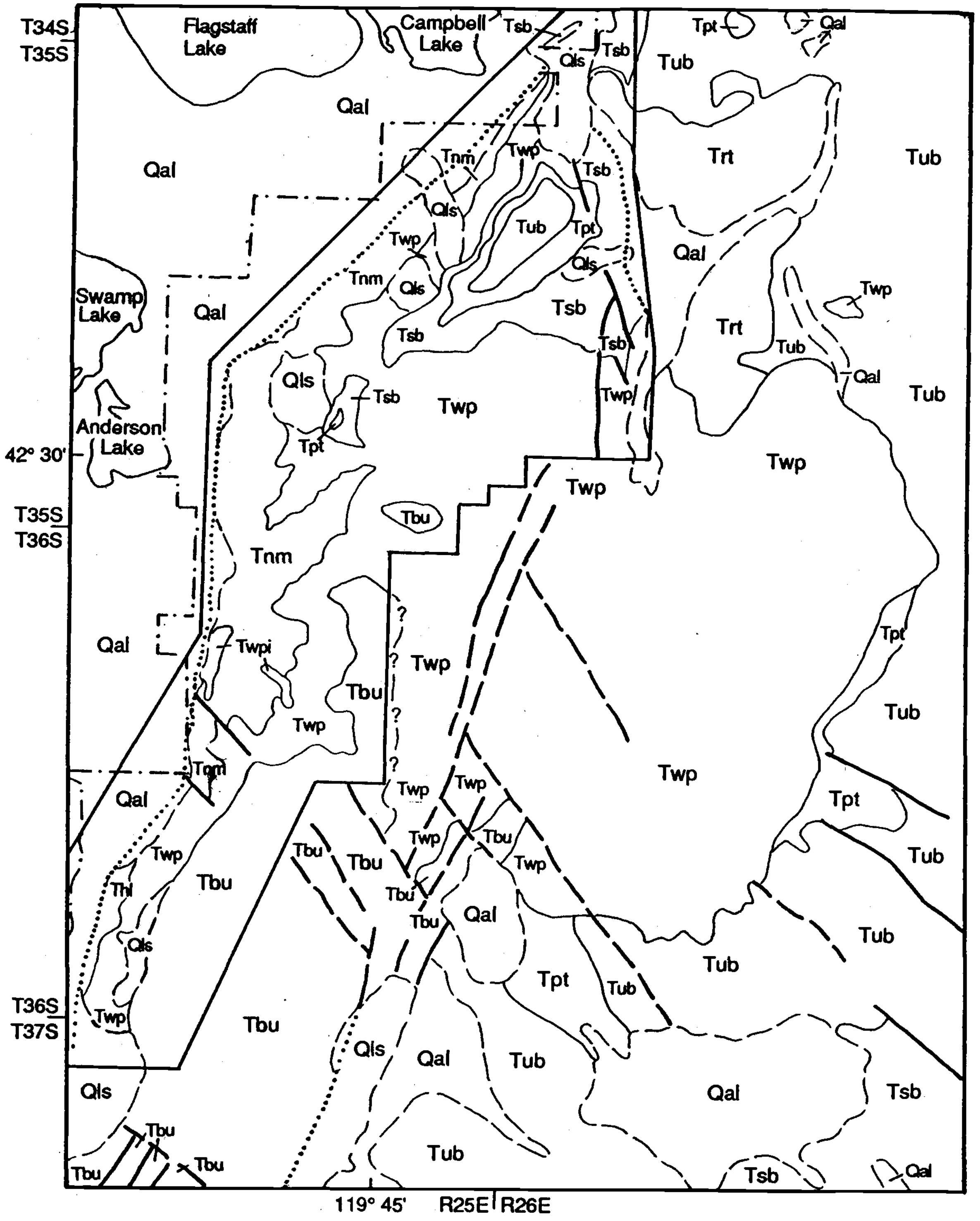
T34S
T35S
Flagstaff Lake
Campbell Lake
Swamp Lake
Anderson Lake
42° 30'
T35S
T36S
T36S
T37S
119° 45'
R25E
R26E
Qal
Qls
Tsb
Tub
Trt
Tpt
Twp
Twpi
Tnm
Tbu
Thl

Generalized Geology of Hart Mountain and Vicinity

Explanation

Quaternary	
Qal	Quaternary alluvium and colluvium
Qls	Quaternary landslide deposits
Tertiary	
Trt	Rattlesnake Ash Flow Tuff
Tub	Upper basalt (HAOT)
Tpt	Plush tuff
Tsb	Steens Basalt
Tbu	Tertiary basalts undivided (HAOT and Steens Basalts)
Hart Mountain volcanic complex	
Twp	Warner Peak rhyolite undivided
Twpi	Warner Peak rhyolite intrusions
Hart Mountain trachyandesite suite	
Thl	Hart Lake section
Tnm	North Mountain section

Scale

1:125,000

0 1 2 3 4 Miles

0 1 2 3 4 5 Kilometers

SYMBOLS

Approximate location of fault (dotted if buried)

Location of lithologic contact (dotted if buried)

Inferred lithologic contact

Boundary of Field Area

Boundary of Hart Mountain National Antelope Refuge

Geology in the Field Area: Allyson Mathis

Geology outside the Field Area: after Walker and Repenning (1965)

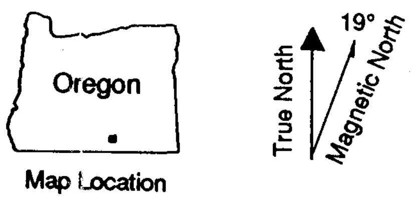
Oregon
Map Location
True North
Magnetic North
19°

Figure 2

a short time interval and likely represent a single magmatic system. Additionally, the pantellerites of the Hart Mountain volcanic complex are the oldest and most peralkaline rhyolites in the Great Basin (Noble et al., 1974; Noble and Parker, 1974). Peralkaline rhyolites usually form in extensional tectonic environments by extensive shallow level crystal fractionation from a basaltic or trachytic parent (Mahood and Baker, 1986; Bailey, 1974; Bailey et al., 1974). The occurrence of 26.4-Ma pantellerites at Hart Mountain suggests that extension-related volcanism in the northern Great Basin may have commenced much earlier than previously postulated (i.e., Hart and Carlson, 1987; Eaton, 1982; Christiansen and McKee, 1978).

The goal of this research project was to establish the age and composition of the volcanic rocks exposed underneath the Steens Basalt at Hart Mountain, and to model their petrologic evolution. These objectives were accomplished by detailed geologic mapping (1:24,000) and ^{40}Ar-^{39}Ar age determinations to provide the stratigraphic and chronologic framework. Petrography, electron microprobe analysis, and whole rock major and trace element (XRF and INAA) analysis of samples collected during field work provided the data necessary for the petrologic study.

LOCATION

The field area is located in and around Hart Mountain National Antelope Refuge in Lake County, southern Oregon (Figures 1 and 2). The 108 km^2 area includes the northern half of Hart Mountain (informally referred to as North Mountain) and the western fault escarpment of Hart Mountain from 42°35'N to 42°23'N. The field and petrologic study focuses on the rocks of the Hart Mountain volcanic complex exposed on the western flank of Hart Mountain. The fault escarpment there exposes the thickest and most complete sequence of these rocks and the full compositional spectrum from basalt to peralkaline rhyolite (SiO_2 52-71 wt %).

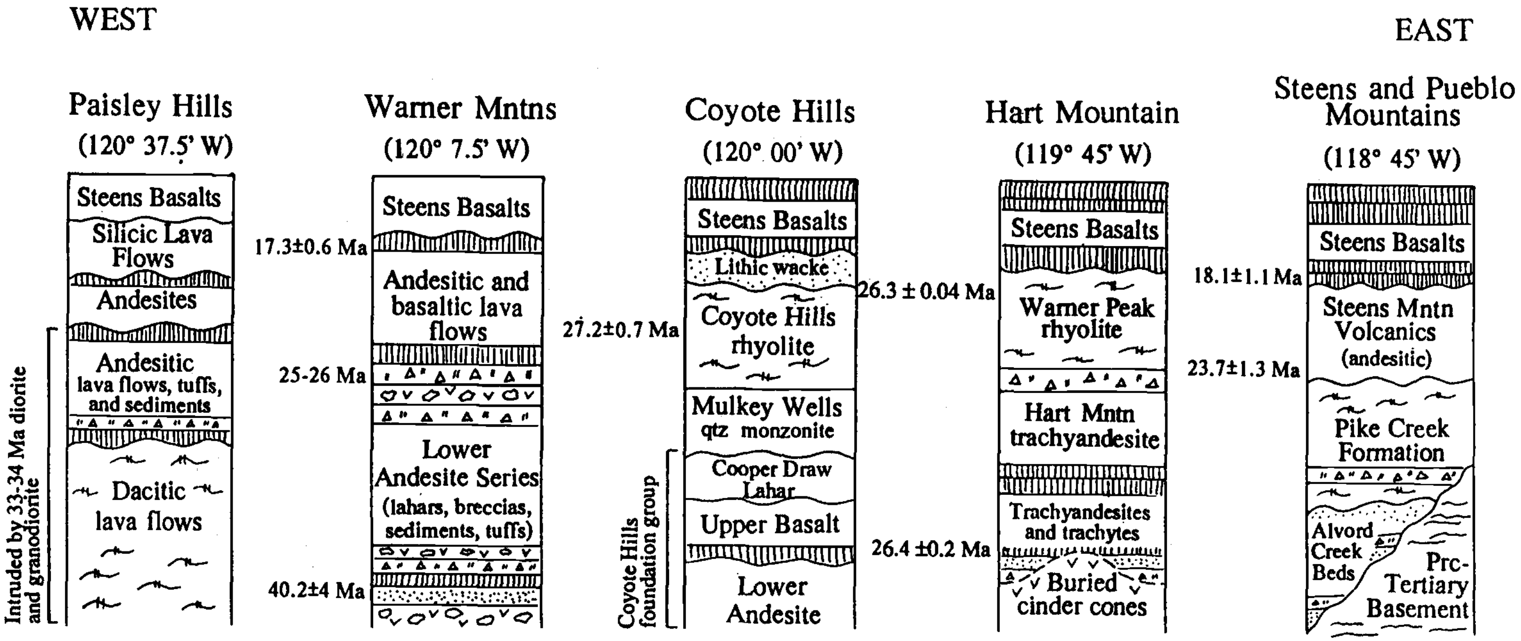
WEST
EAST
Paisley Hills
(120° 37.5' W)
Warner Mntns
(120° 7.5' W)
Coyote Hills
(120° 00' W)
Hart Mountain
(119° 45' W)
Steens and Pueblo Mountains
(118° 45' W)
Steens Basalts
Silicic Lava Flows
Andesites
Andesitic lava flows, tuffs, and sediments
Dacitic lava flows
Intruded by 33-34 Ma diorite and granodiorite
17.3±0.6 Ma
Andesitic and basaltic lava flows
25-26 Ma
Lower Andesite Series (lahars, breccias, sediments, tuffs)
40.2±4 Ma
27.2±0.7 Ma
Lithic wacke
Coyote Hills rhyolite
Mulkey Wells qtz monzonite
Cooper Draw Lahar
Upper Basalt
Lower Andesite
Coyote Hills foundation group
26.3 ± 0.04 Ma
Warner Peak rhyolite
Hart Mntn trachyandesite
Trachyandesites and trachytes
Buried cinder cones
26.4 ±0.2 Ma
18.1±1.1 Ma
Steens Mntn Volcanics (andesitic)
23.7±1.3 Ma
Pike Creek Formation
Alvord Creek Beds
Pre-Tertiary Basement

Figure 3: Schematic sections for rocks older than Steens Basalts in southern Oregon and adjacent parts of California and Nevada. Stratigraphic information and age determinations compiled from: Paisley Hills: Muntzert (1969), Peterson and McIntry (1970); Warner Mountains: Duffield and McKee (1986), Wells (1979); Coyote Hills: Thomas (1981); and Steens and Pueblo Mountains: Fuller (1931), Minor et al. (1987), Harrold (1973).

Additional exposures of the Hart Mountain volcanic complex, including most of the peralkaline rhyolite near-vent rocks, are located a few kilometers east of the field area (Figure 2).

Elevation in the field area ranges from 1371 m above sea level in Warner Valley to 2316 m on the crest of North Mountain. Bedrock is well exposed except where locally covered by landslide deposits or talus.

STRUCTURAL SETTING

Southeastern Oregon and adjacent parts of California, Nevada, and Idaho lie within the northwestern part of the Basin and Range physiographic province (Figure 1). This area is designated the Oregon Plateau by Carlson and Hart (1987). The northwestern Basin and Range is characterized by a thinned crust of 25-35 km and high heat flow (Hart et al., 1984). The distinctive topography of north-south trending mountain ranges, uplifted relative to deep broad valleys by large faults, results from large-scale rifting of the North American plate during the last 17 Ma. Prior to 17 Ma, basin-range topography probably did not exist in the northern Great Basin (Mankinen et al., 1987). Numerous early Miocene ignimbrite sheets in central Nevada indicate there was little topographic relief at the time (Christiansen and McKee, 1978). The approximately 15-Ma Steens Basalts flowed onto a hilly terrain with considerable (as much as 1000 m) topographic relief in southern Oregon (Larson, 1965; Wells, 1979; Mankinen et al., 1987). Most of the paleotopographic highs were volcanic edifices, such as the edifice of the Hart Mountain volcanic complex, rather than fault scarps (Larson, 1965; Wells, 1979; Thomas, 1981; Mankinen et al., 1987).

Prominent uplifted blocks in southeastern Oregon include those at Steens Mountain, Hart Mountain, Abert Rim, Warner Mountains, and Summer Rim (Figure 1). The NNE-striking normal faults have offsets of as much as 2,000 m (Walker and Repenning, 1965). More than 700 m of displacement occurred on the western fault scarp at Hart Mountain and at Poker Jim Ridge, which is a large monoclinal warp immediately north of Hart Mountain (Walker and Swanson, 1968b). Approximately 300 m of displacement occurred in a zone of normal faults which bound the north and east sides of Hart Mountain (Walker and Swanson, 1968b). The age of Basin and Range faulting at Hart Mountain is less than 6.9 Ma as constrained by displacement of a 6.9 Ma rim capping lava flow at Hart Mountain (Hart and Mertzman, 1982). Displacement occurred at Abert Rim between 6 and 15 Ma (Hart and Mertzman, 1982).

Four major zones of northwest-striking faults also cut southeastern Oregon (Figure 1). The inferred right-lateral strike-slip offset in these fault zones results from a northward decrease in Basin and Range extension (Lawrence, 1976). However, field evidence indicates normal displacement on the Brothers Fault Zone and suggests that east-west dextral shear accommodates extension along the northern margin of the Basin and Range (Clayton, 1989). The two northernmost zones, the Vale Zone and the Brothers Fault Zone, mark the northern terminus of the Basin and Range province in Oregon. Physiographic expression of Basin and Range structure north of the Eugene-Denio and Mount McLoughlin zone suggests that faulting is younger north of the zones (Lawrence, 1976). Movement along the northwest-striking fault zones in southeastern Oregon appears to have occurred prior to the emplacement of the Steens Basalts and prior to the initiation of the NNE-striking normal faulting (Larson, 1965).

REGIONAL STRATIGRAPHY

Three major periods of Cenozoic volcanism occurred in southeastern Oregon (Lipman et al., 1972; Christiansen and McKee, 1978; Carlson and Hart, 1987). The earliest period of volcanism produced predominantly calc-alkaline intermediate to silicic volcanic rocks between 50 and 18 Ma (Christiansen and McKee, 1978). Following a regional hiatus in volcanic activity, voluminous outpourings of Fe-rich continental flood basalts, the Steens Basalt, occurred between 18 and 12 Ma in southeastern Oregon and adjacent areas (Christiansen and McKee, 1978; Carlson and Hart, 1987). Also during this period, silicic volcanism began in the northern Great Basin and has continued into the Holocene (MacLeod et al., 1976). Between 18-15 Ma numerous calderas, including McDermitt caldera complex, the Pueblo caldera, and the Whitehorse caldera (Rytuba, 1989; Rytuba et al., 1981), erupted along the Orevada Rift (Figure 1) in southeastern Oregon and northwestern Nevada. Between about 11 and 0 Ma, the silicic volcanism decreased roughly in age to the northwest (MacLeod et al., 1976). Between 9 and 6 Ma, approximately 425 km^3 of silicic ash flow tuffs were erupted from the Harney Basin during the most voluminous period of silicic volcanism in eastern Oregon (Greene, 1973; Davenport, 1971). During the last 11 Ma, primitive high alumina olivine tholeiite (HAOT) basalts were erupted throughout the northwestern Great Basin (Hart et al., 1984).

EARLY VOLCANIC ROCKS

Rocks older than the Steens Basalts in southeastern Oregon are generally exposed only in fault scarps such as at the Warner Mountains, Hart Mountain, and Steens and Pueblo Mountains, or where they were incompletely buried by the Steens Basalts (at the Coyote Hills and east of Hart Mountain). These suites consist of Cenozoic volcanic rocks with minor amounts of sedimentary material. The nearest pre-Tertiary basement rocks are exposed in the Pueblo Mountains in northern Nevada (Rytuba and McKee, 1984). Figure 3 shows generalized stratigraphic columns of rocks exposed underneath the Steens Basalt in southern Oregon.

Pre-Steens rocks in southeastern Oregon range in age from at least 40 Ma to 18 Ma. In the Paisley Hills, there are dacitic and andesitic lava flows which may be older and are intruded by 33-34 Ma diorite and granodiorite. These pre-

Steens suites generally consist of metaluminous intermediate to silicic rocks similar in age and composition to the Clarno Formation in central Oregon (>30-50 Ma; Enlows and Parker, 1972). The rocks in southern Oregon are richer in alkalies than the Clarno Formation (Figure 4). The Hart Mountain volcanic complex is the only pre-Steens suite that includes strongly peralkaline rhyolites in southern Oregon (Noble et al., 1974; this study).

Rocks exposed in the Coyote Hills on the west side of Warner Valley are the closest in age, location, and composition to the rocks of the Hart Mountain volcanic complex (Figure 4). A 27.2±0.7 Ma K-Ar age determination (Fiebelkorn et al., 1983) of the Coyote Hills rhyolite near the top of the exposed stratigraphic section suggests that the Coyote Hills rhyolite is essentially coeval to the Hart Mountain volcanic complex (26.4±0.1 Ma). However, unlike the Hart Mountain volcanic complex, the Coyote Hills is bimodal consisting predominantly of basalts and high silica rhyolites, and has undergone hydrothermal mineralization contemporaneously with the silicic volcanism (Thomas, 1981).

STEENS BASALT

The Steens Basalt and Steens-type basalt are found throughout much of the Oregon Plateau and are largely composed of sequences of thin (averaging 3 m; Larson and Stern, 1983), diktytaxitic, ophitic, and plagioclase-phyric flows of moderately fractionated olivine tholeiites (Gunn and Watkins, 1970). The type section and the most conspicuous occurrence of the Steens Basalt is at Steens Mountain 90 km to the east where 1,000 m of basaltic and basaltic andesite flows and feeder dikes are exposed (Figure 1; Fuller, 1931). Steens-type basalts span a wider age interval (18 to 11 Ma) than the Steens Basalt, and were erupted from feeder dikes throughout its area of exposure (Hart and Carlson, 1985; Mankinen et al., 1987). The Steens and Steens-type basalts cover approximately 75,000 km^2 in the northwestern Great

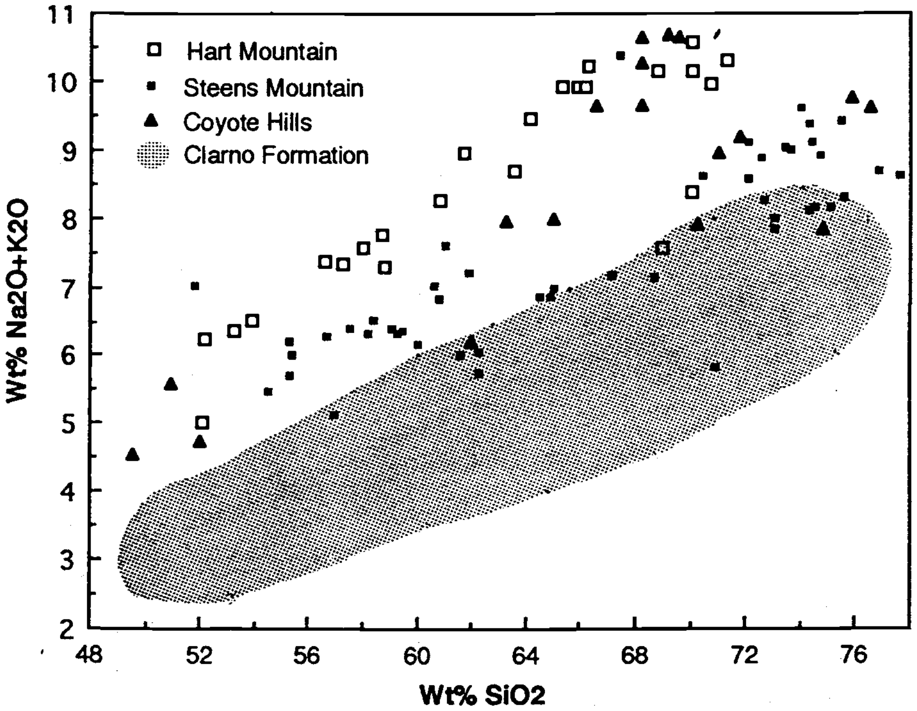

Figure 4: Plot of weight percent Na_2O+K_2O versus weight percent SiO_2 for volcanic rocks older than Steens Basalt in eastern Oregon. Data compiled from: Steens Mountain: Langer (1991), Carlson and Hart (1987), Harrold (1973), and Fuller (1931); Coyote Hills: Thomas (1981). The field for the Clarno Formation is from Rogers and Novitsky-Evans (1977), Noblett (1981), Mullen (1978), and Oles and Enlows (1972).

Basin, and are estimated to have a total volume of at least 30,000 km^3 (Larson and Stern, 1983). Peaks of Steens Basalt volcanism occurred at 15-16 and 11-12 Ma (Hart and Mertzman, 1982; Hart and Carlson, 1985). Regional correlation of the Steens Basalt with the Steens Mountain as a reference section has been done by magnetostratigraphic techniques, which indicate that the early Steens (Steens-type) basalts had eruptive centers in the Santa Rosa, Owyhee, and Jarbridge mountain ranges (Hart and Carlson, 1985). Larson (1965) reported a Steens-type vent on the on the west side of the Warner Valley about 15 km south of Hart Mountain. The vents became progressively more localized as volcanism proceeded until Steens lavas were erupted from the single centralized vent at Steens Mountain (Mankinen et al., 1987). Basalts erupted at Steens Mountain flowed to the west and south. The dominant volume of the Steens Basalt was erupted at 15.5 Ma from NNE trending feeder dikes at Steens Mountain within a short period of time as evidenced by the lack of intraflow soils or sedimentary strata (Fuller, 1931; Gunn and Watkins, 1970; Mankinen et al., 1987).

Other researchers, including Carlson and Hart (1983) and Hart and Carlson (1985), correlate Steens Basalts using Sr isotopic compositions to differentiate between Steens and Steens-type basalts. Steens Basalts have a narrow range of initial Sr isotopic composition suggesting that they were derived from a depleted oceanic type mantle without contamination by evolved continental crust ($^{87}Sr/^{86}Sr_i$ = 0.70367-0.70391; Carlson and Hart, 1983; 1987). Steens-type basalts are found east of Steens Mountain and have higher initial $^{87}Sr/^{86}Sr$ (0.70408-0.70647), which may reflect a continental mantle source for these magmas (Carlson and Hart, 1983; 1987).

Petrogenetic modeling (Helmke and Haskin, 1973; Gunn and Watkins, 1970) suggested that the Steens Basalt can be related to a single parental magma by extensive fractionation of plagioclase, olivine, and clinopyroxene; aided perhaps by minor contamination with young, isotopically unevolved, continental crust (Carlson and Hart, 1987). Hart et al. (1989) further refined this model for Steens-type basalts exposed in the Pueblo Mountains suggesting distinct "parental" magmas resulting from progressive increase in contamination with continental crust during the later phases of volcanism. Fractionation of these "parental" magmas then produced the observed chemical variations within the suite exposed in the Pueblo Mountains.

HIGH-ALUMINA OLIVINE THOLEIITE (HAOT)

High-alumina olivine tholeiites (HAOT) cover an estimated 22,000 km^2 in southeastern Oregon and adjacent parts of California, Nevada, and Idaho, and have a minimum volume of 650 km^3 (Hart et al., 1984). Peaks of HAOT volcanism occurred between 0-2.5, 3.5-6, and 7-10 Ma (Hart et al., 1984). HAOT is the most primitive basalt in the northwestern Great Basin. The unfractionated nature of these basalts is evidenced by high Mg/Fe ratios, high Ni and Ca contents, and low concentrations of Ba, Rb, and K. Modeling suggests that HAOT was generated by partial melting of incompatible element-depleted upper mantle sources (Hart, 1985; Draper, 1991). Minor variations in composition of HAOT lavas can be attributed to modest amounts of shallow level crystal fractionation (Draper, 1991). Hart and Carlson (1987) contend that the major and trace element composition of HAOT remains nearly uniform throughout its area of occurrence; however, Draper (1991) found that Mg# increases systematically to the northwest along the Brothers Fault Zone. $^{87}Sr/^{86}Sr_i$ ratios increase west to east from 0.703 to 0.707 with an abrupt increase near 118° attributed to differences in the source mantles: oceanic mantle in the west, and subcontinental mantle towards the east (Hart, 1985; Hart and Carlson, 1987). The primitive nature of the HAOT magmas results from thinning of the crust by extension allowing rapid transport of the mantle melts (Draper, 1991).

PREVIOUS WORK AT HART MOUNTAIN

Walker (1961) first reported "soda rhyolites" exposed at Hart Mountain. He described pantellerite from Hart Mountain and provided two major element analyses. K-Ar age determinations (25-28 Ma; Noble et al., 1974) established that these pantellerites are the oldest peralkaline rhyolites found in the Great Basin. High Ba/Sr (≈ 25) and high K/Rb (830-430) indicate that prolonged fractionation of plagioclase and mafic minerals from the parental magmas occurred before anorthoclase fractionated to produce the peralkaline rhyolites (Noble et al., 1974). Low REE and trace element (Nb, Y, Zr) concentrations relative to other pantellerites, and low initial $^{87}Sr/^{86}Sr$ (0.7034) in these samples suggest that they fractionated from parental magmas derived from depleted mantle sources (Noble et al., 1974).

Reconnaissance mapping at Hart Mountain has been done by Larson (1965), Walker and Repenning (1965), and Walker and Swanson (1968b). Larson (1965) reported that Hart Mountain has the thickest and most lithologically diverse section of pre-Steens rocks exposed in south-central Oregon. These regional studies did not focus on the petrology of the Hart Mountain volcanic complex.

Chapter Two: Stratigraphy and Structure

STRATIGRAPHY

Up to 1000 m of Tertiary volcanic rocks are exposed along the western fault escarpment of Hart Mountain. These rocks range in age from 6.5 to 26.4 Ma with the pre-Tertiary basement not exposed (Figure 5; Plates I and III). The lower half of the section consists of a mostly conformable sequence of alkali basaltic to trachytic lava flows and tuffs with several small cinder cones exposed near the base of the section, and is herein informally designated the Hart Mountain trachyandesite suite. The Hart Mountain trachyandesite suite is capped by the lava flows and tuffs of a peralkaline rhyolite vent complex informally named the Mount Warner rhyolite (Larson, 1965). I redesignated the Mount Warner rhyolite as the Warner Peak rhyolite in order to avoid confusion with the Warner Mountains to the west. In the field area, the Warner Peak rhyolite consists of trachytic to peralkaline rhyolitic lava flows and ignimbrites with minor amounts of interlayered tuffaceous sediments, and numerous small shallow intrusions and dikes. Together, the Hart Mountain trachyandesite suite and the Warner Peak rhyolite make up the Hart Mountain volcanic complex.

^{40}Ar-^{39}Ar age determinations of mineral separates from near the base of the Hart Mountain trachyandesite suite and from the Warner Peak rhyolite yield ages of 26.4±0.2 and 26.3±0.04 Ma, respectively. The analytically indistinguishable dates indicate that these rocks were erupted within a very short time interval. This conclusion is supported by the paucity of sedimentary rocks and angular unconformities within the sections. At the base of the Hart Mountain escarpment are exposures of several small cinder cones that are buried by a few meters of tuffaceous sediments and the overlying generally conformable sequence of lava flows and tuffs.

The Warner Peak tuff, which usually marks the base of the Warner Peak rhyolite, consists mostly of tuffaceous

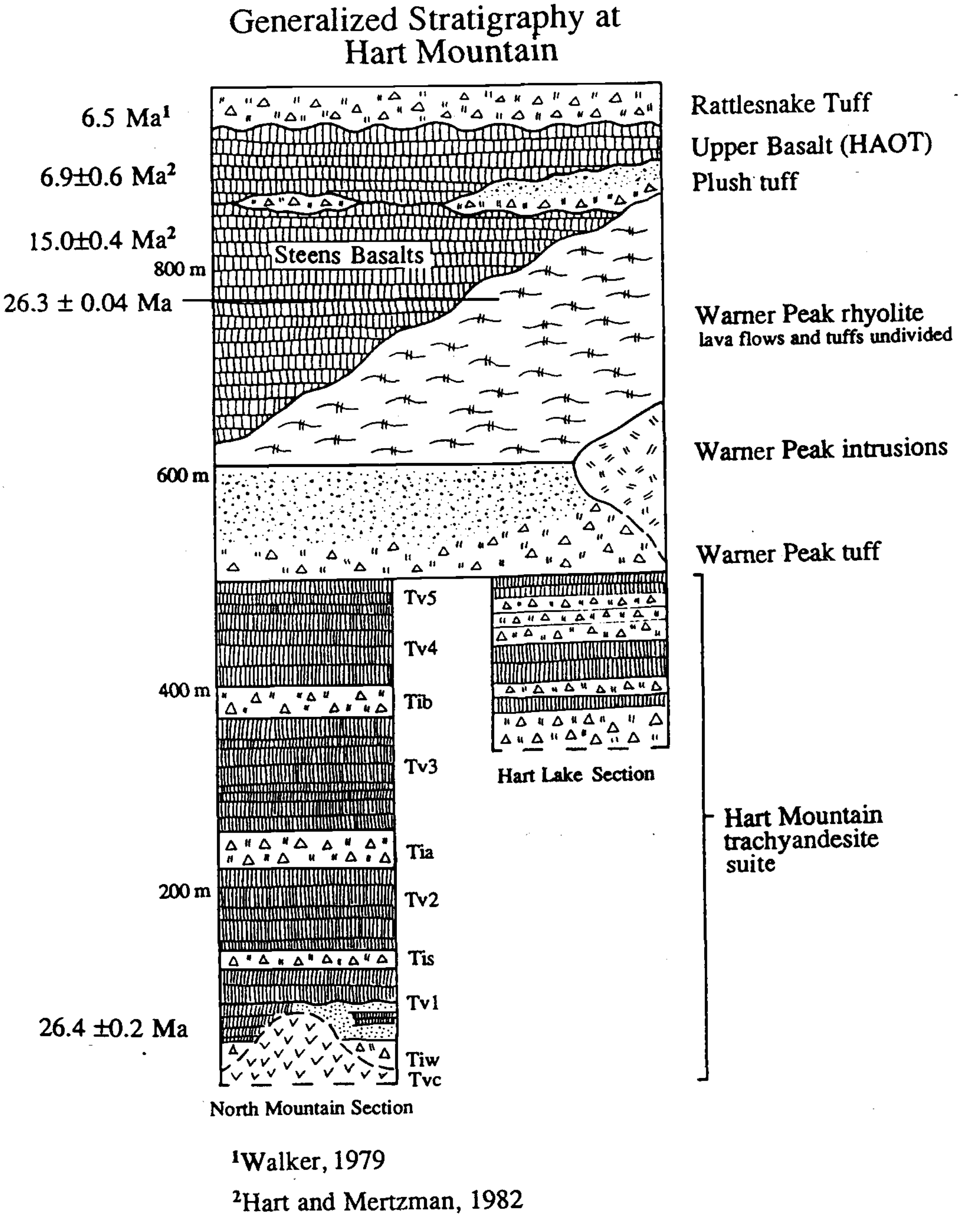
Generalized Stratigraphy at Hart Mountain
6.5 Ma[1]
6.9±0.6 Ma[2]
15.0±0.4 Ma[2]
800 m
26.3 ± 0.04 Ma
600 m
400 m
200 m
26.4 ±0.2 Ma
Steens Basalts
Rattlesnake Tuff
Upper Basalt (HAOT)
Plush tuff
Warner Peak rhyolite
lava flows and tuffs undivided
Warner Peak intrusions
Warner Peak tuff
Tv5
Tv4
Tib
Tv3
Tia
Tv2
Tis
Tv1
Tiw
Tvc
North Mountain Section
Hart Lake Section
Hart Mountain trachyandesite suite
[1]Walker, 1979
[2]Hart and Mertzman, 1982

Figure 5: Generalized stratigraphy at Hart Mountain. The Warner Peak rhyolite and the Hart Mountain trachyandesite suite make up the Hart Mountain volcanic complex. Unit abbreviations are from Plate I.

sediments in the central part of the field area. These tuffaceous sediments, which appear to be only slightly reworked volcanic material, suggest that at least a short hiatus in volcanic activity accompanied the change from predominantly intermediate to predominantly silicic volcanism. However, the lower portion of the Warner Peak rhyolite contains trachytic lava flows similar in mineralogy and composition to the trachytes in the Hart Mountain trachyandesite suite. Therefore, the Hart Mountain trachyandesite suite and the Warner Peak rhyolite appear to represent a single magmatic system which produced compositions ranging from alkali basalt to peralkaline rhyolite (Figure 6).

The edifice of the Hart Mountain volcanic complex formed a topographic high at the onset of Steens flood basalt volcanism at 17 Ma, and was incompletely buried by the Steens Basalts. The unconformity between the Hart Mountain volcanic complex and the Steens Basalt in the Hart Mountain/Poker Jim Ridge area has at least 500 m of relief. The uppermost Steens Basalt flow on the north end of Hart Mountain was dated at 15.0±0.4 Ma by Hart and Mertzman (1982). A package of rhyodacitic and rhyolitic tuffs and tuffaceous sediments informally known as the Plush tuff (Larson, 1965) locally unconformably overlies the Steens Basalts on the north end of Hart Mountain. The Plush tuff is found in the vicinity of Hart Mountain and Warner Valley which suggests that it had a local source. Uncomformably overlying the Plush tuff are basalt flows with compositions of high alumina olivine tholeiite (HAOT) informally designated the Upper Basalt. The rim capping HAOT flow on the north end of Hart Mountain is 6.9±0.6 Ma (Hart and Mertzman, 1982). The Plush tuff is not found in the southern half of the field area. There, the Steens Basalts and the Upper Basalt were mapped together as Tertiary basalts undivided (Tbu) because lithologic distinction of separate units is difficult.

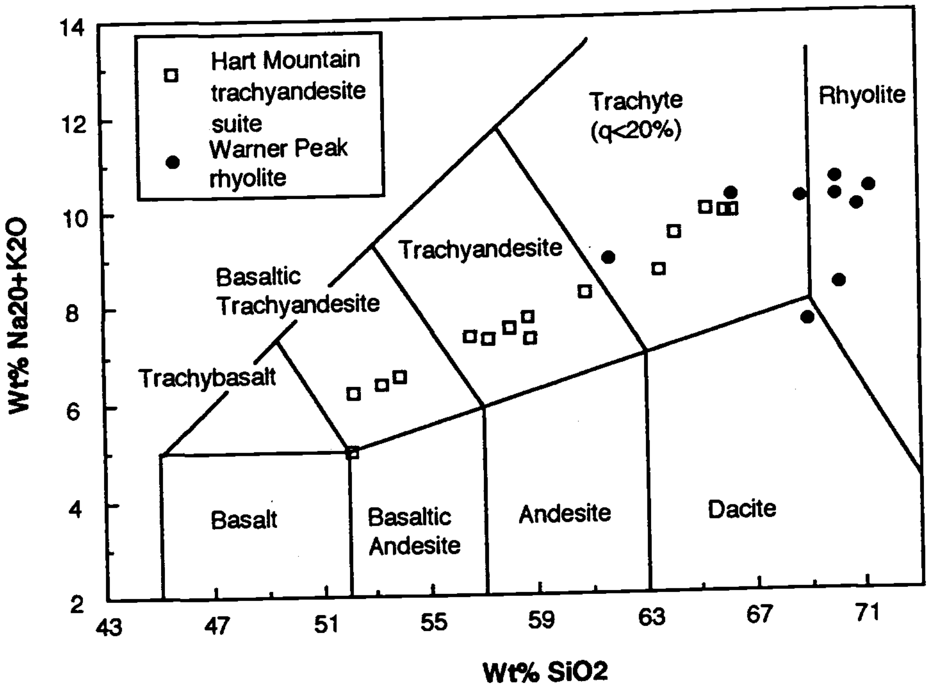

Figure 6: Weight percent SiO_2 versus weight percent Na_2O+K_2O for samples analyzed from the Hart Mountain volcanic complex. Classification follows LeBas et al. (1986).

The youngest unit exposed in the vicinity of Hart Mountain is the regionally extensive Rattlesnake Ash Flow Tuff which was probably erupted from the Harney Basin to the northeast (Walker, 1979; Enlows, 1976). New ^{40}Ar-^{39}Ar geochronology of the Rattlesnake Tuff yielded a date of 7.2 Ma (M. Streck and A.L. Grunder, personal communication, 1992) which is older than the previously published average age of 6.5 Ma (Walker, 1979).

Volcanic stratigraphy, field descriptions and generalized petrologic characteristics of the mapped units are presented in the following section. The geologic map with sample locations are in Plates I and II. Figure 5 is a generalized stratigraphic column of the rocks exposed at Hart Mountain. Plate III consists of detailed stratigraphic columns showing north-south lateral variations in the character and thicknesses of the mapped units.

HART MOUNTAIN VOLCANIC COMPLEX

The Warner Peak rhyolite makes up the dominant volume (approximately 85%) of the Hart Mountain volcanic complex, most of which is exposed a few miles east of the field area (Figure 2). The western fault escarpment of Hart Mountain cuts through a flank of this volcanic complex, exposing the earlier products of the magmatic system in the Hart Mountain trachyandesite suite. The Hart Mountain trachyandesite suite otherwise would likely be buried by the Warner Peak rhyolite and/or the overlying Steens Basalt.

HART MOUNTAIN TRACHYANDESITE SUITE

Rocks of the Hart Mountain trachyandesite suite are exposed as a mostly conformable sequence of slightly eastward dipping lava flows and tuffs. In places, thin dikes and shallow intrusions of trachyandesite invade the sequence of flows. The rocks of the Hart Mountain trachyandesite suite are roughly divisible into two sections: The North Mountain section and the Hart Lake section (Figure 5). The North

Mountain section, with a thickness of 90 to 450 meters, is exposed in the northern half of the field area. It consists of approximately 70% lava flows with at least four interlayered ignimbrites, which serve as stratigraphic markers within the section and are mapped separately. Thin lenses of unwelded ignimbrite, airfall tuff and tuffaceous sediment are found irregularly throughout the section, but are not laterally continuous and appear to represent only a minor volume of material. In general, it was not possible to distinguish individual lava flows throughout the field area because of textural and morphological similarities between many of the lava flows, and because of lateral changes in flow morphologies.

The Hart Lake section, exposed in the southern portion of the field area (Figure 5, Plate I), has a maximum thickness of 200 meters, and consists predominantly of silicic tuffs (approximately 70%) with only a few interlayered lava flows. The Hart Lake section was mapped undivided because it was not possible to map individual lavas flows and tuffs at this scale (1:24,000). There are at least 10 separate lava flows and tuffs. The lava flows and tuffs in the Hart Lake section are similar in morphology, mineralogy, and composition to the rocks in the North Mountain section, and are interpreted to be similar in age, or perhaps slightly younger than the North Mountain rocks. The Hart Lake rocks may represent a higher stratigraphic portion of the Hart Mountain trachyandesite suite because they are generally more silicic. The two sections are separated by a near-vertical NW-striking fault with apparent down-to-the-south displacement near Deep Canyon (Plates I and III). No lava flows or ignimbrites could be definitely correlated between the two sections (Figure 7). The character and thickness of the Warner Peak tuff also changes across the fault: it consists predominantly of tuffaceous sediments north of the fault and is approximately 50 m thick; whereas, south of the fault, it consists of predominantly of ignimbrites with only a few meters of

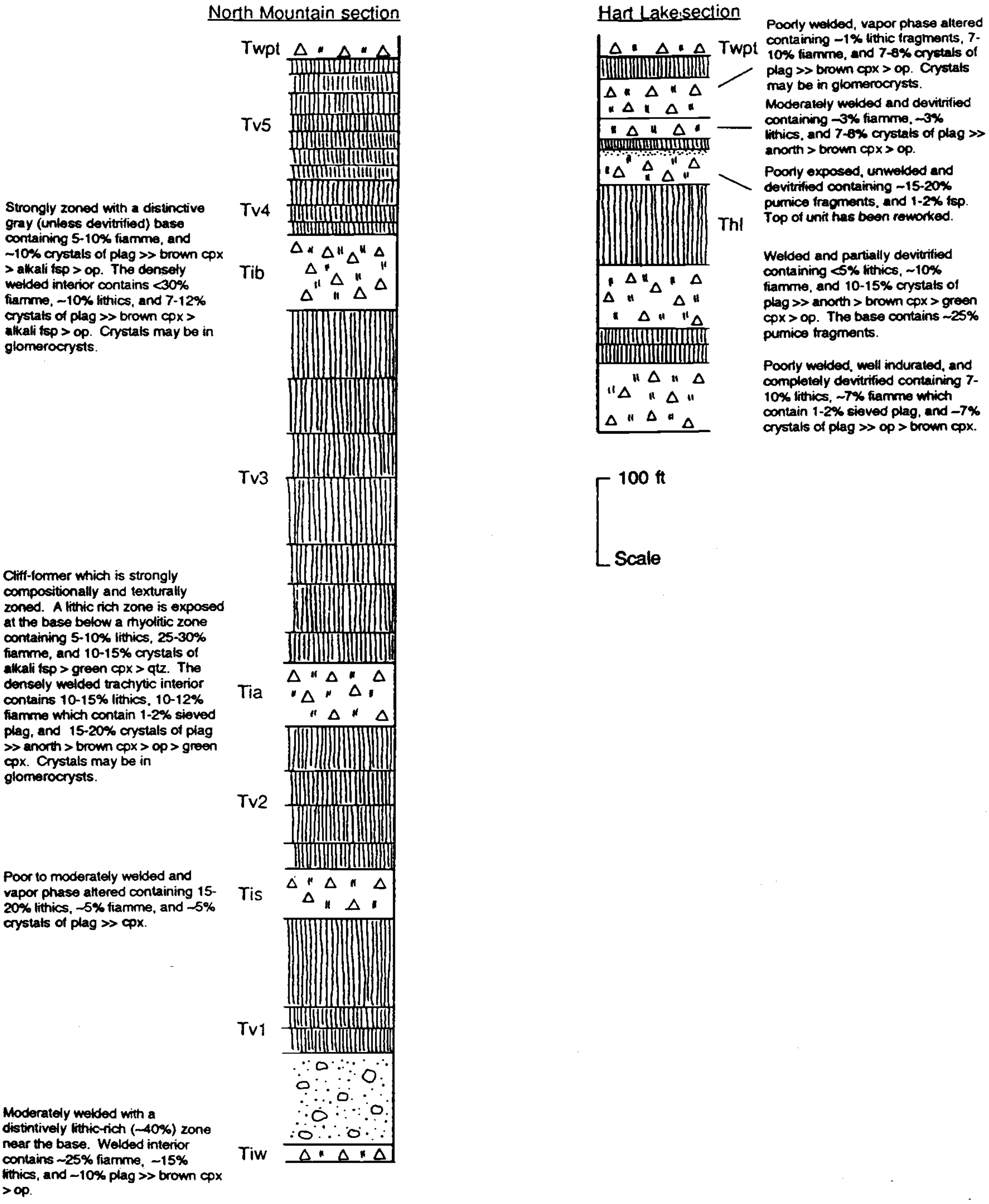

Strongly zoned with a distinctive gray (unless devitrified) base containing 5-10% fiamme, and ~10% crystals of plag >> brown cpx > alkali fsp > op. The densely welded interior contains <30% fiamme, ~10% lithics, and 7-12% crystals of plag >> brown cpx > alkali fsp > op. Crystals may be in glomerocrysts.

Cliff-former which is strongly compositionally and texturally zoned. A lithic rich zone is exposed at the base below a rhyolitic zone containing 5-10% lithics, 25-30% fiamme, and 10-15% crystals of alkali fsp > green cpx > qtz. The densely welded trachytic interior contains 10-15% lithics, 10-12% fiamme which contain 1-2% sieved plag, and 15-20% crystals of plag >> anorth > brown cpx > op > green cpx. Crystals may be in glomerocrysts.

Poor to moderately welded and vapor phase altered containing 15-20% lithics, ~5% fiamme, and ~5% crystals of plag >> cpx.

Moderately welded with a distintively lithic-rich (~40%) zone near the base. Welded interior contains ~25% fiamme, ~15% lithics, and ~10% plag >> brown cpx > op.

Poorly welded, vapor phase altered containing ~1% lithic fragments, 7-10% fiamme, and 7-8% crystals of plag >> brown cpx > op. Crystals may be in glomerocrysts.

Moderately welded and devitrified containing ~3% fiamme, ~3% lithics, and 7-8% crystals of plag >> anorth > brown cpx > op.

Poorly exposed, unwelded and devitrified containing ~15-20% pumice fragments, and 1-2% fsp. Top of unit has been reworked.

Welded and partially devitrified containing <5% lithics, ~10% fiamme, and 10-15% crystals of plag >> anorth > brown cpx > green cpx > op. The base contains ~25% pumice fragments.

Poorly welded, well indurated, and completely devitrified containing 7-10% lithics, ~7% fiamme which contain 1-2% sieved plag, and ~7% crystals of plag >> op > brown cpx.

Figure 7: Detailed composite stratigraphic columns of the North Mountain and Hart Lake sections. Descriptions of the ignimbrites demonstrates the lack of correlation between the sections. Plag=plagioclase, cpx=clinopyroxene, fsp=feldspar, op=opaque oxides, qtz=quartz, anorth=anorthoclase.

tuffaceous sediments at the base and is approximately 60 m thick. The stratigraphic differences north and south of the fault near Deep Canyon suggests that faulting may have occurred while the Hart Mountain volcanic complex was active. Perhaps the predominance of ignimbrites within the Hart Lake section and the down-to-the-south displacement indicate that it was a fault-controlled paleovalley into which more ignimbrites flowed.

North Mountain Section

The North Mountain section is exposed from the northern boundary of the field area south to Deep Canyon. The thickest section of North Mountain rocks is found between Juniper and Mulkey Canyons where two small buried cinder cones or near vent accumulations of ash and tephra are exposed near the base of the western fault escarpment. A third cinder cone is exposed south of Hart Canyon, but extensive intrusions of Warner Peak rhyolite there make stratigraphic relationships difficult to discern.

In this section, field and petrographic characteristics will be described for the base of the North Mountain section (Tvc, Tiw, Tvl), for the generalized characteristics of the lava flows (Tvl, Tv2, Tv3, Tv4, Tv5 and the lava flows of the Hart Lake section), and for the ignimbrites (Tis, Tia, Tib).

Base of the North Mountain section (Tvc, Tiw, Tvl)

Three mapped units (vent complexes, Tvc; Ignimbrite W, Tiw; and lava flows and tuffaceous sediments, Tvl) make up the lowest exposed portion of the Hart Mountain escarpment, and the oldest exposed rocks at Hart Mountain. These three map units are discussed here as a group because they appear to record an early phase of volcanism including a short hiatus in volcanic activity in which small scattered trachybasalt to basaltic trachyandesite cinder cones were formed and then buried by tuffaceous sediments, an ignimbrite, and lava flows. These map units also include the most mafic rock (sample AM-90-23, SiO_2 = 52.1 wt %) collected from Hart Mountain.

Tvc consists of near-vent accumulations of reddened scoriaceous ash lapilli and bombs and related feeder dikes and lava flows which appear to have formed small edifices less than a hundred meters high (Figure 8). The structure of the northern-most (T36S R25E, section 21) vent is the best preserved: a trachyandesitic conduit (sample AM-89-92) is exposed in the center of the pile of radially dipping tephra. A basaltic lava flow (AM-89-70, AM-90-23) is found on the northern flank of the cone. This seriate and glomeroporphyritic lava flow contains 10-15% subhedral to anhedral phenocrysts of plagioclase (bytownite to labradorite), olivine (Fo_{85-65}), augite, and Fe-Ti oxides in a pilotaxitic groundmass. Phenocrysts are as large as 3 mm. Olivine is commonly replaced by iddingsite and/or calcite.

Tiw, a moderately welded trachytic ignimbrite (sample AM-89-85), flowed out onto the vent complexes of Tvc. Maximum exposed thickness is 8 meters, with the unwelded top and bottom not exposed. A distinctive lithic-rich zone with approximately 40% rounded silicic volcanic lithic clasts, as large as 10 cm, in size is exposed near the base. The welded interior consists of approximately 25% crystal-poor fiamme which have perlitic fracture and approximately 10% crystals (plagioclase > alkali feldspar > clinopyroxene > Fe-Ti oxides > apatite), and approximately 15% volcanic lithics, in a thoroughly devitrified matrix.

In the field, Tvl is distinguished as the lava flows and tuffaceous sediments above Tiw and below Tis; however, the character of Tvl changes dramatically along the extent of its exposure. In the region of Hart Canyon, it consists of distinctive porphyritic pilotaxitic basaltic trachyandesitic lava flow with abundant (25-30%) plagioclase laths up to 2.5 cm long in a microcrystalline hyalopilitic groundmass of plagioclase > Fe-Ti oxides > clinopyroxene > brown clay minerals replacing glass.

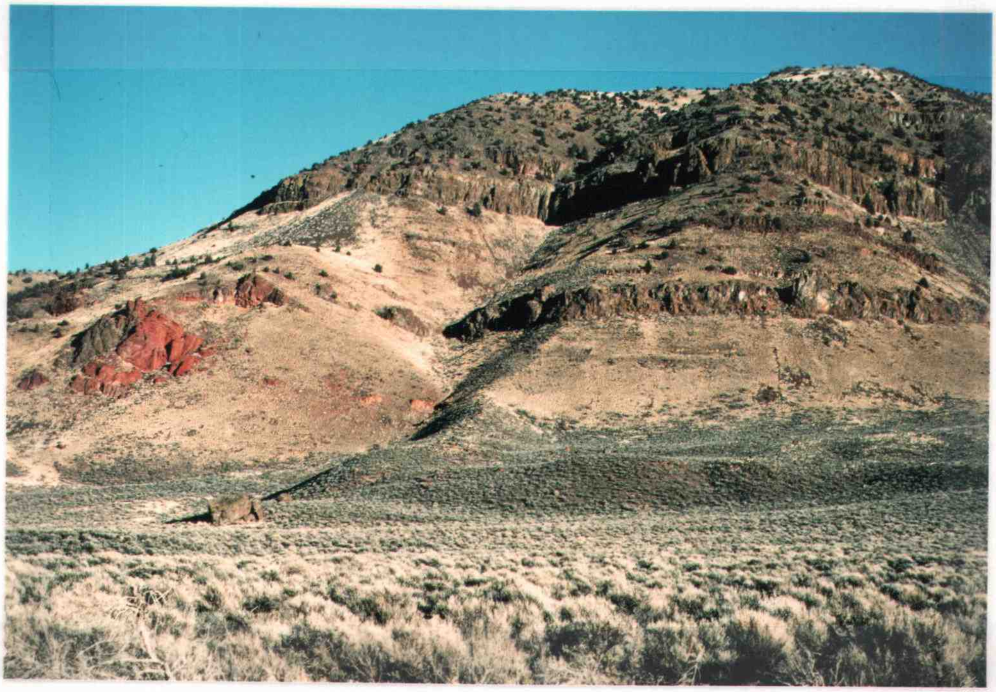

Figure 8: View of North Mountain section showing one of the buried vent complexes exposed at the base of the section.

Between Juniper and Mulkey Canyons, Tv1 consists of up to 45 m of tuffaceous sediments overlain by aphanitic lava flows. The tuffaceous sediments are generally poorly bedded, locally conglomeratic (especially adjacent to the paleotopographic highs of the vent complexes), with poorly sorted, angular mafic and silicic volcanic clasts up to 15 cm in diameter, in a matrix of coarse sand. The finer-grained sediments are tan to green in color, and may contain fragments of petrified wood, and abundant plagioclase crystals up to 1.5 cm long, which may have been eroded from the plagioclase-rich lava flows of Tv1.

North Mountain lava flows (Tv2, Tv3, Tv4, Tv5)

Map units Tv2, Tv3, Tv4, and Tv5 consist of basaltic trachyandesitic to trachytic lava flows with minor amounts of interlayered unwelded ignimbrite, airfall tuffs and tuffaceous sediments. These units are interlayered with the ignimbrites Tis, Tia, and Tib, which were mapped separately. Because of the difficulties in recognizing individual lava flows within the sequence, Tv2, Tv3, and Tv4 were mapped as groups of lava flows between the more distinctive ignimbrites. Tv5 consists of a group of 6 to 10 thin (1 to 3 m) crystal-poor trachyandesitic lava flows which form a distinctive 60-75 m thick cliff-forming unit at the top of the North Mountain section, and must have been erupted within a very short time interval.

The lava flows of the Hart Mountain trachyandesite suite are dark-gray to black in color and weather to a reddish-brown. Individual flows are as thick as 50 meters. They are usually crystal-poor with only 1-3 volume % phenocrysts. Less abundant crystal-rich lava flows may have up to 15% phenocrysts. Closely spaced, irregular platy jointing is present in nearly all flows, and spheroidal weathering is only present in the more mafic lava flows. The flow tops and bottoms may either be vesicular or brecciated, and a few flows consist entirely of autobrecciated clasts. Vesicles, when present, are usually elongate and may have amygdaloidal fillings of chalcedony, opal, calcite, and/or zeolites (including stilbite). Brecciated flows generally have platy jointed dense interiors, and reddened oxidized massive zones of breccia and scoria along the margins. The thicknesses of the brecciated zones within the flows are variable, and commonly make up most of the lava flow.

Petrographically, the lava flows of the Hart Mountain trachyandesite suite can be divided into five main textural groups: crystal-poor hyalopilitic, crystal-poor intersertal, crystal-poor pilotaxitic, mingled or inclusion-rich, and crystal-rich pilotaxitic lava flows. Intersertal lava flows are the least common. A rough correlation between texture and composition exists: The more silicic (SiO_2 61-66 wt %) lava flows are crystal rich (samples AM-89-74, AM-89-55, AM-89-90), and the basaltic trachyandesitic lava flows are hyalopilitic (AM-89-61, AM-89-43). The chemically analyzed pilotaxitic lava flows (AM-89-65, AM-90-22) are trachyandesitic. The mingled or inclusion-rich lava flows (AM-89-42, AM-89-92, AM-89-60) also have trachyandesitic compositions.

The crystal-rich lava flows include trachytes and trachyandesites and contain 10-20% phenocrysts of plagioclase >> clinopyroxene ≈ olivine > Fe-Ti oxides > apatite, which occur in glomerocrysts and as lone phenocrysts. Plagioclase phenocrysts are subhedral to euhedral 0.2-5.0 mm in size, and commonly have inclusions of the other phases. Plagioclase phenocrysts are oligoclase to andesine (An_{16-33}) in the trachytes, andesine to labradorite (An_{45-50}) in the trachyandesites, and are generally unzoned to weakly normally zoned. Subhedral olivine (?) phenocrysts 0.2-1.0 mm in size have been completely replaced by iddingsite. Pale green slightly pleochroic augite/ferroaugite crystals are subhedral, up to 2.0 mm in size, and are commonly partially replaced by iddingsite. Fe-Ti oxides are up to 0.6 mm in size, and occur commonly as inclusions in the ferromagnesian phases, and, in turn, have abundant apatite inclusions. The pilotaxitic groundmass of the crystal-rich lava flows consists of feldspar microlites (anorthoclase in the trachytes, and anorthoclase to andesine in the trachyandesites) >> Fe-Ti oxides > ferromagnesian minerals > brown alteration material replacing glass > euhedral apatite microphenocrysts.

The mingled or inclusion-rich lava flows exhibit textural and compositional disequilibrium: microphenocrysts (xenocrysts?) of plagioclase and clinopyroxene generally are anhedral, and plagioclase crystals have sieved interiors and/or fritted edges. Plagioclase phenocrysts are normally or reversely zoned. Additionally, the groundmasses of these lava flows are heterogeneous: zones of distinctly different grain sizes appear to result from the incomplete mingling of magmas or the partial incorporation of inclusions within the magma (Figure 9). The composition of feldspar microlites differs among the grain size zones in the groundmass. For example, in AM-89-42, groundmass feldspar in the coarser zones (>0.05 mm) is andesine, whereas, anorthoclase is found in the finer-grained zones.

Crystal-poor lava flows have rare phenocrysts of plagioclase > clinopyroxene ≈ olivine ≈ Fe-Ti oxides 1-2 mm in size, and may have apatite microphenocrysts in the more silicic samples. Groundmasses consist mostly of plagioclase microlites (< 0.5 mm) with interstices occupied by Fe-Ti oxides, clinopyroxene, olivine, brown alteration material, and/or glass. Pilotaxitic texture is more commonly observed than hyalopilitic texture among the crystal poor lava flows.

North Mountain Ignimbrites (Tis, Tia, Tib)

Four ignimbrites are found in the North Mountain section (Figures 5 and 7). These ignimbrites, which are individually as thick as 30 m, have some common characteristics: each consists of a single cooling unit, and is generally lithic- and crystal-rich with mineralogy similar to that found in the

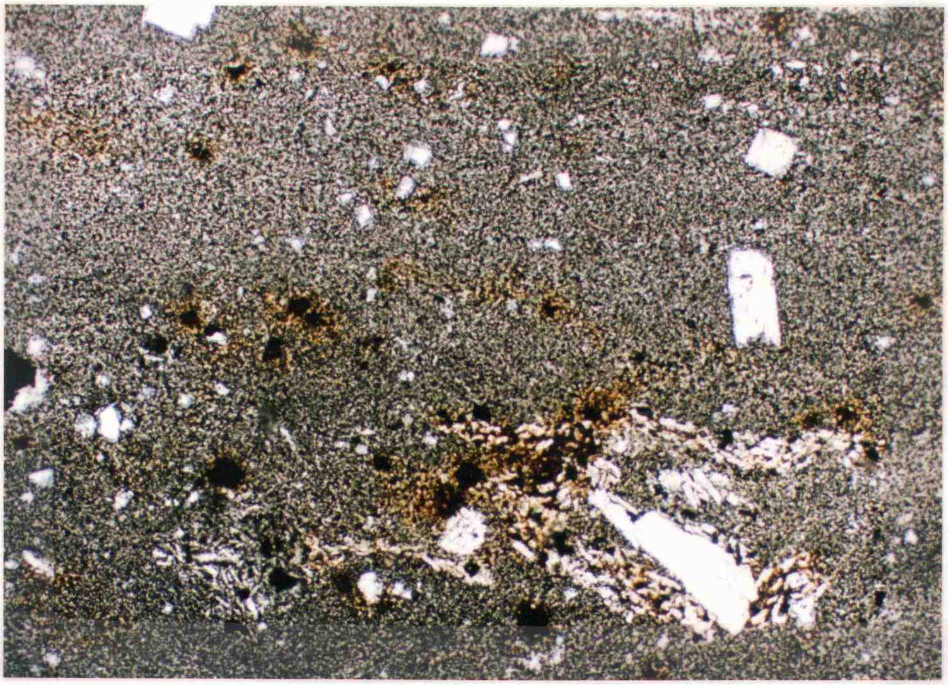

Figure 9: Photomicrograph of sample AM-89-42 showing mingled texture and anhedral plagioclase crystals. The field of view equals 6.7 mm.

crystal-rich lava flows. Abundant lithic fragments in these ignimbrites have textures and compositions similar to those found in the lava flows of the Hart Mountain trachyandesite suite. The abundance (15-40%) of these large (as large as 10 cm) lithic fragments supports the conclusion that these ignimbrites are near vent deposits which were erupted from the Hart Mountain volcanic complex.

The lowest exposed ignimbrite Tiw is moderately welded with phenocrysts of plagioclase > alkali feldspar > clinopyroxene > Fe-Ti oxides > apatite.

Tis is exposed above the lava flows and tuffaceous sediments of Tvl between Juniper and DeGarmo Canyons, and between Potter and Hart Canyons. It is a poorly to moderately welded, vapor-phase altered, ignimbrite, is 20-25 m thick, and is generally completely devitrified. Sample AM-89-75 contains 15-20% angular volcanic lithic fragments as large as 3 cm in diameter, approximately 5% pumice/fiamme fragments as large as 4 cm long, which may weather out due to vapor phase alteration, and approximately 5% crystals of andesine plagioclase and augite 1-2 mm in size. Devitrification of the matrix has partially to completely destroyed the glass shard structure. Fiamme sample AM-89-81 was collected near the base and consists of slightly hydrated obsidian containing approximately 2% plagioclase phenocrysts up to 3 mm in size.

Tia is a distinctive cliff-former within the North Mountain section, with a total thickness of 25-30 m, and is strongly compositionally (peralkaline rhyolite to trachyte) and texturally zoned. At the base, a distinctive lithic-rich zone may be exposed which contains up to 40% rounded volcanic lithics which decrease in size and number upsection. A light tan devitrified partially welded rhyolitic zone up to 6 m thick contains 5-10% subrounded lithics mostly <1 cm in diameter, 25-30% fiamme which contain 1-2 mm euhedral phenocrysts, and 10-15% crystals of sanidine and anorthoclase >> green ferrohedenbergite > quartz. The densely welded vitric zone (AM-89-83) contains 10-15% subrounded lithic fragments mostly < 1 cm, but as large as 5 cm, 15-20% crystals of plagioclase (An_{20-28}) >> anorthoclase >> augite > Fe-Ti oxides > ferrohedenbergite, and 10-12% fiamme which contain 2-4% sieved subhedral plagioclase phenocrysts. Microprobe analyses of glass from sample AM-89-83 yield a trachytic composition (Table 1). The red vapor-phase altered unwelded to poorly welded top is as thick as 18 m and contains approximately 25% lithics as large as 10 cm in diameter.

Tib is exposed throughout the North Mountain section. It may actually consist of more than one ignimbrite in nearly the same stratigraphic position, or a single strongly zoned ignimbrite. Samples collected near Deep Canyon were generally more crystal rich (20%) than samples collected elsewhere (7-20%). Tib was mapped as a single unit because of its distinctive stratigraphic position beneath the thin cliff-forming lava flows of Tv5, and because the strong textural zonation made definite correlation of samples collected in different locations difficult. It is 18-20 m thick, and moderately to densely welded. The base is generally gray in color, but may be pink if it is devitrified. The base contains 8-10% angular lithic fragments as large as 5 mm in size, 5-10% round fiamme or cognate glass lithic fragments, and 10-12% crystals of plagioclase >> augite > sanidine and anorthoclase > Fe-Ti oxides. Fiamme sample AM-90-02 is slightly hydrated and contains approximately 4% plagioclase crystals as large as 3 mm in size. The densely welded interior is distinctly cliff-forming and contains <30% fiamme as large as 2 cm long, 10-12% lithics as large as 1 cm in size, and 7-12% crystals of plagioclase >> augite > sanidine and anorthoclase > Fe-Ti oxides. The top of the unit has undergone vapor phase alteration.

Table 1: Microprobe analysis of glass in ignimbrite AM-89-83 (Tia).

	Point 1	Point 2	Point 3
wt %			
SiO_2	66.74	66.38	66.43
Al_2O_3	15.36	16.18	15.14
TiO_2	0.43	0.42	0.48
FeO*	3.61	3.66	3.68
MnO	0.20	0.14	0.15
CaO	1.22	1.68	1.30
BaO	0.08	0.13	0.04
MgO	0.40	0.52	0.40
K_2O	5.10	2.77	5.01
Na_2O	4.32	6.88	4.48
P_2O_5	0.11	0.04	0.09
Total	97.56	98.79	97.20

Analysis by Rick Weingarz. FeO* is total iron. Variation in Na_2O and K_2O likely results from hydration.

Hart Lake Section (Thl)

The Hart Lake section is exposed from Deep Canyon to the southern boundary of the field area. Because it is composed of a greater proportion of less resistant tuffs, the Hart Lake section is not as well exposed as the North Mountain section.

At least five ignimbrites and minor amounts of tuffaceous sediment are found in the Hart Lake section. These ignimbrites are generally altered by vapor phase and/or secondary alteration, poorly to moderately welded, plagioclase crystal rich, 10-20 m thick, and generally have significantly fewer lithics than those of the North Mountain section. Detailed stratigraphy and petrography (Figure 7) failed to definitively correlate any ignimbrites in the North Mountain and Hart Lake sections, although strong compositional and textural zoning in many of the flows makes correlation potentially feasible with further sampling and petrography.

Most lava flows of the Hart Lake section are 5 m thick but one crystal-poor flow is approximately 30 m thick. These lava flows have commonly undergone secondary alteration.

WARNER PEAK RHYOLITE

Most of the exposed rocks of the Warner Peak rhyolite lie east of the field area (Figure 2), in an area of irregular topographic highs (T36S, R26E), and at Warner Peak (T36S, R25E, section 11). Both areas appear to be remnants of the central vent complex (Larson, 1965; Walker and Repenning, 1965; Walker and Swanson, 1968b). The vent rocks are mostly flow-banded porphyritic trachytes and peralkaline rhyolites found in intrusive and exogenous domes and associated lava flows (Walker and Swanson, 1968b). Other irregularly shaped dikes, sills, and shallow intrusions of Warner Peak rhyolite are found in the field area, especially between DeGarmo and Deep Canyons (T36S, R25E, Section 16), where they invade the

Hart Mountain trachyandesite suite and the lava flows and tuffs of the Warner Peak rhyolite.

On the west side of the field area, rocks of the Warner Peak rhyolite are exposed overlying the Hart Mountain trachyandesite suite. The Warner Peak tuff, at the base of the section, was mapped separately from the overlying lava flows and tuffs. Dikes, sills, and shallow intrusions of Warner Peak rhyolite were also mapped. On the east side of the field area, closer to the main vent complex, it was possible to map the trachytic lava flows and tuffs separately from the rhyolitic lava flows. In general, the rocks of the Warner Peak rhyolite on the west side of the field area have undergone less secondary alteration, and therefore, the petrologic study focuses on the rocks there.

In the following section, field and petrographic characteristics of the Warner Peak tuff (Twpt), Warner Peak lava flows and tuffs undivided (Twpu), Warner Peak intrusions (Twpi), and the trachytic and rhyolitic lava flows (Twpa and Twpr) will be described.

Warner Peak tuff (Twpt)

The Warner Peak tuff is recognizable in the field as a 60 to 120-m-thick white to green layer of ignimbrite, airfall tuff, and tuffaceous sediment at the base of the Warner Peak rhyolite. At the top of the North Mountain section, it consists mostly of poorly sorted, poorly bedded tuffaceous sediments with thin trachyandesitic lava flows locally interbedded near the top of the unit. Near DeGarmo Canyon, a 5-m-thick, light gray, incipiently welded ignimbrite (AM-89-33) is found at the base of the unit. The tuffaceous sediments of Twpt at the top of the North Mountain section are locally conglomeratic with angular volcanic clasts as large as 15 cm in diameter in matrix support. Reverse grading and poorly developed cross bedding is present in some outcrops.

Above the Hart Lake section, the Warner Peak tuff consists of three unwelded ignimbrites 10-25 m thick with a few meters of bedded tuffaceous sediments exposed at the base of the unit. All three of these ignimbrites have undergone extensive secondary alteration, and are megascopically similar to one another. They are lithic-rich, with approximately 5% feldspar crystals in a matrix of thoroughly devitrified glass shards.

AM-89-33 is a thoroughly devitrified ignimbrite which has undergone some vapor phase alteration. It contains approximately 30% pumice fragments as large as 2 cm in diameter which contain less than 1% subhedral alkali feldspar >> green pleochroic pyroxene, 1-2 mm in size. The matrix contains approximately 5 percent feldspar >> green pyroxene crystals, 5% mafic to intermediate volcanic lithics as large as 1 cm in size, and 60% devitrified glass shards.

Warner Peak lava flows and tuffs undivided (Twpu)

The Warner Peak rhyolite on the west side of the field area consists mostly of a sequence of peralkaline rhyolitic lava flows 30-60 m thick with minor amounts of interlayered trachytic lava flows, ignimbrites, lahar deposits, and tuffaceous sediments. Near Juniper Canyon up to 60 m of slightly reworked tuffaceous sediments are included in this unit. This unit has a total thickness of 150-370 m, and is locally uncomformably overlain by the Steens Basalt.

The peralkaline rhyolite lava flows (AM-90-27, AM-90-34, AM-90-35) are mostly green in color, porphyritic and glomeroporhyritic, and may be crudely columnarly jointed. They contain approximately 8-10% crystals of subhedral anorthoclase > sodic sanidine as large as 5 mm in size >> euhedral green ferrohedenbergite as large as 0.5 mm in size > pleochroic blue to green to brown arfvedsonite > Fe-Ti oxides. Weakly pleochroic brown amphibole with compositions ranging between richterite and eckermanite is present in some flows and may be partially replaced by arfvedsonite. The holocrystalline groundmasses are microporhyritic or pilotaxitic with the interstices between feldspar microlites filled by the mafic phases.

Interlayered porphyritic trachytic lava flows (AM-90-26, AM-90-36) are generally thinner than the rhyolitic flows, and have mineralogies and textures very similar to the crystal-rich trachytes in the Hart Mountain trachyandesite suite.

At least one ignimbrite is found in this unit near Hart Canyon. It is moderately to strongly welded and consists of 10-15% fiamme, 2-3% lithic fragments > 1 cm, and 5-8% crystals of anorthoclase > sanidine > green ferrohedenbergite > Fe-Ti oxides.

Warner Peak trachytic and rhyolitic lava flows (Twpa and Twpr)

Up to 330 m of trachytic lava flows and ignimbrites (Twpa) are exposed on the east side of the field area, and are overlain by rhyolitic lava flows of the Warner Peak rhyolite (Twpr) or unconformably overlain by the Steens Basalt (Tsb). The trachytic lava flows are generally crystal rich with 20% plagioclase phenocrysts as large as 1 cm in length in a black aphanitic groundmass. Some flows are highly vesicular. The rhyolitic lava flows generally have textures and mineralogies identical to the peralkaline rhyolites found in Twpu, however, some lahar deposits are found within Twpr.

Warner Peak rhyolitic intrusions (Twpi)

Intrusions of Warner Peak rhyolite (AM-89-14, AM-89-40/41, AM-89-93) are most common in the central part of the field area. These intrusions, which include dikes and sills, have very irregular shapes and appear to be very shallow based on their textural similarity to the volcanic peralkaline rhyolites, with which they share mineralogical characteristics. They generally have vitrophyric margins or consist entirely of vitrophyre. These intrusions also appear to have been forceful: many wall rock inclusions are found along margins, some margins have well developed slickensides, and the intrusions commonly invade the Warner Peak tuff, perhaps because it was less resistant to intrusion. In the field, these cliff-forming intrusions display well developed columnar jointing.

STEENS BASALT (Tsb)

The Steens Basalt exposed at Hart Mountain is composed of a sequence of medium gray, thin (averaging 3 m), diktytaxitic, and ophitic lava flows containing plagioclase >> clinopyroxene > olivine > Fe-Ti oxides (Larson, 1965). Some flows are porphyritic and contain abundant (40%) plagioclase laths as large as 5 cm in length. These flows may be highly vesicular and contain pipe vesicles. Thinly spaced platy jointing is common, but columnar jointing is generally lacking. Within the field area the Steens Basalt reaches a maximum thickness of 250 m, but immediately north of the field area up to 650 m of Steens Basalts are exposed along Poker Jim Ridge (Larson, 1965; Walker and Repenning, 1965).

The uppermost Steens Basalt flow in the northern end (T34S, R25E, section 36, SE 1/4) of the field area was determined by K-Ar methods to be 15.04±0.79 Ma by Hart and Mertzman (1982). Mankinen et al. (1987) state that all aspects, including lithology, stratigraphy, geochemistry, radiometric age, and magnetostratigraphy, of the sequence of Steens Basalts in the Hart Mountain region indicate that it is equivalent to the section exposed at Steens Mountain.

PLUSH TUFF (Tpt)

The Plush tuff was informally designated by Larson (1965) as a late Miocene series of rhyodacitic to rhyolitic tuffs and tuffaceous sediments found between the Steens Basalt and the overlying upper basalt (Tub). In the field area, the Plush tuff has a maximum thickness of 20 m. Where the Plush tuff is not exposed it was not possible to distinguish the flows of the Steens Basalt and the overlying upper basalt, so they were mapped as Tertiary basalts undivided (Tbu). As much as 400 m of undivided Tertiary basalts were mapped in the southern part of the field area.

The Plush tuff is orange to light tan to white, is poorly bedded, and mostly consists of friable tuffaceous sandstone deposited under fluvial and lacustrine conditions (Larson, 1965). The Plush tuff obtains a maximum thickness of 90 m on the west side of Warner Valley (Larson, 1965), and pinches out near paleotopographic highs, such as the edifice of the Hart Mountain volcanic complex. Beaty's Butte seems to have been a volcanic source for at least some of the tuffaceous material within the Plush tuff (Larson, 1965).

UPPER BASALT (HAOT, Tub)

The upper basalt exposed at Hart Mountain is chemically classified as low potassium high-alumina olivine tholeiite (HAOT) by Hart and Carlson (1982), Hart and Mertzman (1982), and Hart et al. (1984). HAOT is a chemical type of magma erupted throughout the northwestern Basin and Range since 11 Ma (Hart et al., 1984; Hart and Carlson, 1987). HAOT was most commonly erupted in small volumes from fissures, but also formed small buttes, cones, and craters (Hart et al., 1984). Important centers of HAOT volcanism were in northeastern California, the Warner Mountains, northeast of Winnemucca, Nevada, and in the Owyhee Region (Hart et al., 1984). Larson (1965) reported that feeder dikes for HAOT basalts are present at several localities along the west side of Warner Valley. No such dikes were identified in the study area.

In the field area, Tub is medium gray, fine to medium grained, generally diktytaxitic, and contains plagioclase >> clinopyroxene > olivine > Fe-Ti oxides. Maximum thickness is 18 m.

RATTLESNAKE ASH FLOW TUFF (Trt)

The Rattlesnake Ash Flow Tuff is exposed in the northeastern corner of the field area as a beige poorly welded ignimbrite containing 3-5% fiamme, <1% lithic fragments, and <1% crystals of anorthoclase, plagioclase, quartz, and clinopyroxene. It is less than 1 m thick and banks against the horst that makes up the northern end of Hart Mountain.

QUATERNARY DEPOSITS (Qal and Qls)

Quaternary alluvium and colluvium (Qal) and landslide deposits (Qls) cover bedrock in parts of the field area. Alluvium and colluvium are found mostly in canyon bottoms and at the base of the fault escarpments. Landslide deposits are found throughout the field area, but are most common on the western side of the field area which has more relief. These deposits are recognized usually by a break in the slope of the fault escarpment and by their hummocky topography. The largest landslide deposit (T36S, R25E, section 27) in the field area covers an area of approximately 1.5 km.

STRUCTURE

Despite Basin and Range block faulting, and the presence of NW striking faults of the Eugene-Denio fault zone within the field area, the exposed rock units exposed are generally only mildly deformed. Beds throughout most of the field area strike N to NW and dip 3-5° to the east (Figure 10), except where locally deformed by forceful intrusions of Warner Peak rhyolite. Small fault bound blocks within the zone of normal faults which define the east side of the Hart Mountain horst have measured dips as steep as 43° east.

Movement along the NW striking faults initiated prior to movement along the N to NE striking range faults. Faults of the Eugene-Denio zone mostly strike N40° to 50°W (Larson, 1965), and the Eugene-Denio zone itself trends N55° to 60°W (Lawrence, 1976). Faults within the field area trend from

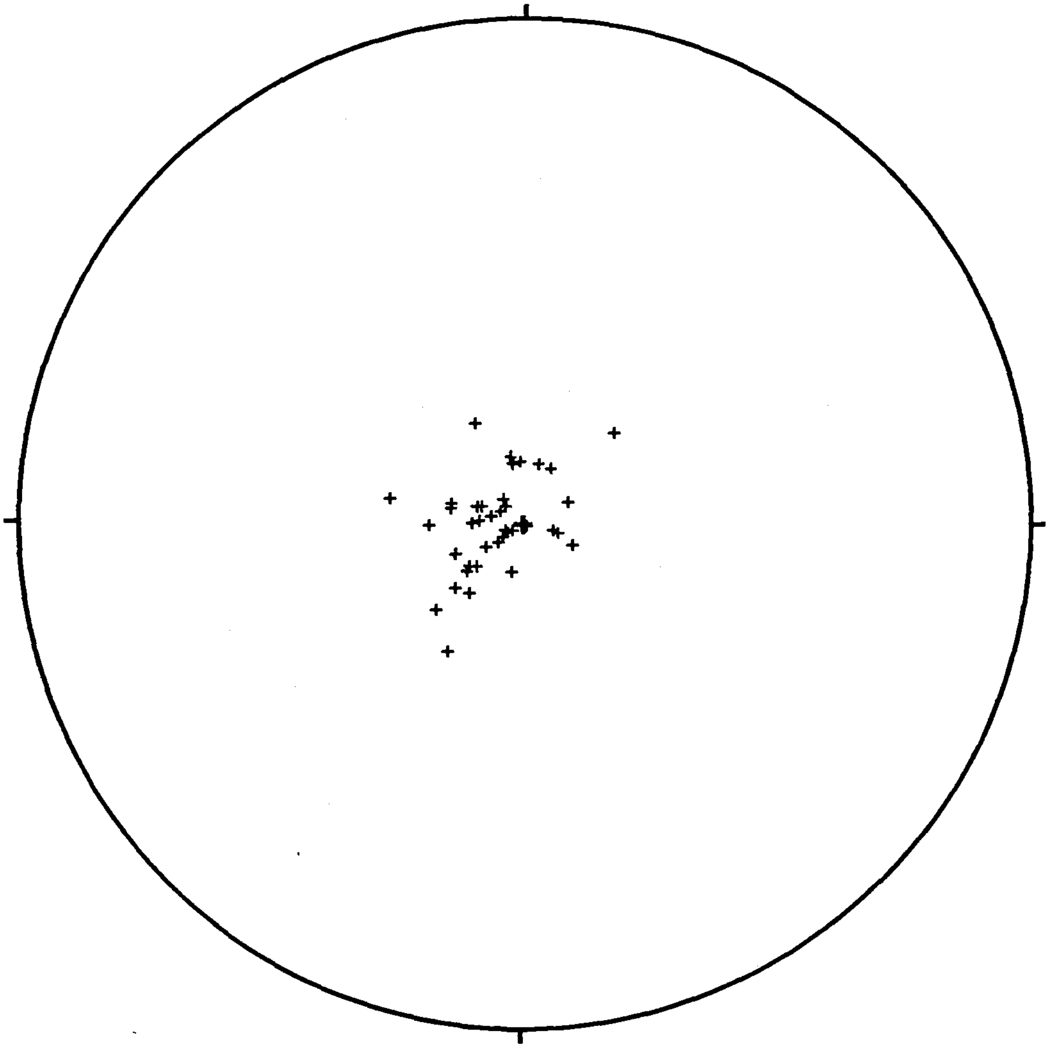

Figure 10: Schmidt equal area projection of poles to eutaxitic foliation in ignimbrites and platy jointing in lava flows in the Hart Mountain volcanic complex. All data points are from the western half of the field area. Some of the scatter in the data may result from eutaxitic foliation and platy jointing not equal to paleohorizontal.

N17° to 60°W. These faults displace rocks of the Hart Mountain volcanic complex, but do not displace the Steens Basalt or younger units in the field area. Thomas (1981) reported that NW-striking faults cut the Steens Basalt in the Coyote Hills. No fault planes of the NW striking faults were exposed in the field area, but Larson (1965) reported near-vertical fault planes where they were exposed in the Plush area.

The earliest movement along the Eugene-Denio zone is generally thought to be late to latest Miocene (Lawrence, 1976). Field evidence at Hart Mountain and at the Coyote Hills suggests that this structural trend was established by late Oligocene. Thomas (1981) reports a NW-trending alignment of volcanic plugs of the 27-Ma Coyote Hills rhyolite. Dikes of the Hart Mountain trachyandesite suite have NW strikes roughly in agreement with the trend of the Eugene-Denio zone. However, the dikes, sills, and shallow intrusions of the Warner Peak rhyolite have irregular orientations and shapes.

The western range-front fault at Hart Mountain has a minimum displacement of roughly 900 m in the field area, as reflected in the relief difference between the crest of Hart Mountain and the Warner Valley. If basin fill in the Warner Valley is considered, displacement could be two to three times as much. The set of normal faults which define the east side of the Hart Mountain horst has a total minimum displacement of 300 m in the field area.

No fault planes of the range faults are exposed in the field area because they are covered by talus and landslide deposits. In the Plush area, Larson (1965) reports a 72° dip to the east on an exposed fault plane on the west side of Warner Valley near Adel. Displacement along the range faults at Hart Mountain began after the deposition of the HAOT Upper Basalt rim capping lava flow (6.9±0.6 Ma; Hart and Mertzman, 1982). It appears that the Rattlesnake Ash Flow Tuff flowed against the Hart Mountain horst in the eastern portion of the field area, suggesting that movement along those faults began at least in part before deposition of the Rattlesnake Ash Flow Tuff (7.2 Ma). No Pleistocene-Holocene fault scarps are found in the Hart Mountain-Warner Valley region (Craven, 1988); however, 13 m of displacement of Pleistocene shorelines in Warner Valley are interpreted to be part of regional warping (Craven, 1988). In 1968, a swarm of 10 earthquakes up to 5.1 in magnitude on the Richter Scale occurred south of Hart Mountain near Adel in the Warner Valley. First motion studies of these earthquakes indicate mostly normal displacement on north-trending faults (Couch and Johnson, 1968).

The amount of regional extension in the Hart Mountain area is small. Assuming rotational planar normal faulting, and 60-70° dips of fault planes and 3-5° dips of bedding, calculated extension is less than 10% using the method of Thompson (1960). Decreasing dip of the fault plane to 45°, and increasing dip of bedding to 8° (the dip of Poker Jim Ridge north of the field area, Larson, 1965), increases estimated extension to 13%.

Chapter Three: Geochemistry

AGE DETERMINATIONS

Single crystal ^{40}Ar-^{39}Ar age determinations were performed on two samples from the Hart Mountain volcanic complex by Alan Deino, Institute of Human Origins, Berkeley, CA. A plagioclase (150-300 mm) separate was prepared from sample AM-90-29, a plagioclase-rich (25-30% phenocrysts) basaltic trachyandesite collected from map unit Tvl in Hart Canyon. Sodic sanidine (150-300 mm) was separated from a pantellerite lava flow (AM-90-34) from map unit Twpu near Deep Canyon approximately 50 meters below the base of the Steens Basalt. These samples yielded dates of 26.48±0.13 and 26.33±0.04 Ma respectively (Table 2), which are standard weighted averages of 15 determinations on crystals from AM-90-29 and 8 determinations from AM-90-34. Errors are one sigma standard errors of the weighted mean.

These data are in accordance with previously published K-Ar dates of 28.2±0.8 to 25.6±0.8 Ma for anorthoclase separates from peralkaline rhyolites from the Warner Peak rhyolite (Noble et al., 1974; and Fiebelkorn et al., 1983).

The greater analytical precision of the Ar-Ar dates provide a tighter restraint on the timing of volcanism at Hart Mountain. The two samples dated spanned nearly the complete stratigraphic range of the Hart Mountain volcanic complex exposed on the western fault escarpment and indicate rapid eruption of the whole volcanic pile.

Table 2: ^{40}Ar-^{39}Ar analytical data, Hart Mountain, southeastern Oregon.

Lab ID#	Ca/K	$^{36}Ar/^{39}Ar$	$\%(^{36}Ar/^{39}Ar)_{Ca}$	$^{40}Ar^{*}/^{39}Ar$	^{40}Ar (Moles × 10^{14})	$\%^{40}Ar^{*}$	Age (Ma) ±1σ
Sample AM90-29:	Plagioclase, $J = 0.0003522 \pm 0.0000008$						
4108-01	17.75	0.0079	29.7	41.72	2.8	96.2	26.32 ± 0.22
4108-02	20.68	0.0169	16.1	42.10	1.3	90.9	26.56 ± 0.53
4108-03	19.86	0.0106	24.7	41.54	1.9	94.6	26.20 ± 0.31
4108-04	22.95	0.0161	18.8	41.25	1.6	91.4	26.02 ± 0.38
4108-05	19.15	0.0206	12.3	41.84	1.3	88.6	26.39 ± 0.46
4108-06	13.54	0.0132	13.5	40.69	1.6	92.3	25.67 ± 0.36
4108-08	21.54	0.0236	12.0	42.24	1.8	87.2	26.64 ± 0.33
4108-09	17.65	0.0164	14.1	42.84	2.6	91.1	27.02 ± 0.25
					Wtd. Ave.=		26.41 ± 0.16
Sample AM90-29:	Plagioclase, $J = 0.002096 \pm 0.000004$						
4754-02	18.34	0.0049	49.2	7.029	1.2	90.4	26.39 ± 0.34
4754-03	20.53	0.0041	65.2	7.094	1.0	94.3	26.63 ± 0.35
4754-09	23.52	0.0061	50.8	7.154	0.4	88.9	26.85 ± 0.81
4754-10	17.30	0.0029	78.4	7.169	0.7	97.4	26.91 ± 0.47
4754-11	18.54	0.0098	25.0	7.067	2.5	76.4	26.53 ± 0.23
4754-12	17.31	0.0036	63.8	6.956	0.7	94.8	26.11 ± 0.48
4754-13	19.31	0.0039	65.7	7.119	0.7	94.7	26.72 ± 0.49
					Wtd. Ave.=		26.54 ± 0.10
Sample AM-90-34:	Sanidine, $J = 0.01526 \pm 0.00002$						
4004-01	0.0207	0.00004	6.9	0.9657	27.8	98.8	26.39 ± 0.07
4004-02	0.0255	0.00003	11.4	0.9661	31.6	99.1	26.40 ± 0.07
4004-03	0.0264	0.00004	8.3	0.9663	25.2	98.8	26.41 ± 0.07
4004-04	0.0196	0.00007	3.9	0.9619	11.5	98.0	26.29 ± 0.08
4004-05	0.0210	0.00009	3.2	0.9611	14.9	97.4	26.27 ± 0.08
4004-06	0.0214	0.00004	8.0	0.9565	24.0	98.9	26.14 ± 0.07
4004-07	0.0225	0.00007	4.5	0.9628	9.7	98.0	26.31 ± 0.09
4004-08	0.0208	0.00002	12.8	0.9664	21.8	99.3	26.41 ± 0.07
					Wtd. Ave.=		26.33 ± 0.04
Omitted due to low $^{40}Ar^{*}$ content:							
4108-07	19.70	0.0774	3.4	44.91	2.6	66.9	28.31 ± 0.48
4754-01	18.12	0.0142	16.9	7.073	2.7	66.9	26.55 ± 0.29

Notes: Errors in age quoted for individual runs are 1σ analytical uncertainty. Weighted averages are calculated using the inverse variance as the weighting factor (Taylor, 1982), while errors in the weighted averages are 1σ standard error of the mean (Samson and Alexander, 1987). Ca/K is calculated from $^{37}Ar/^{39}Ar$ using a multiplier of 1.96. $^{40}Ar^{*}$ refers to radiogenic argon. 'Moles ^{40}Ar' refers to the estimated total moles of ^{40}Ar released during fusion based on spectrometer sensitivity considerations. $\lambda = 5.543 \times 10^{-10}\ y^{-1}$. Isotopic interference corrections: $(^{36}Ar/^{37}Ar)_{Ca} = 2.58 \times 10^{-4} \pm 6 \times 10^{-6}$, $(^{39}Ar/^{37}Ar)_{Ca} = 6.7 \times 10^{-4} \pm 3 \times 10^{-5}$, $(^{40}Ar/^{39}Ar)_{K} = 8 \times 10^{-4} \pm 7 \times 10^{-4}$.

MINERAL CHEMISTRY

Electron microprobe analysis was used to obtain mineral compositions of feldspar, pyroxene, olivine, and amphibole from representative samples from the Hart Mountain volcanic complex. Analyses of cores and rims of phenocrysts, and of groundmass phases were performed where possible. These data were used to document mineral composition and zonation, and to provide mineral compositions for petrogenetic modeling.

Analyses were done using the Oregon State University Cameca SX-50 electron microprobe operating with standard beam conditions (15 kV acceleration voltage, 20 nA beam current, and a focused beam diameter of ~5 microns). Calibration used mineral standards, and were checked by replicate analyses of standards at the beginning and the end of each analytical session. Mineral compositions were calculated with standard Cameca software.

Nine samples encompassing the complete compositional spectrum of the Hart Mountain volcanic complex, including three peralkaline rhyolites of the Warner Peak rhyolite, were analyzed. These samples include AM-89-70 (equivalent to AM-90-23; trachybasalt, Tvc); AM-89-61 (basaltic trachyandesite, Tv3), AM-89-42 (mingled trachyandesite, Thl), AM-89-74 (crystal-rich trachyandesite, Tv1), AM-89-90 (trachyte, Tv3), AM-89-83 (trachytic ignimbrite, Tia), AM-90-34 (pantellerite lava flow, Twpu), and AM-89-14 and AM-89-93 (comendite intrusions, Twpi). Complete petrographic descriptions are in Appendix I. Tables 3 and 4 contain summaries of the modal mineralogies for the Hart Mountain trachyandesite suite and the Warner Peak rhyolite, respectively.

FELDSPAR

Feldspar compositions (Tables 5 and 6; Figures 11 and 12) range from bytownite to sodic sanidine in rocks from the Hart Mountain volcanic complex. Plagioclase is ubiquitous as phenocrysts in the Hart Mountain trachyandesite suite, and is usually the most abundant phase. Anorthoclase occurs in the

Table 3: Mineralogy of selected samples from the Hart Mountain trachyandesite suite.

	%	phenocrysts and microphenocrysts						groundmass			
Sample	phenos	feldspar	cpx	olivine	Fe-Ti ox	apatite	proportions	feldspar	cpx+ol	Fe-Ti ox	other
AM-89-70	10-15%	An81-52	Aug+Di	Fo85-65	X		plg>ol>cpx>ox	55-60%	15-25%	20-25%	
AM-89-61	<1%	An50-35	Augite	X	X		plg>ol≈cpx>ox	~70%	~10%	~10%	~10%
AM-89-74	10-12%	An50-45	Augite	idd.	X	X	plg>>ol>cpx>ox>ap	~55%	1-3%	15-20%	25-30%
AM-89-90	~20%	An39-15	Aug+FA	idd.	X	X	plg>>cpx≈ol>ox	~70%	~5%	10-15%	10-15%

Notes: Aug=augite; Di=diopside; FA=ferroaugite; idd.=olivine replaced by iddingsite; plg=plagioclase; ol=olivine; cpx=clinopyroxene, ox=Fe-Ti oxides, ap=apatite. X designates the presence of a phase. "Other" includes glass and/or brown alteration material in the groundmass.

Table 4: Mineralogy of the peralkaline rhyolites.

	Rock	%	phenocrysts				groundmass					
Sample	Type	phenos	feldspar	cpx	amph	Fe-Ti ox	feldspar	cpx	amph	Fe-Ti ox	quartz	texture
AM-90-27	L	~3%	~3%				50-60%	20%		X		microporphrytic
AM-89-40/41	VI	8-10%	8-10%				5-8%	10-15%		X		microporphyritic
AM-90-35	L	~9%	~8%	X	X	X	~80%		X	X		pilotaxitic
AM-90-34*	L	~8%	~8%		X	X	~60%	X	~40%		X	pilotaxitic
AM-89-14*	I	12-15%	12-15%	X		X	~45%	X		X		microporphyritic
AM-89-93*	I	20-25%	~20%	~2%	X	X	~80%	~7%	~3%	~10%	X	intergranular

Notes: Rock types: L=lava; VI=vitric magrin of intrusion; I=intrusion. Most alkali feldspar phenocrysts are anorthoclase; clinopyroxene phenocryst range in composition from hedenbergite to sodic ferrohedenbergite. X=present in trace or minor amounts. * designates samples used for microprobe analyses. Sample AM-90-27 also contains trace amounts of a completely altered mafic phase as a phenocryst.

Table 5: Representative analyses of feldspar crystals from the Hart Mountain trachyandesite.

Sample #	AM-89-70		AM-89-70		AM-89-70		AM-89-70		AM-89-61		AM-89-61	
	rim	core	rim	core	rim	core	grdms	grdms	grdms	grdms	grdms	grdms
SiO2	49.95	47.37	54.67	50.83	51.99	50.74	51.82	53.73	57.91	58.52	55.82	60.42
Al2O3	31.15	33.40	28.40	31.56	30.04	31.12	29.83	28.78	26.36	26.06	27.90	24.32
MgO	0.05	0.03	0.02	0.02	0.05	0.12	0.03	0.02	0.05	0.02	0.06	0.02
CaO	14.29	16.60	10.63	14.14	12.91	14.05	12.84	11.13	8.31	7.78	9.71	5.76
FeO*	0.74	0.49	0.85	0.56	0.89	0.58	0.98	0.96	0.70	0.61	0.59	0.56
BaO	0.03	0.00	0.02	0.00	0.06	0.02	0.00	0.05	0.02	0.05	0.03	0.10
Na2O	3.22	2.11	5.07	3.42	4.10	3.54	3.94	4.86	6.19	6.45	5.35	7.34
K2O	0.20	0.07	0.47	0.18	0.29	0.16	0.29	0.44	0.61	0.77	0.46	0.97
Total	99.63	100.08	100.13	100.71	100.33	100.31	99.74	99.98	100.15	100.26	99.92	99.49
Or	1.20	0.43	2.77	1.02	1.67	0.91	1.72	2.59	3.60	4.52	2.76	5.74
Ab	28.63	18.62	45.07	30.15	35.91	31.01	35.10	42.99	55.36	57.30	48.55	65.75
An	70.17	80.94	52.16	68.83	62.42	68.08	63.18	54.43	41.04	38.19	48.70	28.51

Sample #	AM-89-61		AM-89-42		AM-89-42		AM-89-42		AM-89-42		AM-89-74	
	grdms	grdms	rim	core	rim	core	rim	core	grdms	grdms	rim	core
SiO2	59.02	56.24	55.79	53.80	55.38	57.70	61.44	60.96	61.32	64.54	57.06	56.55
Al2O3	25.83	26.84	27.98	29.81	28.31	27.07	25.11	24.64	24.13	21.68	27.94	27.43
MgO	0.01	0.07	0.01	0.03	0.01	0.02	0.02	0.00	0.07	0.04	0.04	0.05
CaO	7.03	9.03	10.04	12.04	10.34	8.76	6.28	6.23	5.60	2.89	9.52	9.40
FeO*	0.80	0.82	0.64	0.52	0.53	0.38	0.53	0.49	0.75	0.73	0.42	0.46
BaO	0.09	0.04	0.08	0.04	0.05	0.05	0.08	0.11	0.12	0.09	0.05	0.07
Na2O	6.54	5.67	5.47	4.55	5.37	6.22	7.08	7.14	7.38	6.77	5.60	5.79
K2O	0.87	0.56	0.49	0.36	0.43	0.50	0.94	0.99	1.13	4.06	0.51	0.44
Total	100.19	99.28	100.50	101.16	100.43	100.70	101.47	100.56	100.50	100.80	101.13	100.17
Or	5.20	3.32	2.85	2.09	2.51	2.90	5.52	5.78	6.62	24.21	2.97	2.56
Ab	59.49	51.44	48.24	39.79	47.26	54.59	63.40	63.56	65.78	61.30	50.04	51.36
An	35.31	45.24	48.91	58.13	50.23	42.50	31.08	30.66	27.60	14.49	46.99	46.08

Mol percent orthoclase (Or), albite (Ab), and anorthite (An) calculated with standard CAMECA software by cation proportion of K, Na, and Ca normalized to 100%. Vertical lines separate analyses of individual crystals.

Table 5, continued.

Sample #	AM-89-74		AM-89-74		AM-89-74		AM-89-74		AM-89-90		AM-89-90	
	rim	core	rim	core	grdms	grdms	grdms	grdms	rim	core	rim	core
SiO2	56.33	55.28	56.15	55.78	58.13	62.78	65.04	65.34	61.86	61.39	62.74	60.64
Al2O3	27.63	28.19	27.57	28.27	26.07	22.20	20.98	20.30	22.68	23.69	21.94	23.40
MgO	0.01	0.02	0.02	0.04	0.00	0.04	0.00	0.00	0.00	0.01	0.02	0.00
CaO	9.53	10.16	9.66	10.03	8.02	4.07	2.39	1.37	4.14	4.78	3.21	4.87
FeO*	0.58	0.46	0.56	0.42	0.80	0.58	0.41	0.51	0.30	0.29	0.57	0.32
BaO	0.07	0.03	0.05	0.05	0.15	0.17	0.16	0.15	0.18	0.12	0.20	0.15
Na2O	5.63	5.32	5.62	5.49	6.42	7.53	7.37	6.61	8.39	7.98	8.23	8.03
K2O	0.51	0.42	0.43	0.40	0.60	2.07	4.05	5.73	1.27	0.96	1.78	0.89
Total	100.28	99.88	100.05	100.47	100.20	99.45	100.40	100.00	98.82	99.22	98.69	98.30
Or	2.96	2.44	2.53	2.34	3.50	12.25	23.45	33.87	7.27	5.64	10.50	5.16
Ab	50.13	47.46	49.98	48.58	57.09	67.56	64.93	59.35	72.84	70.89	73.63	71.03
An	46.91	50.10	47.49	49.08	39.42	20.19	11.63	6.79	19.89	23.47	15.87	23.81

Sample #	AM-89-90		AM-89-90		AM-89-90		AM-89-83		AM-89-83		AM-89-83	
	rim	core	rim	core	grdms	grdms	rim	core	rim	core	rim	core
SiO2	63.47	60.14	64.65	58.49	64.52	64.50	59.72	60.61	61.13	62.61	66.80	66.18
Al2O3	23.22	24.67	19.96	24.51	20.38	21.30	24.81	24.66	23.32	22.90	19.50	20.16
MgO	0.02	0.02	0.00	0.00	0.00	0.00	0.01	0.01	0.12	0.04	0.00	0.00
CaO	3.98	5.96	0.90	6.39	1.40	2.32	5.53	5.80	5.01	4.02	0.14	0.22
FeO*	0.42	0.36	0.47	0.36	0.87	0.56	0.31	0.38	0.83	0.58	0.22	0.17
BaO	0.15	0.11	0.17	0.09	0.46	0.30	0.16	0.10	0.15	0.12	0.08	0.16
Na2O	8.11	7.52	8.04	7.39	8.41	8.44	7.53	7.49	7.62	8.10	6.74	7.06
K2O	1.16	0.74	4.31	0.72	3.31	2.25	0.81	0.84	0.87	0.84	6.43	5.94
Total	100.52	99.52	98.50	97.96	99.34	99.67	98.89	99.89	99.04	99.21	99.91	99.91
Or	6.88	4.29	24.95	4.18	19.16	13.21	4.79	4.92	5.24	5.08	38.28	35.25
Ab	73.26	66.56	70.67	64.82	74.04	75.36	67.72	66.61	69.48	74.49	61.05	63.64
An	19.86	29.15	4.38	31.00	6.80	11.43	27.49	28.48	25.27	20.43	0.68	1.11

Table 6: Representative analyses of feldspar crystals from the Warner Peak rhyolite.

Sample #	AM-89-14		AM-89-14		AM-89-14		AM-89-14		AM-89-93		AM-89-93	
	rim	core	rim	core	rim	core	grdms	grdms	rim	core	rim	core
SiO2	65.98	65.81	66.50	66.01	64.21	64.28	64.92	66.62	67.23	66.63	67.14	67.23
Al2O3	19.36	19.24	18.94	19.36	21.07	20.73	20.16	18.98	19.71	19.44	19.64	19.82
MgO	0.00	0.00	0.01	0.01	0.00	0.00	0.00	0.00	0.00	0.01	0.01	0.00
CaO	0.17	0.15	0.10	0.16	1.63	1.34	0.93	0.03	0.13	0.38	0.05	0.17
FeO*	0.59	0.45	0.71	0.41	0.42	0.31	0.75	0.91	0.40	0.29	0.37	0.24
BaO	0.31	0.20	0.15	0.30	0.91	0.92	0.40	0.11	0.28	0.32	0.18	0.42
Na2O	7.79	7.75	7.56	7.80	8.35	8.36	8.06	7.53	7.83	8.09	7.87	8.07
K2O	4.88	4.79	4.83	4.88	2.29	2.44	3.71	5.13	5.06	4.87	5.03	4.95
Total	99.08	98.40	98.79	98.92	98:88	98.39	98.93	99.31	100.63	100.02	100.29	100.91
Or	28.95	28.71	29.43	28.90	14.01	15.00	22.16	30.89	29.67	27.85	29.54	28.50
Ab	70.21	70.52	70.03	70.32	77.59	78.06	73.18	68.95	69.71	70.34	70.20	70.67
An	0.84	0.77	0.54	0.78	8.40	6.94	4.66	0.15	0.62	1.80	0.26	0.83

Sample #	AM-89-93		AM-89-93		AM-90-34		AM-90-34		AM-90-34		AM-90-34	
	rim	core	grdms	grdms	rim	core	rim	core	rim	core	grdms	grdms
SiO2	67.18	66.88	67.34	66.97	66.97	67.11	67.71	66.58	66.86	66.93	67.28	67.12
Al2O3	19.45	19.57	19.38	19.24	18.79	19.11	18.52	19.30	19.29	18.99	18.61	18.22
MgO	0.00	0.00	0.00	0.00	0.00	0.00	0.00	0.00	0.00	0.00	0.00	0.03
CaO	0.09	0.11	0.04	0.00	0.05	0.09	0.02	0.12	0.07	0.05	0.02	0.00
FeO*	0.41	0.38	0.61	0.63	0.81	0.35	0.98	0.46	0.50	0.51	0.85	1.34
BaO	0.21	0.27	0.18	0.14	0.20	0.25	0.15	0.31	0.23	0.18	0.14	0.14
Na2O	7.58	7.73	7.53	6.67	7.26	7.94	7.55	7.98	7.87	7.80	6.80	6.67
K2O	5.27	5.21	5.67	6.75	5.46	4.71	5.11	4.77	5.05	4.79	6.20	6.72
Total	100.20	100.16	100.75	100.40	99.54	99.58	100.04	99.53	99.88	99.26	99.90	100.23
Or	31.24	30.55	33.06	39.97	33.01	27.95	30.81	28.08	29.59	28.72	37.44	39.85
Ab	68.30	68.90	66.74	60.03	66.75	71.60	69.11	71.31	70.07	71.01	62.48	60.15
An	0.47	0.55	0.20	0.00	0.24	0.45	0.08	0.61	0.34	0.27	0.08	0.00

Mol percent orthoclase (Or), albite (Ab), and anorthite (An) calculated with standard CAMECA software by cation proportion of K, Na, and Ca normalized to 100%. Vertical lines separate analyses of individual crystals.

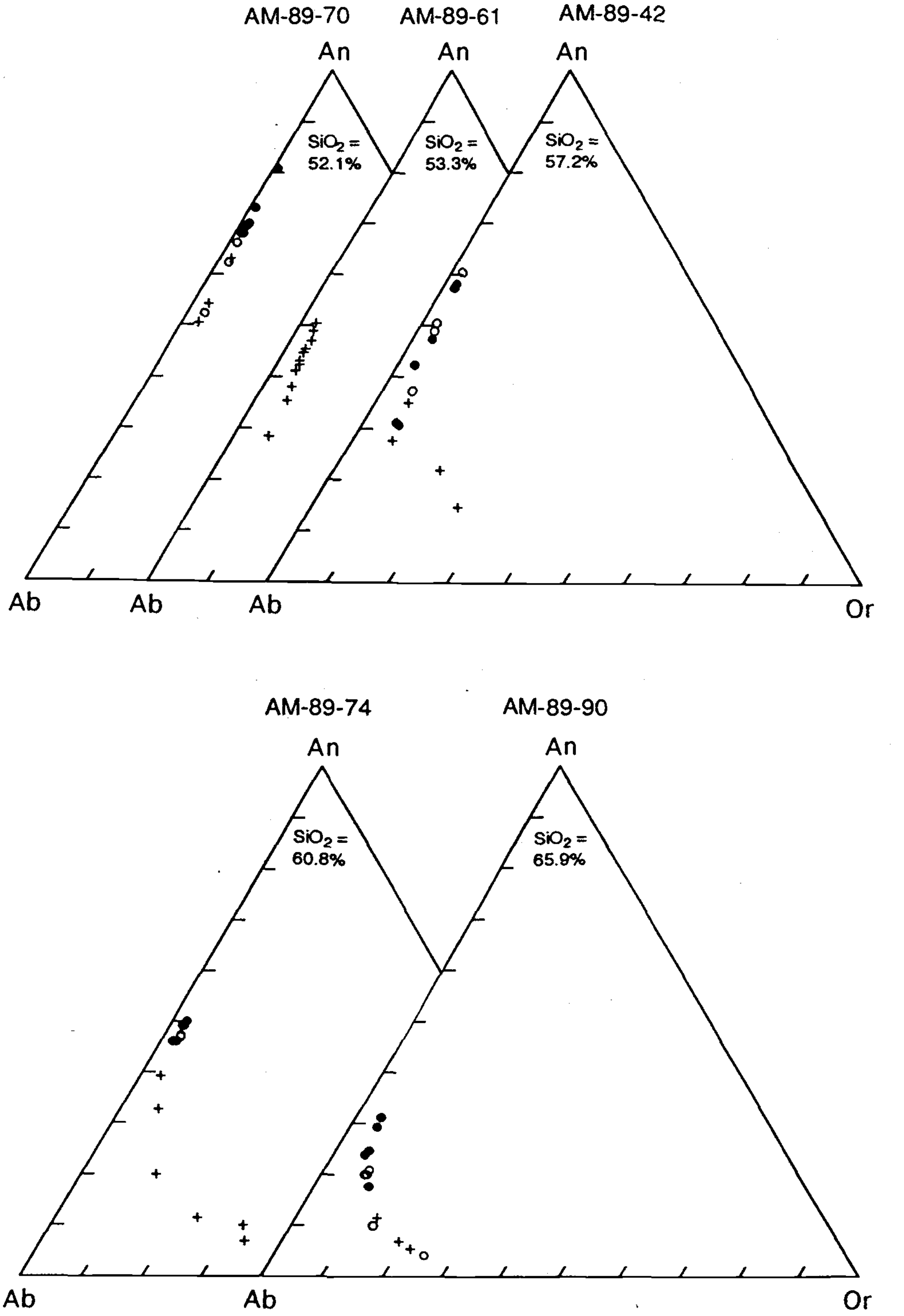

Figure 11: Ternary projections of feldspar compositions from the Hart Mountain trachyandesite. Open circles are rim compositions, filled are core compositions, plus symbols represent groundmass compositions. SiO_2 values are for whole rock.

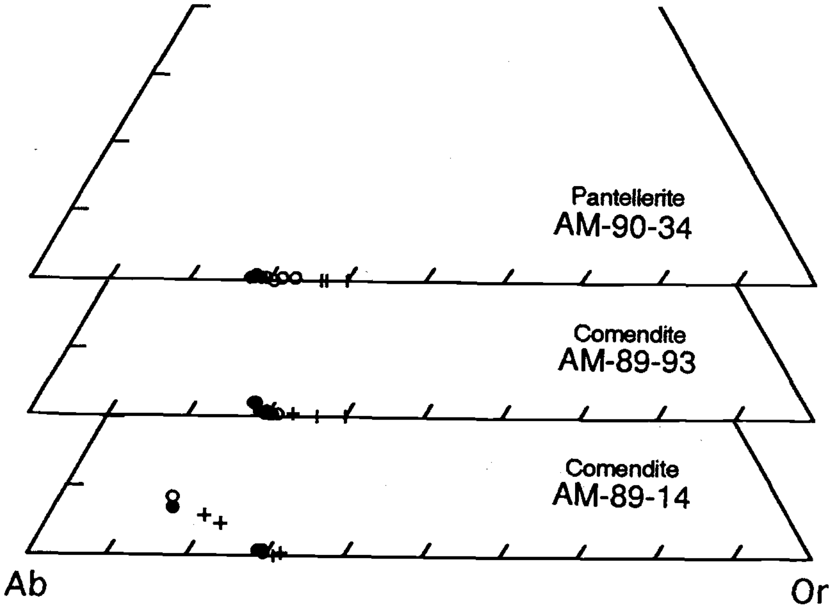

Figure 12: Ternary projections of feldspar compositions from the Warner Peak rhyolite. Open circles are rim compositions, filled are core compositions, plus symbols represent groundmass compositions.

groundmass in the more silicic samples, and rarely as overgrowths on plagioclase phenocrysts. Feldspar phenocrysts in the Warner Peak rhyolite are anorthoclases. Anorthoclase and sodic sanidine are found in the groundmass of these rocks. This systematic change in feldspar composition with increasing silica, the predominance of normal zoning or the lack of zonation in plagioclase phenocrysts, and euhedral to subhedral crystal morphologies support crystal fractionation as the dominant process involved in the petrogenesis of the Hart Mountain volcanic complex as argued further below. The normal zoning and slight oscillatory zoning present in these feldspars is interpreted to be the result of sluggish response to compositional changes during fractionation. Large amounts of undercooling during crystallization of some samples (i.e., AM-89-70, AM-89-61) is suggested by the skeletal morphologies of some plagioclase crystals (Lofgren, 1974; 1980; Mathis, 1988).

Core compositions of plagioclase crystals within individual samples vary over a range of approximately 15 mol % An. Most analyzed plagioclase phenocrysts (samples AM-89-70, AM-89-90) display normal zoning with core and rim compositions differing by 3 to 15 mol % An. Anorthoclase occurs as an overgrowth on some plagioclase phenocrysts in AM-89-90. The rim compositions of plagioclase phenocrysts generally have the same range of compositions as feldspar microlites in the groundmass (except in AM-89-74). Therefore, rim compositions are interpreted to be closer to equilibrium with the melt than the core compositions.

All analyses of phenocrysts in sample AM-89-74 yield compositions within a narrow range (An_{45-50}). However, feldspar microlites in the groundmass display a very wide range of compositions from $An_{39}Ab_{57}Or_4$ to $An_7Ab_{59}Or_{34}$ (Figure 11). The phenocrysts in this sample have subhedral to euhedral morphologies, and do not display any disequilibrium textures such as skeletal or sieved cores, or dendritic rims. Hence, the phenocrysts compositions are interpreted to represent equilibrium feldspar compositions. The range in feldspar compositions in the groundmass may result from rapid quenching of the melt. Nucleation of feldspar microlites at progressively greater amounts of undercooling and slow diffusion of components may explain the range of compositions found in these groundmass feldspars. Further evidence for a rapidly quenched groundmass in this lava flow includes remnants of glass present between microlites, and the presence of pigeonite as a groundmass phase.

Groundmass feldspar microlites in sample AM-89-42 range in composition from $An_{28}Ab_{66}Or_7$ to $An_{14}Ab_{61}Or_{24}$. Plagioclase phenocrysts (xenocrysts?) may display normal or reverse zoning, or be unzoned. Compositions of phenocrysts range from mildly reversely zoned at An_{60} to An_{57} to unzoned at An_{30}. Zoned crystals have compositions between these values with rim and core compositions within individual crystals differing by as much as 15 mol % An. Compositions of the feldspar phenocrysts at each end of the compositional spectrum probably represent equilibrium compositions of feldspars of at least two different batches of mafic magma included into the more silicic matrix. Sample AM-89-42 is one of a few samples of the Hart Mountain trachyandesite suite which exhibits disequilibrium textures such as sieved and fritted crystals and texturally inhomogeneous groundmasses. These samples also contain a wide range of plagioclase compositions. They apparently result from the mingling of magmas or incorporation of cognate inclusions within the Hart Mountain volcanic system.

Anorthoclase phenocrysts in the Warner Peak rhyolite are generally euhedral. Within individual samples, the anorthoclase phenocrysts typically have Carlsbad, albite, and/or albite and pericline ("anorthoclase grid") twinning. In thin section, some crystals appear untwinned. Feldspars from two comendites (AM-89-93, AM-89-14) and one pantellerite (AM-90-34) were analyzed (Table 6, Figure 12). Anorthoclase was the only feldspar present in sample AM-89-14, and samples

AM-89-93 and AM-90-34 had sanidine as groundmass feldspar phases in addition to anorthoclase. Anorthoclase in AM-89-14 has the most compositional variability of these samples: An content ranges from $An_{8.4}$ to $An_{0.15}$. Alkali feldspars in AM-89-93 and AM-90-34 all have very low An contents (<1 mol %), and range in Or contents by less than 12 mol %.

PYROXENE

Pyroxene crystals with compositions ranging from diopside to ferroaugite (Table 7, Figure 13) are found in at least trace amounts in all described samples from the Hart Mountain trachyandesite suite. Pigeonite is found as a groundmass phase in rapidly quenched samples of the Hart Mountain trachyandesite suite (AM-89-74, AM-89-42). Ferrohedenbergite and hedenbergite (Table 8, Figure 13) are the pyroxene phases which, if present, are found in samples of the Warner Peak rhyolite. Some hedenbergite/ferrohedenbergite crystals have a significant sodic component (as much as 3.5 wt % Na_2O). AM-89-93 also contains aegerine-augite in the groundmass.

Pyroxene crystals found in samples of the Hart Mountain volcanic complex are generally euhedral to subhedral. Color varies systematically with composition: augite crystals are light brown, augite/ferroaugite crystals have weak light green pleochroism, and hedenbergite/ferrohedenbergite crystals display weak olive green to jade green pleochroism.

Since most samples from the Hart Mountain volcanic complex contain only one pyroxene, pyroxene thermometry could only be used to estimate minimum temperatures of formation (Figure 14; Lindsley, 1983). Phenocryst compositions were used when possible because groundmass phases may have crystallized metastably (Lindsley, 1983). However, a pigeonite analysis from the groundmass of trachyandesite AM-89-74 yielded a temperature of formation in agreement with that of the augite phenocrysts from that sample (~900°C). Ferrohedenbergite compositions from the Warner Peak rhyolite were not included in Figure 4 because they yielded

Table 7: Representative analyses of pyroxene crystals from the Hart Mountain trachyandesite.

Sample #	AM-89-70		AM-89-70		AM-89-70		AM-89-70		AM-89-61		AM-89-61	
	rim	core	rim	core	rim	core	grdms	grdms	rim	core	rim	core
SiO2	52.12	48.75	49.04	49.08	48.68	48.90	50.71	51.89	48.71	51.90	49.78	51.60
TiO2	0.90	1.23	1.59	1.62	1.60	1.56	1.17	0.96	2.00	0.90	1.73	1.03
Al2O3	2.16	7.05	6.26	6.07	5.72	5.57	1.88	1.53	4.08	1.75	3.59	1.81
Cr2O3	0.16	0.25	0.14	0.10	0.00	0.00	0.00	0.04	0.02	0.00	0.00	0.00
Fe2O3	0.41	2.33	2.25	2.14	2.49	3.48	2.37	1.04	2.67	1.23	1.96	1.27
MgO	15.97	14.57	14.36	14.20	13.87	14.38	14.65	14.90	12.79	15.47	13.11	14.89
CaO	18.53	20.27	19.89	19.67	19.57	20.00	19.41	18.80	19.23	16.97	20.69	18.68
MnO	0.30	0.14	0.15	0.16	0.20	0.14	0.37	0.30	0.45	0.49	0.30	0.33
FeO	9.15	5.02	6.38	7.03	7.33	6.14	8.45	10.17	10.25	11.88	9.16	10.76
Na2O	0.32	0.49	0.53	0.52	0.50	0.51	0.41	0.39	0.41	0.25	0.37	0.23
Total	100.03	100.11	100.60	100.61	99.96	100.67	99.41	100.02	100.60	100.83	100.71	100.60
Wo	38.51	45.47	44.24	43.84	43.73	44.53	41.57	39.41	42.37	35.24	44.66	38.87
En	46.15	45.48	44.42	43.68	43.13	44.55	43.67	43.46	39.21	44.69	39.38	43.11
Fs	15.34	9.05	11.35	12.47	13.14	10.92	14.75	17.13	18.42	20.07	15.96	18.02

Sample #	AM-89-61		AM-89-42		AM-89-42		AM-89-42		AM-89-42		AM-89-74	
	rim	core	rim	core	rim	core	grdms	grdms	grdms	grdms	rim	core
SiO2	49.52	51.26	51.72	51.61	50.37	49.92	51.07	50.88	51.47	52.76	51.54	51.80
TiO2	1.70	0.89	0.91	1.23	1.76	2.06	1.53	0.41	0.40	0.26	0.72	0.70
Al2O3	3.92	1.96	1.16	1.70	2.53	3.22	2.59	0.30	0.49	0.63	1.04	1.74
Cr2O3	0.00	0.02	0.02	0.00	0.04	0.01	0.02	0.03	0.03	0.00	0.01	0.01
Fe2O3	1.72	1.02	0.70	0.57	0.88	1.14	2.28	0.00	0.47	0.79	0.77	1.21
MgO	12.94	13.40	12.98	14.18	12.30	12.69	14.41	13.29	13.49	13.03	13.12	14.08
CaO	20.53	18.66	18.38	20.15	19.94	20.09	20.62	3.96	7.47	19.77	17.67	20.09
MnO	0.31	0.46	0.59	0.26	0.36	0.23	0.23	1.02	0.97	0.56	0.79	0.54
FeO	9.14	12.28	14.15	10.07	12.32	11.14	8.25	30.21	26.59	12.75	13.99	9.73
Na2O	0.41	0.34	0.26	0.30	0.36	0.41	0.40	0.07	0.15	0.31	0.32	0.32
Total	100.20	100.28	100.87	100.07	100.86	101.00	101.39	100.18	101.54	100.86	99.97	100.22
Wo	44.72	37.49	38.34	42.03	42.46	43.09	43.60	8.46	15.64	40.93	37.22	42.12
En	39.22	39.45	37.66	41.15	36.44	37.86	42.39	39.47	39.30	37.54	38.46	41.06
Fs	16.06	21.05	24.00	16.82	21.10	19.05	14.01	52.07	45.06	21.53	24.31	16.82

FeO, Fe2O3, and mol percent wollastonite (Wo), enstatite (En), and ferrosilite (Fs) calculated with standard CAMECA software: FeO and Fe2O3 calculated by charge balance; Wo, En, and Fs calculated by cation proportion of Mg, Fe, and Ca normalized to 100%. Vertical lines separate analyses of individual crystals.

Table 7, continued.

Sample #	AM-89-74		AM-89-74		AM-89-74		AM-89-74		AM-89-74		AM-89-90	
	rim	core	rim	core	rim	core	grdms	grdms	grdms	grdms	rim	core
SiO2	52.01	51.96	51.64	51.29	51.80	51.21	50.47	51.09	50.53	51.27	50.10	50.99
TiO2	0.69	0.68	0.75	0.57	0.80	0.82	0.35	0.92	0.87	0.66	0.44	0.45
Al2O3	1.61	1.50	1.89	1.40	1.82	2.10	0.28	1.17	1.14	0.82	0.84	1.06
Cr2O3	0.00	0.00	0.03	0.00	0.00	0.00	0.00	0.00	0.00	0.02	0.00	0.00
Fe2O3	1.20	1.60	1.40	1.43	0.83	1.07	0.00	0.68	0.61	0.50	0.72	0.13
MgO	14.29	14.39	14.12	14.26	14.26	13.95	12.91	13.10	12.36	12.74	8.77	9.11
CaO	19.94	20.06	20.17	18.82	19.94	19.78	3.91	17.55	15.89	16.79	19.35	19.88
MnO	0.48	0.50	0.54	0.54	0.44	0.53	1.41	0.66	0.93	0.72	0.94	0.87
FeO	9.83	9.39	9.30	10.51	9.81	9.66	30.65	14.08	16.52	15.53	17.58	17.54
Na2O	0.32	0.32	0.34	0.27	0.31	0.34	0.08	0.29	0.29	0.31	0.29	0.27
Total	100.36	100.42	100.17	99.08	100.00	99.47	100.06	99.53	99.14	99.35	99.04	100.30
Wo	41.65	41.97	42.47	39.79	41.74	41.95	8.33	37.12	34.01	35.57	42.05	42.35
En	41.53	41.88	41.35	41.95	41.52	41.17	38.29	38.54	36.81	37.54	26.51	27.01
Fs	16.82	16.16	16.19	18.25	16.74	16.89	53.38	24.34	29.18	26.88	31.44	30.64

Sample #	AM-89-90		AM-89-90		AM-89-90		AM-89-83		AM-89-83		AM-89-83	
	rim	core	rim	core	rim	core	rim	core	rim	core	rim	core
SiO2	53.48	51.23	51.09	51.36	50.61	51.18	52.78	51.52	51.00	51.46	48.42	47.99
TiO2	0.51	0.47	0.43	0.48	0.74	0.49	0.41	0.46	0.41	0.36	0.59	0.54
Al2O3	4.46	1.50	1.09	0.88	0.97	1.07	0.94	1.07	1.00	0.89	0.64	1.06
Cr2O3	0.00	0.00	0.02	0.00	0.06	0.02	0.03	0.00	0.00	0.02	0.04	0.00
Fe2O3	0.00	0.00	0.14	0.60	0.55	1.01	0.00	0.28	1.69	0.61	0.00	0.00
MgO	6.43	9.35	9.63	10.54	9.12	10.14	11.67	11.67	11.99	10.98	0.28	0.17
CaO	15.81	19.33	19.77	19.63	18.92	19.65	19.07	18.53	19.26	18.92	19.12	18.70
MnO	0.95	0.99	0.83	0.84	1.00	0.91	0.97	1.06	0.99	1.01	1.47	1.35
FeO	15.95	16.82	16.84	15.67	18.19	16.24	14.59	14.85	12.91	15.30	29.11	29.10
Na2O	1.82	0.28	0.28	0.30	0.32	0.26	0.29	0.34	0.30	0.37	0.40	0.53
Total	99.42	99.98	100.13	100.30	100.48	100.98	100.73	99.77	99.54	99.93	100.08	99.43
Wo	41.66	41.80	42.10	41.60	40.60	41.67	40.19	39.27	41.15	40.31	44.06	43.78
En	23.56	28.13	28.51	31.09	27.22	29.92	34.20	34.40	35.65	32.55	0.91	0.56
Fs	34.78	30.08	29.39	27.32	32.17	28.41	25.61	26.33	23.20	27.14	55.03	55.66

Table 8: Representative analyses of pyroxene crystals from the Warner Peak rhyolite.

Sample #	AM-89-93		AM-89-93		AM-89-93		AM-89-93	
	rim	core	rim	core	rim	core	grdms	grdms
SiO2	48.37	47.85	47.60	48.08	49.27	48.39	51.35	48.24
TiO2	0.44	0.63	0.44	0.52	0.64	0.51	0.41	0.64
Al2O3	0.23	0.40	0.29	0.31	0.15	0.31	0.17	0.28
Cr2O3	0.01	0.05	0.00	0.01	0.00	0.02	0.01	0.00
Fe2O3	1.65	1.77	12.48	2.04	5.62	0.32	23.10	1.78
MgO	0.14	0.28	0.05	0.12	0.04	0.15	0.03	0.10
CaO	19.20	19.69	16.94	19.41	15.14	19.07	5.42	18.01
MnO	1.76	1.91	1.51	1.91	1.50	1.69	0.78	1.87
FeO	28.30	27.81	17.98	27.96	25.50	29.11	9.08	28.95
Na2O	0.71	0.50	3.45	0.64	2.81	0.60	9.68	0.90
Total	100.82	100.89	100.74	101.01	100.65	100.17	100.03	100.76
Wo	44.79	45.49	52.54	45.23	41.74	44.01	41.16	42.66
En	0.45	0.90	0.23	0.40	0.14	0.49	0.33	0.31
Fs	54.76	53.61	47.23	54.38	58.12	55.50	58.51	57.02

Sample #				AM-89-14				
	core	core	core	core	core	core	core	core
SiO2	47.71	47.62	47.35	47.76	47.67	47.90	48.16	47.26
TiO2	0.67	0.53	0.64	0.42	0.48	0.59	0.54	0.50
Al2O3	0.32	0.33	0.37	0.30	0.31	0.48	0.59	0.23
Cr2O3	0.01	0.01	0.00	0.08	0.01	0.02	0.04	0.01
Fe2O3	1.60	1.80	1.60	1.87	1.09	1.52	1.32	1.68
MgO	0.19	0.31	0.30	0.19	0.32	2.24	2.88	0.27
CaO	18.04	18.83	18.66	18.14	18.73	19.30	19.33	18.59
MnO	1.90	1.87	1.83	1.83	1.74	1.87	1.78	1.66
FeO	28.58	27.64	28.00	27.82	27.96	25.07	24.11	27.64
Na2O	0.80	0.69	0.63	0.91	0.68	0.46	0.49	0.72
Total	99.84	99.64	99.38	99.32	99.00	99.45	99.24	98.56
Wo	42.84	44.50	44.03	43.64	44.20	44.39	44.38	44.42
En	0.62	1.02	0.99	0.64	1.06	7.18	9.19	0.90
Fs	56.53	54.48	54.98	55.72	54.74	48.42	46.43	54.68

FeO, Fe2O3, and mol percent wollastonite (Wo), enstatite (En), and ferrosilite (Fs) calculated with standard CAMECA software: FeO and Fe2O3 calculated by charge balance; Wo, En, and Fs calculated by cation proportion of Mg, Fe, and Ca normalized to 100%. Vertical lines separate analyses of individual crystals.

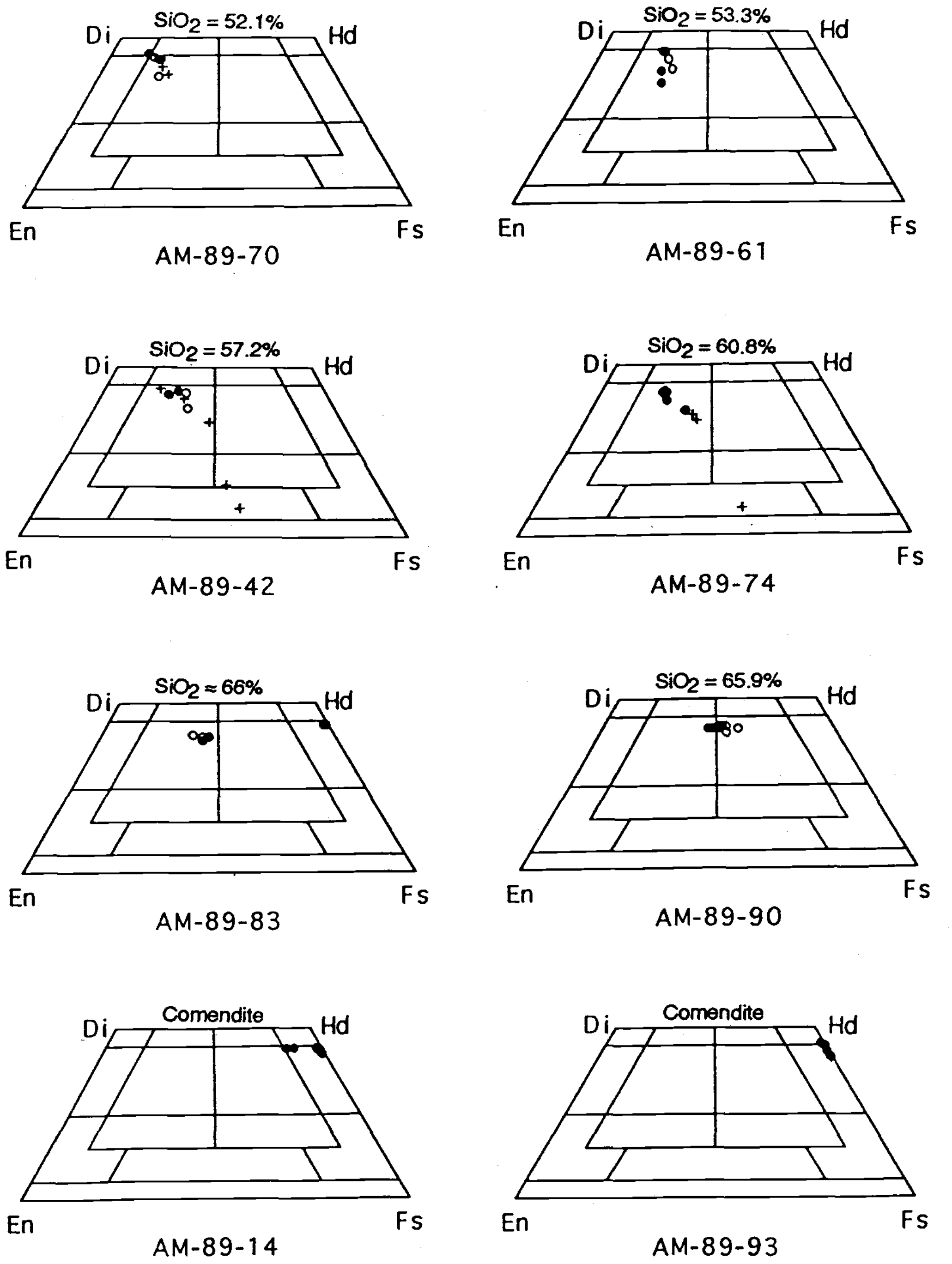

Figure 13: Compositions of pyroxenes from the Hart Mountain volcanic complex. Open circles are rim compositions, filled are core compositions, plus symbols represent groundmass compositions. SiO_2 values are for whole rock.

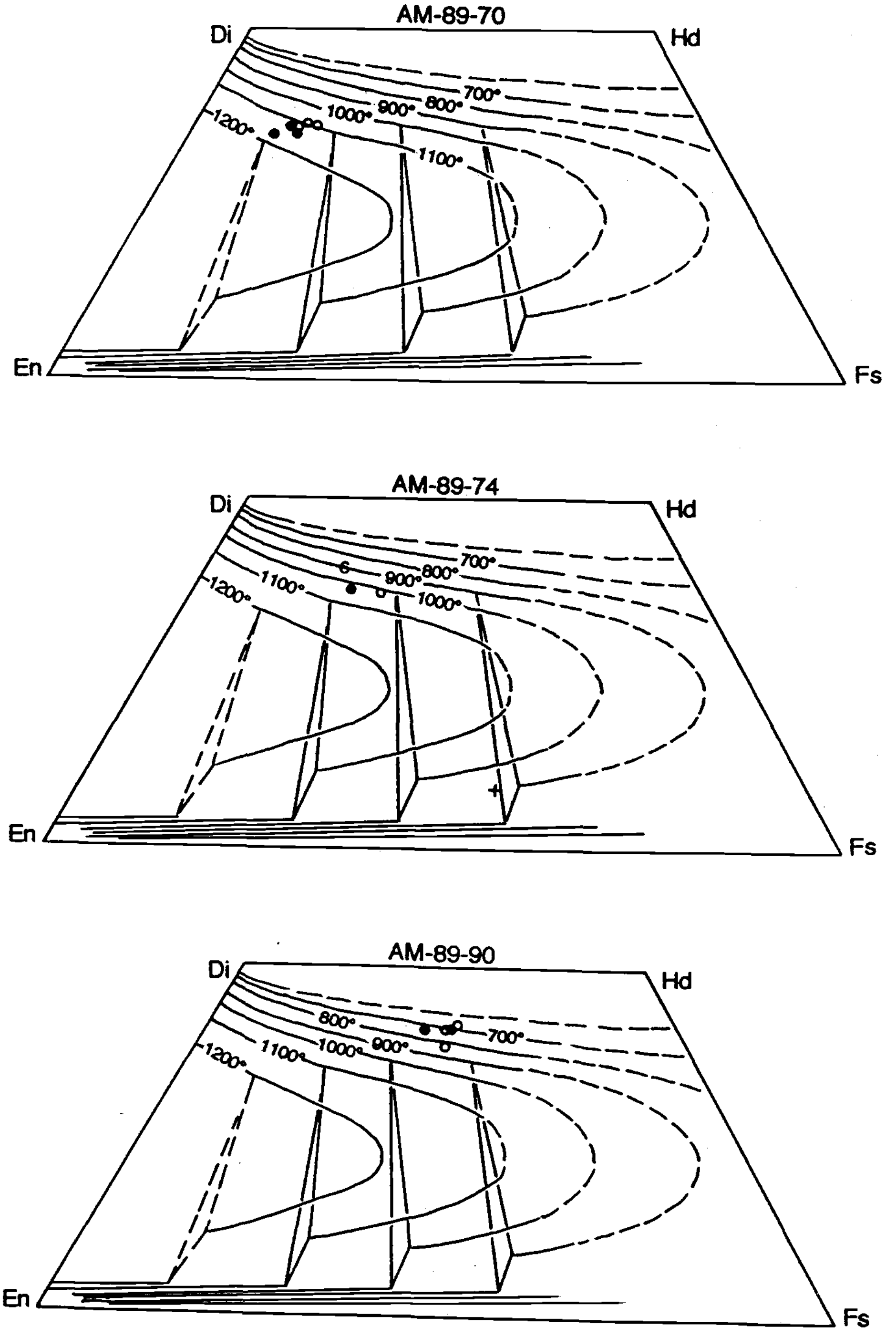

Figure 14: Minimum temperature of formation for pyroxenes from selected samples of the Hart Mountain trachyandesite. Compositions recalculated according to Lindsley (1983), and plotted relative to isotherms also determined by Lindsley (1983). Open circles are rim compositions, filled are core compositions, plus symbols represent groundmass compositions. The number "6" represents 6 analyses at that composition.

anomalously low temperatures of formation (500-600°C) compared to other peralkaline rhyolites which typically have high magmatic temperatures (900-1000°C; Mahood, 1984).

OLIVINE

Samples AM-89-70 and AM-90-23, collected from Tvc, are the only samples which contain appreciable amounts of unaltered olivine. Altered olivine crystals are present (1-2 volume %, or in trace amounts) in many samples of the Hart Mountain trachyandesite. Petrographically, olivine was generally recognized as red-brown (iddingsite?) crystals without cleavage.

Olivine phenocrysts in AM-89-70 range in composition from Fo_{64} to Fo_{85} (Table 9), and are normally zoned. Core compositions range from Fo_{85} to Fo_{77}. Olivine crystals within this compositional range are common in trachybasalts (Deer et al., 1966).

AMPHIBOLE

Two different amphiboles were present in some samples of the Warner Peak rhyolite: strongly pleochroic blue to green to brown arfvedsonite, and weakly pleochroic brown amphibole. Pleochroic green amphibole crystals were present in the trachytic portion of ignimbrite A (AM-89-83).

Acceptable electron microprobe analyses (Table 10) of amphibole crystals were only obtained on arfvedsonite in sample AM-89-93. Other amphibole analyses yielded systematically low totals below 96 wt %. Recalculation of these analyses was based on 23 oxygens, and Fe_2O_3 was calculated as average Fe_2O_3 value by the method of Spear and Kimball (1984). All analyses of the blue-green amphibole have $Na_B \geq 1.34$ and are therefore classified as alkali amphiboles. $Mg/Mg+Fe^{2+} > 0.5$ and $(Na+K)_A \geq 0.50$ values place these amphiboles well within the arfvedsonite field (Leake, 1978). These crystals display very little zonation or chemical variation between grains. For example, Fe/Fe+Mg

Table 9: Representative analyses of olivine phenocrysts in sample AM-89-70.

	rim	core	rim	core	rim	core	rim	core
SiO2	38.74	39.59	37.01	38.46	36.60	40.33	36.03	38.68
TiO2	0.0	40.01	0.05	0.00	0.05	0.02	0.06	0.01
MgO	42.33	45.46	36.03	40.26	34.43	44.32	31.34	42.55
CaO	0.17	0.23	0.13	0.19	0.17	0.34	0.18	0.22
MnO	0.23	0.17	0.45	0.33	0.54	0.22	0.61	0.23
FeO*	18.25	13.93	25.94	20.44	27.14	15.10	30.74	17.67
NiO	0.24	0.25	0.14	0.19	0.19	0.31	0.08	0.33
Total	100.01	99.65	99.76	99.86	99.11	100.64	99.04	99.69
Fo	80.5	85.4	71.0	77.8	69.1	84.1	64.2	81.2
Fa	19.5	14.7	28.7	22.2	30.6	16.1	35.3	18.1

Mol percent forsterite (Fo) and Fayalite (Fa) calculated with standard Cameca software by cation proportion of Mg and Fe normalized to 100%. Vertical lines separate analyses of individual crystals.

Table 10: Representative analyses of amphibole crystals in sample AM-89-93.

	rim	core	rim	core	rim	core	rim	grdms
SiO2	49.61	49.73	49.69	50.05	50.08	49.60	48.73	52.30
TiO2	0.60	0.56	0.35	0.31	0.45	0.59	0.06	0.47
Al2O3	0.14	0.19	0.22	0.21	0.17	0.18	0.25	0.31
MgO	0.07	0.06	0.09	0.05	0.08	0.05	0.05	0.00
FeO*	35.37	35.30	35.31	35.42	34.20	35.36	35.49	29.81
MnO	1.63	1.67	1.70	1.72	1.66	1.65	1.85	0.53
CaO	1.56	1.83	1.45	1.58	1.45	1.74	1.62	2.35
Na2O	7.62	7.31	7.65	7.61	7.82	7.48	7.72	11.09
K2O	1.33	1.26	1.25	1.19	1.32	1.38	1.02	0.04
H2O	0.61	0.57	0.54	0.69	0.61	0.69	0.55	1.88
Cl	0.03	0.03	0.03	0.04	0.05	0.02	0.03	0.01
F	2.59	2.68	2.72	2.42	2.58	2.42	2.65	0.00
Total	103.79	103.90	103.77	103.75	103.07	103.62	102.71	98.80
O=F,Cl	-1.10	-1.13	-1.16	-1.03	-1.09	-1.03	-1.13	0.00
Total	102.69	102.77	102.61	102.73	101.98	102.60	101.58	98.80
Si iv	7.978	7.982	7.984	8.000	8.000	7.974		
Al iv	0.022	0.018	0.016	0.000	0.000	0.026		
Al vi	0.005	0.018	0.026	0.040	0.033	0.008		
Ti	0.073	0.068	0.042	0.037	0.054	0.071		
Fe3+	0.540	0.571	0.631	0.630	0.504	0.522		
Mg	0.017	0.014	0.021	0.012	0.019	0.012		
Fe2+	4.218	4.167	4.113	4.104	4.077	4.232		
Mn	0.222	0.227	0.232	0.233	0.225	0.225		
Sum oct	5.073	5.066	5.065	5.057	4.931	5.070		
Ca	0.269	0.315	0.250	0.271	0.249	0.300		
Na (M4)	1.658	1.620	1.685	1.673	1.820	1.630		
Na (A)	0.718	0.655	0.698	0.686	0.609	0.701		
K (A)	0.273	0.258	0.257	0.243	0.269	0.283		
Sum (A)	0.991	0.913	0.955	0.928	0.878	0.984		

Standard Cameca software calculates H2O by filling the hydroxyl site with OH after initially allocating F and Cl. Recalculation of analyses use the average Fe2O3 value by the method of Spear and Kimball (1984). Recalculation could not be done on nonstoichiometric analyses. Structural formula was calculated using 23 oxygen. Analyzed Fe content may be high. Vertical lines separate analyses of individual crystals.

values only range between 0.996 and 1.000. They also have high F contents (as high as 2.7 wt %), which is common in arfvedsonite crystals from peralkaline rhyolites (Conrad, 1984; Macdonald et al., 1987).

Attempts to analyze brown amphiboles from sample AM-90-34 were unsuccessful due to low totals (<96 wt % without H_2O). However, rough estimates of their composition suggest sodic-calcic amphibole with compositions ranging between richterite, ferrorichterite, and eckermanite.

DISCUSSION

Changes in mineral compositions and modal proportions reflect differentiation from trachybasalt to trachyte in the Hart Mountain trachyandesite. Anorthite content in feldspar decreases from An_{81} to An_{15}. Ferrosilite content in pyroxene phenocrysts increases from Fs_9 to Fs_{35}.

The trachybasalt and the basaltic trachyandesites contain plagioclase > olivine ≥ clinopyroxene > Fe-Ti oxides. The mineral assemblages in the trachyandesites and the trachytes contain a greater proportion of plagioclase, less olivine, and also contain apatite as microphenocrysts and as inclusions in other phases. Anorthoclase is present as rim overgrowths on a few plagioclase phenocrysts and in the groundmass of the trachytes. The occurrence of oligoclase and andesine as the predominant feldspar phenocryst phases in the trachytes of the Hart Mountain volcanic complex is unusual: alkali feldspar is the principal constituent of most trachytes (Williams et al., 1982). For example, anorthoclase is the feldspar phase found in trachytes at Pantelleria (Civetta et al., 1984; Mahood and Stimac, 1990); at Kane Spring Wash (Novak and Mahood, 1986); and the Paisano Volcano, Trans-Pecos, Texas (Parker, 1983). At Kane Spring Wash and Trans-Pecos Texas, and also at Socorro Island (Bryan, 1970), some anorthoclase phenocrysts have plagioclase cores.

Anorthoclase is the most common phenocryst in the peralkaline rhyolites of the Warner Peak rhyolite, and may be the only phenocryst phase in some samples. Fe-Ti oxide, either as microphenocrysts or as a groundmass phase, is the only other mineral present in all samples described from the Warner Peak rhyolite. Hedenbergite/ferrohedenbergite, arfvedsonite, and richterite-eckermanite may or may not be present in minor amounts. Quartz is present in the groundmass of some samples.

The modal mineralogies of samples of the Warner Peak rhyolite are quite variable despite similar whole rock compositions (see Table 4). For example, pantellerite AM-90-35 contains clinopyroxene and only minor amounts of amphibole in the groundmass. Sample AM-89-34, with almost an identical composition, has amphibole as the only mafic phenocrystic phase. Perhaps higher water or halogen content, or lower crystallization temperature or oxygen fugacity (Conrad, 1984) in AM-89-34 increases the stability of amphibole relative to clinopyroxene.

Aenigmatite, a characteristic mineral of peralkaline rhyolites (Nicholls and Carmichael, 1969), was not observed in the peralkaline rhyolites at Hart Mountain. The ubiquitous presence of Fe-Ti oxides in the Warner Peak rhyolite precludes the presence of aenigmatite because aenigmatite and Fe-Ti oxides cannot coexist in equilibrium in peralkaline rhyolites (Nicholls and Carmichael, 1969). Fayalitic olivine, another phase found in some peralkaline rhyolites (Sutherland, 1974), also was not observed in the Warner Peak rhyolite.

Apatite, as sparse inclusions in Fe-Ti oxides, was the only accessory phase observed in the peralkaline rhyolites. Zircon was not present, which is in keeping with the work of Watson (1979) in which melt peralkalinity decreased the stability of zircon despite high Zr contents (as high as 556 ppm at Hart Mountain).

WHOLE ROCK COMPOSITION

METHODS

Most major and trace element analyses were done with X-ray fluorescence (XRF) at Washington State University. Two XRF analyses (samples AM-90-22 and AM-98-93) were done at Stanford University by Martin Streck. Precision for major elements is estimated to be better than 1% (one-sigma standard deviation, S.D.) except for FeO*, MnO, P_2O_5, and Na_2O ($\leq$3%). One sigma S.D. values for trace elements are estimated to be better than 2 to 10%.

Rare earth elements (REE), Cs, Th, U, Sc, Hf, Ta, Cr, and Co were acquired by instrumental neutron activation (INA) analyses at the OSU Radiation Center following standard procedures. Estimated precision is better than 5% (one-sigma S.D.) for REE (except Nd), Sc, Co, Cs, Hf, Ta, Th, and 5-15% for Cr, Nd, U, and V.

RESULTS

Twenty-four samples from the Hart Mountain volcanic complex were analyzed for major and trace elements. All samples were collected from the western fault escarpment of Hart Mountain (see Plates I and III for sample locations). These samples make up a nearly continuous compositional spectrum from trachybasalt to trachyte in the Hart Mountain trachyandesite suite to the peralkaline rhyolites of the Warner Peak rhyolite (Table 11; Figures 6, 15, and 16). Because $Na_2O - 2.0 > K_2O$ in the trachybasalt, basaltic trachyandesites, and trachyandesites, they could be further classified as hawaiite, mugearites, and benmoreites, respectively (LeMaitre, 1989). The suite is characterized by low MgO (< 3 wt %) except for the most primitive sample (MgO =6.48 wt %), high alkalies (Na_2O+K_2O=5.01 to 10.56 wt %), and low concentrations of many trace elements, including Ni, Cr, Rb, and REEs.

Samples from the Hart Mountain trachyandesite suite range from 52.1 to 66.2 wt % SiO_2. Minor apparent silica gaps exist

Table 11: Compositions of samples from the Hart Mountain volcanic complex.

Sample #	AM-90-23	AM-89-92	AM-89-85	AM-90-29	AM-89-74	AM-89-81	AM-89-55
Rock type:	L	D	F	L	L	F	L
Strat. Unit:	Tvc	Tvc	Tiw	Tv1	Tv1	Tis	Tv2
A.I.	0.460	0.621	0.726	0.512	0.713	0.828	0.897
XRF analysis (wt %)							
SiO2	52.11	58.75	63.51	52.17	60.83	64.11	66.20
Al2O3	16.33	17.19	16.75	17.93	16.65	15.89	15.73
TiO2	1.811	1.530	0.924	2.494	1.348	0.880	0.682
FeO*	9.40	6.56	5.17	9.81	6.45	5.85	4.79
MnO	0.165	0.175	0.167	0.167	0.155	0.182	0.207
CaO	8.23	5.29	3.29	8.07	4.12	2.74	1.96
MgO	6.48	2.51	1.20	2.31	1.68	0.66	0.39
K2O	1.29	2.41	3.80	1.90	3.01	4.23	3.87
Na2O	3.72	4.90	4.89	4.33	5.24	5.21	6.03
P2O5	0.458	0.688	0.301	0.817	0.516	0.256	0.145
Total	99.88	99.72	98.62	98.59	99.97	97.17	99.85
XRF analysis (ppm)							
Ni	103	11	6	12	2	6	7
V	166	71	11	150	28	0	0
Ba	381	784	848	729	887	952	952
Rb	21	45	76	30	57	81	77
Sr	531	601	440	607	452	317	208
Zr	185	257	316	289	328	409	459
Y	28	37	40	40	43	50	53
Nb	27.4	42.4	48.2	47.4	50.8	59.0	64.4
Ga	18	23	23	22	23	25	27
Cu	43	18	16	59	0	5	4
Zn	93	108	94	116	103	121	131
Pb	5	6	9	3	7	10	9
INA analysis (ppm)							
La	23.8	38.5	39.8	40.8	43.5	47.8	49.6
Ce	51.5	82.0	86.6	90.8	94.4	102.3	104.3
Nd	30.1	44.8	39.1	56.8	46.4	48.8	48.8
Sm	6.48	9.06	8.94	11.38	10.16	10.76	10.75
Eu	2.10	2.90	2.56	3.63	2.91	2.89	2.65
Tb	0.92	1.25	1.20	1.60	1.48	1.57	1.55
Yb	2.12	3.22	3.68	3.48	4.16	4.81	5.35
Lu	0.30	0.42	0.58	0.50	0.56	0.66	0.78
Sc	21.1	14.9	11.6	21.7	13.2	11.0	8.7
Cr	177	17	4	7	6	4	2
Co	36.0	10.1	2.5	27.1	6.1	2.7	1.1
Cs	0.36	0.55	1.5	0.55	0.7	1.9	0.8
Hf	4.7	6.7	8.5	7.8	9.1	11.7	13.0
Ta	1.5	2.3	2.4	2.6	2.7	3.2	3.3
Th	2.6	4.8	7.4	4.3	7.6	8.6	9.7
U	nd	1.7	nd	1.8	2.8	3.3	3.2

Rock types: L = lava flows, D = dike, F = fiamme, T = whole rock tuff, I = intrusion, VI = vitric margin of intrusion. A.I. = Agpiatic Index (molar Na2O+K2O/molar Al2O3). Data normalized to 100% anhydrous, totals are prior to normalization. nd = under detection limit. *All trace element data from INA analyses.

Table 11, continued.

Sample #	AM-89-60	AM-89-61	AM-89-90	AM-90-02	AM-89-65	AM-90-22*	AM-89-42
Rock type:	L	L	L	F	L	L	L
Strat. Unit:	Tv3	Tv3	Tv3	Tib	Tv5	Tv5	Thl
A.I.	0.705	0.638	0.901	0.880	0.695	0.696	0.672
XRF analysis (wt %)							
SiO2	58.69	53.29	65.91	65.25	57.99	56.501	57.18
Al2O3	16.05	14.81	15.69	15.44	15.81	15.438	15.98
TiO2	1.620	2.397	0.688	0.855	1.925	2.042	1.861
FeO*	8.23	11.31	5.17	5.18	8.44	9.527	8.83
MnO	0.207	0.341	0.178	0.197	0.206	0.247	0.210
CaO	4.86	7.64	1.94	2.31	5.34	5.729	5.46
MgO	1.94	2.76	0.36	0.59	1.95	2.314	2.36
K2O	2.53	1.85	3.85	4.89	2.54	2.443	2.33
Na2O	5.21	4.53	6.06	5.04	5.01	4.921	4.99
P2O5	0.667	1.079	0.148	0.240	0.779	0.836	0.815
Total	100.05	98.75	99.77	97.77	99.95	99.41	100.08
XRF analysis (ppm)							
Ni	2	0	6	6	0		0
V	22	89	1	0	64		50
Ba	725	578	961	990	780	743	729
Rb	47	25	78	76	43	50	46
Sr	489	503	209	243	465		498
Zr	299	264	465	427	322	245	283
Y	48	47	52	54	51		44
Nb	41.4	39.3	65.7	63.5	47.6		41.4
Ga	26	20	27	22	24		28
Cu	0	0	1	1	1		4
Zn	123	132	131	126	134	125	131
Pb	11	7	9	8	10		11
INA analysis (ppm)							
La	40.1	37.7	49.3	52.4	48.0	43.0	39.2
Ce	85.7	81.6	99.5	104.9	101.1	97.0	84.9
Nd	43.1	41.9	50.0	52.4	56.5	46.8	46.8
Sm	10.59	10.70	10.91	12.79	12.40	11.72	10.62
Eu	3.39	3.41	2.77	3.11	3.35	3.38	3.34
Tb	1.57	1.62	1.54	1.68	1.71	1.70	1.57
Yb	4.10	3.75	5.68	5.15	4.57	4.43	4.05
Lu	0.58	0.54	0.70	0.76	0.59	0.64	0.55
Sc	16.0	19.8	8.9	10.1	18.3	18.2	16.6
Cr	3	2	1	nd	9	9	3
Co	7.7	18.5	1.1	1.8	12.4	11.9	10.3
Cs	0.32	0.34	0.8	2.0	nd	0.3	0.57
Hf	8.4	7.2	13.6	13.0	9.3	8.5	8.0
Ta	2.5	2.2	3.5	3.5	2.6	2.6	2.3
Th	6.1	4.2	10.7	10.0	6.0	5.7	6.0
U	2.0	1.2	3.2	4.5	nd	nd	2.1

Table 11, continued.

Sample #	AM-89-43	AM-90-26	AM-90-27	AM-90-34	AM-90-35	AM-90-36	AM-89-33
Rock type:	L	L	L	L	L	L	T
Strat. Unit:	Thl	Twpu	Twpu	Twpu	Twpu	Twpu	Twpt
A.I.	0.638	0.860	1.290	1.137	1.164	0.831	0.737
XRF analysis (wt %)							
SiO2	53.95	66.23	68.76	70.74	70.02	61.66	68.95
Al2O3	15.10	17.21	11.00	12.13	12.17	15.65	13.35
TiO2	2.53	1.122	0.650	0.482	0.485	1.136	0.577
FeO*	10.77	2.64	8.69	5.95	6.36	7.76	6.17
MnO	0.204	0.038	0.190	0.117	0.152	0.227	0.183
CaO	6.91	2.04	0.40	0.36	0.61	3.40	2.12
MgO	2.79	0.19	0.12	0.24	0.01	0.86	0.96
K2O	1.97	3.57	4.43	4.58	4.53	3.05	4.67
Na2O	4.56	6.65	5.71	5.37	5.63	5.90	2.91
P2O5	1.186	0.313	0.038	0.023	0.023	0.356	0.091
Total	99.43	99.15	99.06	98.73	99.56	98.56	95.41
XRF analysis (ppm)							
Ni	0	11	7	6	5	5	7
V	91	4	21	0	0	3	6
Ba	574	1041	786	561	480	1055	204
Rb	35	64	82	101	100	56	95
Sr	503	360	15	18	13	370	74
Zr	263	411	516	556	552	348	488
Y	48	68	81	51	47	49	68
Nb	37.6	58.7	86.5	94.1	91.1	54.3	72.5
Ga	23	27	31	30	27	25	29
Cu	0	6	7	0	0	3	5
Zn	128	81	268	165	149	122	162
Pb	4	7	13	16	7	7	12
INA analysis (ppm)							
La	39.2	58.3	87.2	58.5	67.6	55.1	57.1
Ce	85.6	107.9	133.6	143.6	127.2	112.3	117.5
Nd	49.4	58.0	91.8	60.8	65.2	59.1	60.8
Sm	11.32	13.34	20.03	13.29	13.96	13.12	12.99
Eu	3.58	3.86	4.71	2.68	2.65	3.81	2.22
Tb	1.70	2.23	2.83	1.63	1.64	1.73	1.82
Yb	3.98	6.98	8.44	5.59	5.59	5.16	6.58
Lu	0.54	1.11	1.26	0.83	0.84	0.72	1.06
Sc	19.9	11.9	7.0	3.1	3.1	15.8	3.0
Cr	3	nd	nd	nd	nd	nd	3
Co	16.9	0.77	0.74	0.34	0.10	4.0	1.1
Cs	0.37	0.64	0.49	0.56	1.8	0.9	2.0
Hf	7.2	13.3	16.9	17.3	17.0	10.3	12.9
Ta	2.2	3.6	4.8	5.3	5.0	3.0	3.5
Th	5.0	8.1	13.3	15.1	14.3	8.4	9.0
U	1.4	1.9	3.6	2.8	2.6	3.0	nd

Table 11, continued.

Sample #	AM-89-14	AM-89-40	AM-89-93*
Rock type:	I	VI	I
Strat. Unit:	Twpi	Twpi	Twpi
A.I.	1.146	1.002	1.123
XRF analysis (wt %)			
SiO2	71.27	70.06	69.998
Al2O3	12.62	12.03	13.170
TiO2	0.377	0.524	0.344
FeO*	4.82	7.29	4.768
MnO	0.120	0.337	0.188
CaO	0.38	1.05	0.860
MgO	0.05	0.30	0.071
K2O	4.45	3.05	4.574
Na2O	5.86	5.32	5.984
P2O5	0.041	0.042	0.042
Total	99.10	96.31	99.31
XRF analysis (ppm)			
Ni	9	9	
V	0	0	
Ba	746	320	754
Rb	95	96	89
Sr	21	14	
Zr	536	527	411
Y	72	84	
Nb	78.1	85.3	
Ga	27	30	
Cu	9	2	
Zn	164	205	160
Pb	13	14	
INA analysis (ppm)			
La	72.0	74.3	70.9
Ce	146.6	158.0	147.2
Nd	71.9	74.9	65.5
Sm	14.75	15.43	14.93
Eu	2.79	2.72	2.82
Tb	2.09	2.37	2.11
Yb	7.29	7.66	7.17
Lu	1.03	1.08	1.05
Sc	2.7	2.5	1.6
Cr	3	4	nd
Co	0.1	0.1	0.24
Cs	0.54	2.5	0.5
Hf	15.8	14.9	16.0
Ta	4.6	4.5	4.7
Th	13.4	9.8	13.3
U	2.1	3.0	2.1

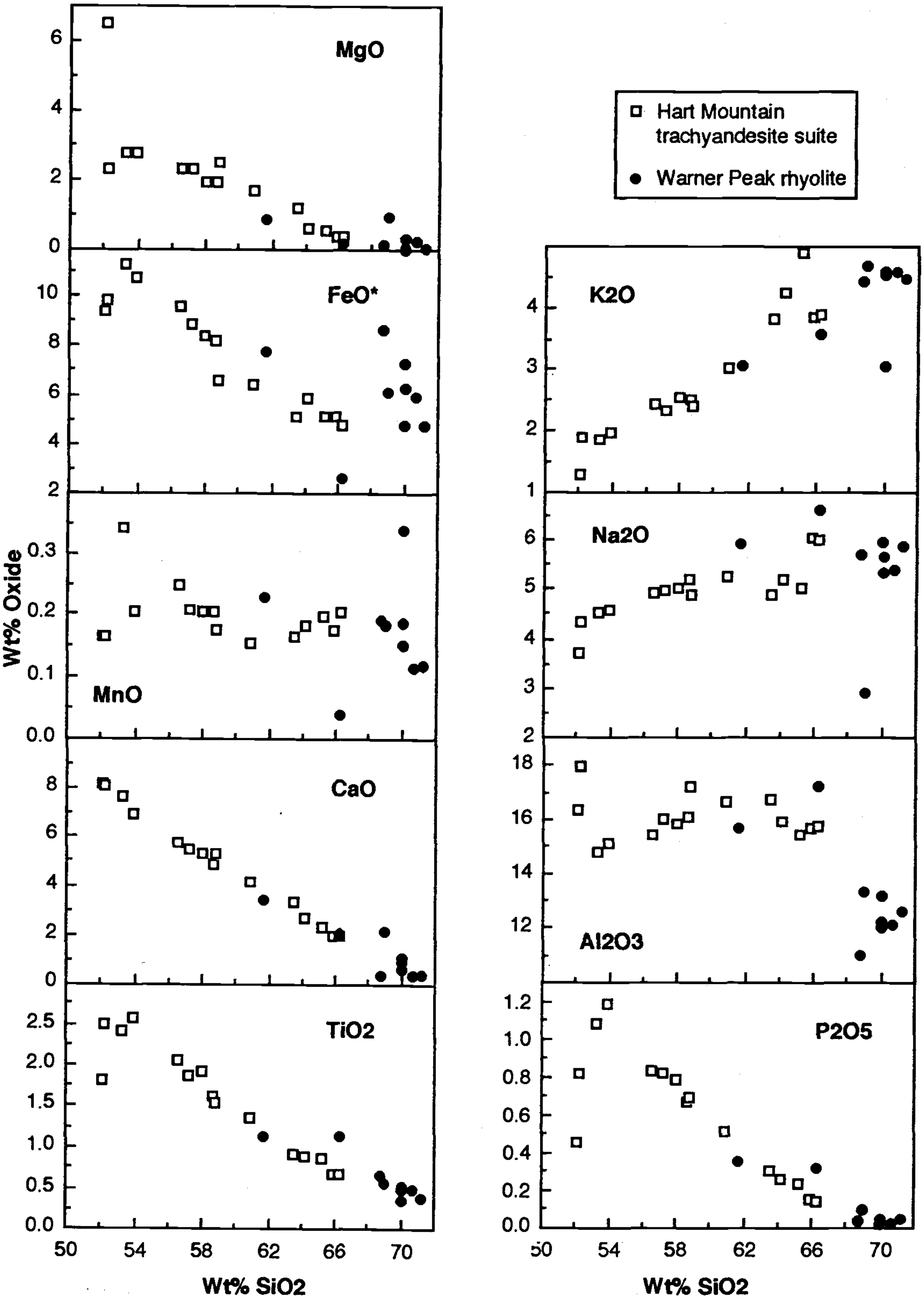

Figure 15: Major element variation diagrams for the Hart Mountain volcanic complex.

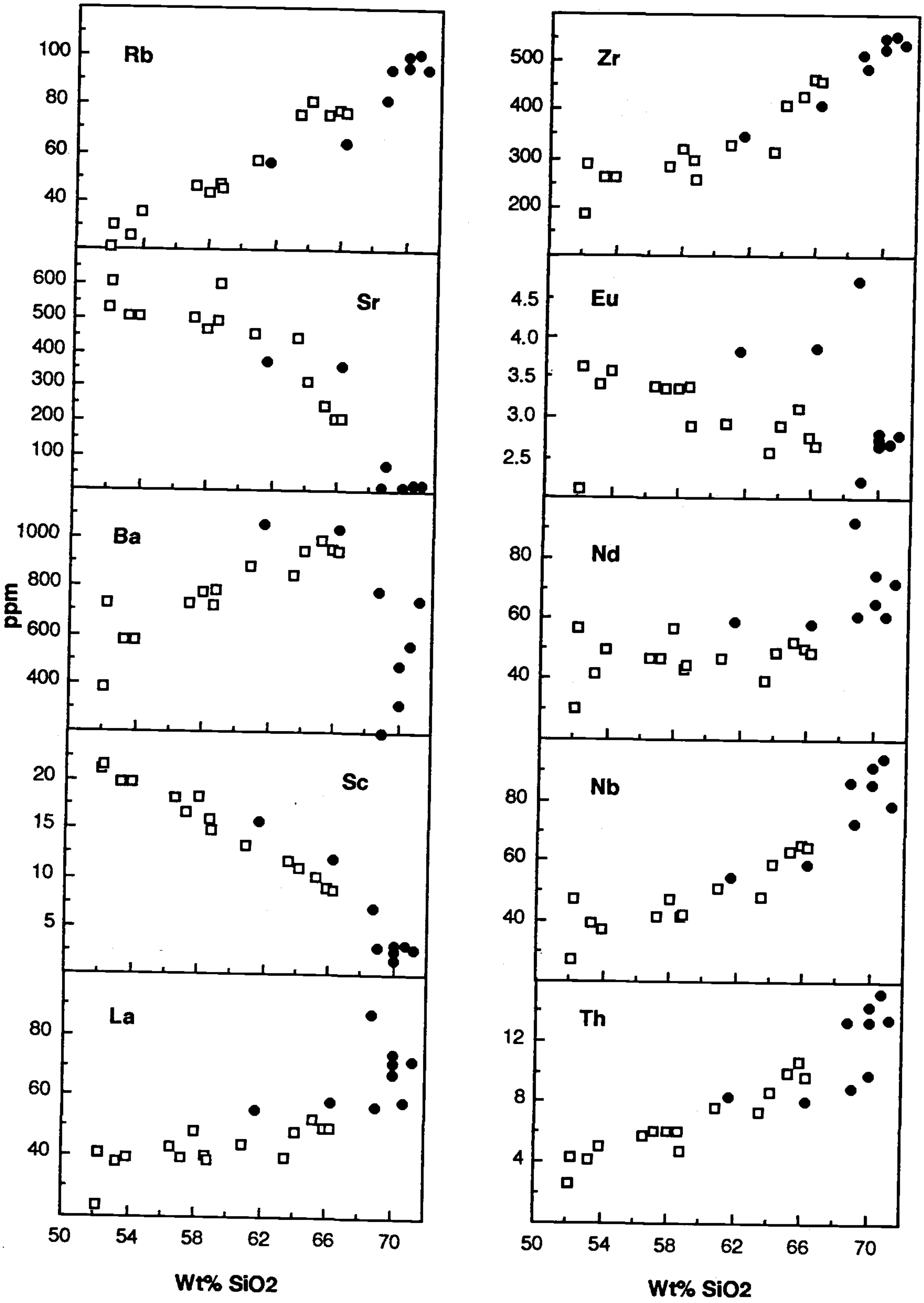

Figure 16: Trace element variation diagrams for the Hart Mountain volcanic complex. Symbols are the same as Figure 15.

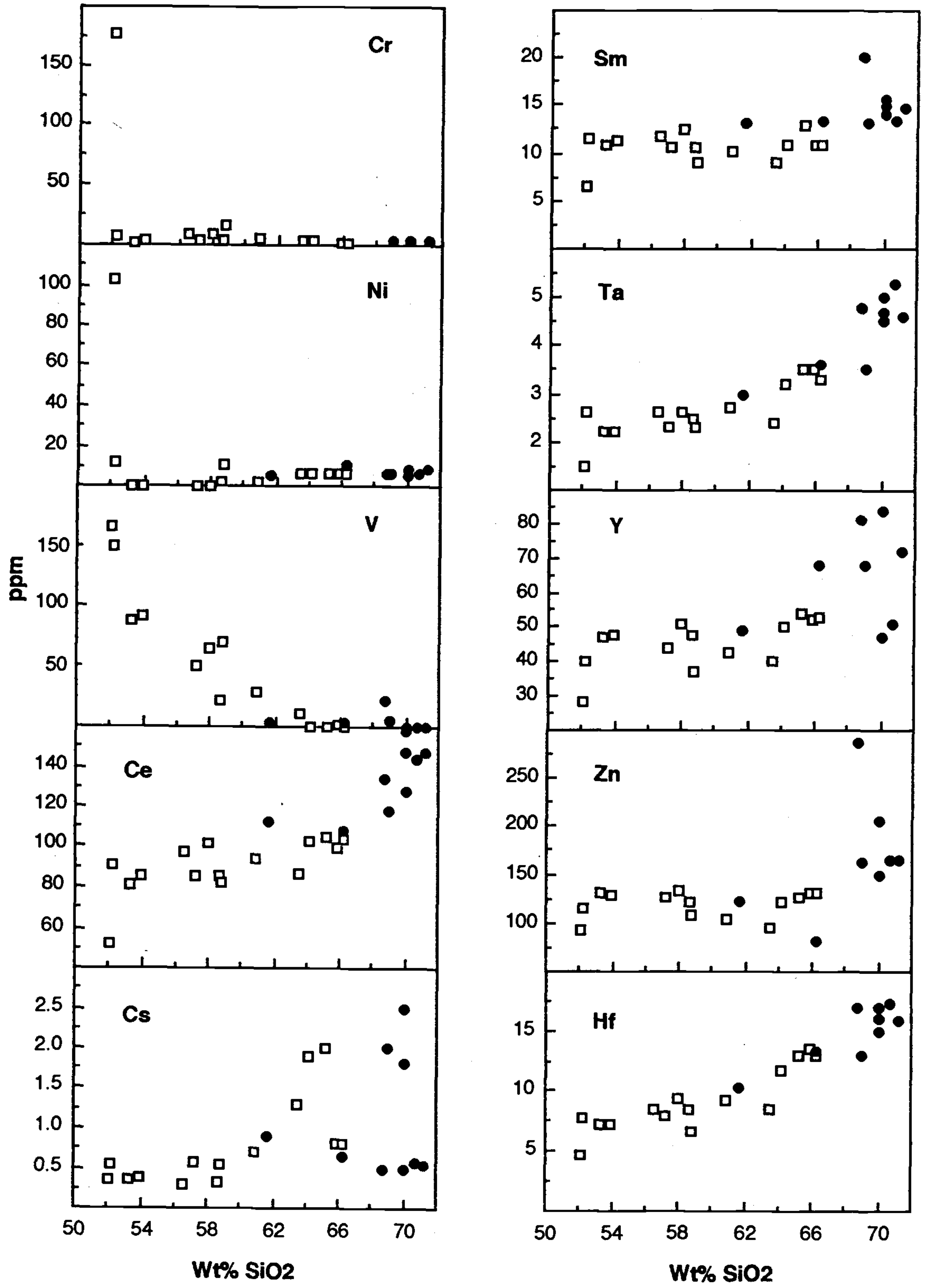

Figure 16, continued.

between 54.0 and 56.5 wt % and between 58.8 and 60.8 wt %, but these may result from incomplete sampling. The agpaitic index (molar Na_2O+K_2O/molar Al_2O_3) ranges from 0.46 to 0.90. All samples are hypersthene normative. MgO and CaO decrease, and K_2O and Na_2O increase with increasing SiO_2 content. FeO*, TiO_2, and P_2O_5 reach maxima in the basaltic trachyandesite field (SiO_2 53-54 wt %) and then systematically decrease with increasing differentiation. Al_2O_3 (17.9 to 14.8 wt %) in the Hart Mountain trachyandesite suite displays no distinctive trend with differentiation.

Samples from the Warner Peak rhyolite range from 61.7 to 71.3 wt % SiO_2, and include two trachytes. The rhyolites are enriched in FeO* (4.82-8.69 wt %) and depleted in Al_2O_3 (11.0-13.3 wt %) relative to the trends in the Hart Mountain trachyandesite suite. A small apparent silica gap (66.2 to 68.8 wt %) exists between the trachytes and most of the rhyolites. All unaltered rhyolites analyzed from the Warner Peak rhyolite are peralkaline with 7.5 to 14.5% normative acmite and with agpaitic index as high as 1.29. Compositions range from pantellerite to comendite (see Figure 22a). Two samples (AM-89-33 and AM-89-40) are hydrated and/or devitrified, and have likely lost alkalies (Figure 6). These samples are interpreted to be peralkaline despite agpaitic indices less than or equal to 1 because they have mineralogies identical to the peralkaline rhyolites, and the more refractory oxides, such as FeO* and Al_2O_3, have values well within the range found in the unaltered samples (see Figure 22a).

Trace element concentrations for the Hart Mountain trachyandesite suite are similar to mafic and intermediate rocks associated with peralkaline rhyolites elsewhere (Mahood and Baker, 1986; Civetta et al., 1984; Novak and Mahood, 1986). Compatible elements, Cr, V, Sc, and Sr decrease and incompatible elements, Rb, Ba, Th, REEs, and the high field strength elements (Zr, Hf, Nb, and Ta) increase with differentiation. Most trace elements in the Warner Peak rhyolite roughly follow the same differentiation trends as in the Hart Mountain trachyandesite suite with the exceptions of a marked enrichment of REE and a strong depletion of Ba concentrations in the rhyolites. Among samples of the Warner Peak rhyolite, most trace element concentrations do not vary systematically with increasing SiO_2 or increasing peralkalinity. A few systematic compositional changes are found within the pantellerite suite: Rb, Nb, and Zr decrease, and REE (except Ce) concentrations increase with increasing peralkalinity. The most peralkaline sample (AM-90-27) has the highest agpaitic index (1.290), the smallest europium anomaly (Eu/Eu* 0.748), and the highest concentrations of Ba, Zn, Sc, and REE (except Ce) among the peralkaline rhyolites.

REE variations within the Hart Mountain volcanic complex are illustrated in Figures 17, 18, and 19. In the Hart Mountain trachyandesite suite (Figure 18), light rare earth elements (LREE) are enriched 76 to 158 times chondrites and heavy rare earth elements (HREE) are 9 to 22 times chondrite with the enrichments increasing with differentiation. The trachybasalts and basaltic trachyandesites have no to negligible positive Eu anomalies (Eu/Eu* 1-1.022), and the trachytes have moderate negative europium anomalies (Eu/Eu* 0.778-0.930). For samples collected between Juniper and Mulkey Canyons, REE increase systematically with stratigraphic position (Figure 18a). In the Warner Peak rhyolite (Figure 19), LREEs are enriched 177 to 280 times chondrites and HREEs are 22 to 39 times chondrite. REE plots lack systematic compositional differences between pantellerites and comendites. Two pantellerites (AM-90-27 and AM-90-34) span the REE compositional range (except Eu) and for Eu anomalies (AM-90-27 and AM-89-40; Eu/Eu* 0.541-0.748) in rhyolites.

Concentrations of some major (Na_2O and K_2O) and trace elements (including REE) in the peralkaline rhyolites cannot be considered magmatic because of compositional changes with

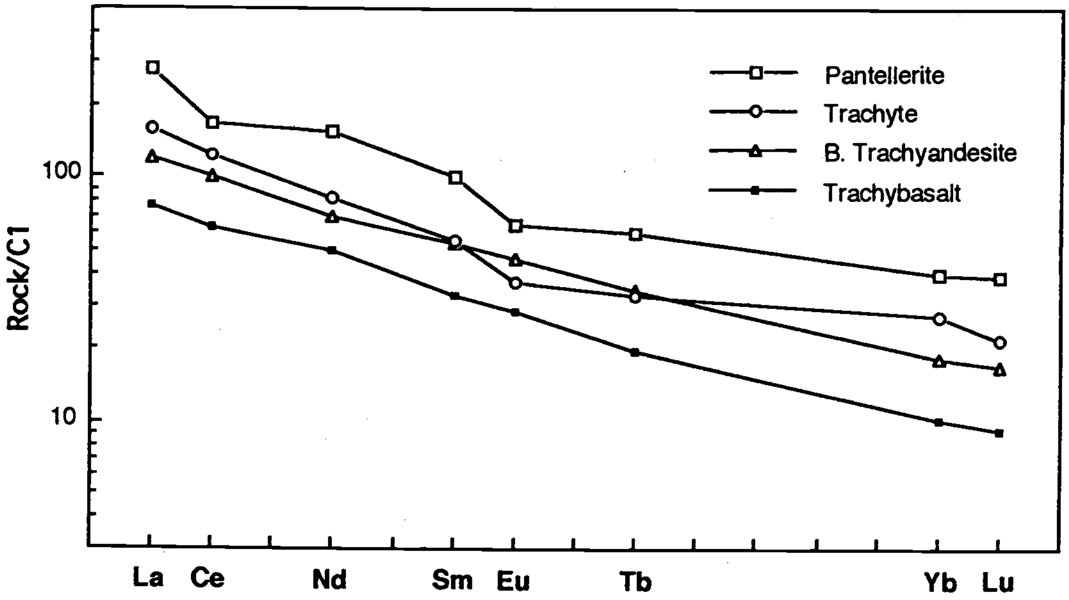

Figure 17: Range of REE concentrations found in samples of the Hart Mountain volcanic complex. Trachybasalt = AM-90-23; b. trachyandesite (basaltic trachyandesite) = AM-89-61; trachyte = AM-89-90; pantellerite = AM-90-27. Values for the non-volatile C1 chrondrite normalization are modified from Anders and Ebihara (1982).

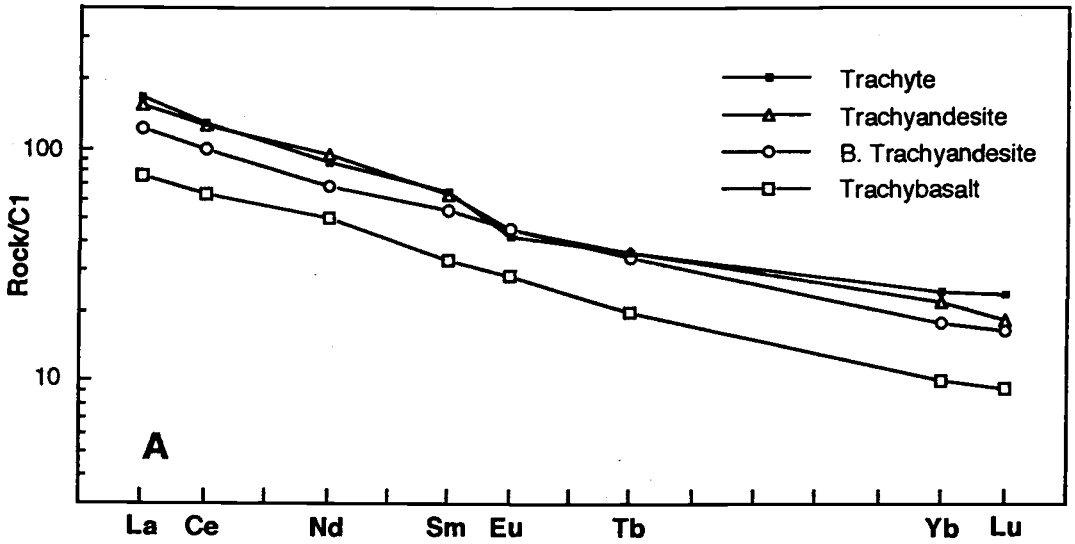

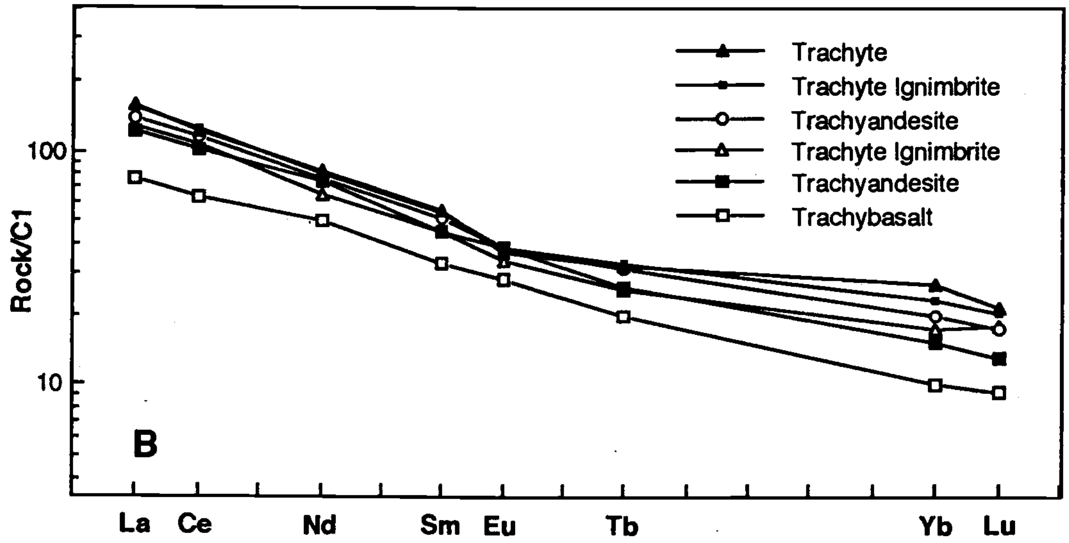

Figures 18A and B: Concentrations of REEs found in selected samples of the Hart Mountain trachyandesite suite. A. The range of REE concentrations found in the Hart Mountain trachyandesite suite. Trachybasalt = AM-90-23; b. trachyandesite = AM-89-61; trachyandesite = AM-89-65; trachyte = AM-90-02. B. Increasing REE concentrations with increasing stratigraphic height. Trachybasalt = AM-90-23 (Tvc); trachyandesite = AM-89-92 (Tvc); trachyte ignimbrite = AM-89-85 (Tiw); trachyandesite = AM-89-74 (Tvl); trachytic ignimbrite = AM-89-81 (Tis); Trachyte = AM-89-90 (Tv3).

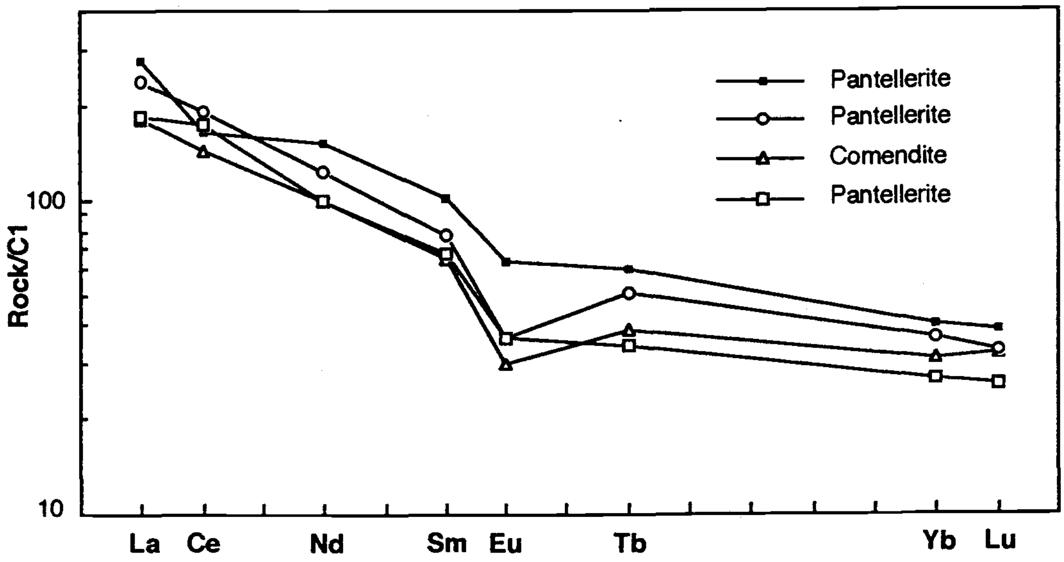

Figures 19: The range of concentrations of REEs found in samples of the Warner Peak rhyolite. Pantellerite = AM-90-27, AM-89-40, and AM-90-34; comendite = AM-89-33.

crystallization and/or hydration (Weaver et al., 1990; Baker and Henage, 1977; Macdonald and Bailey, 1973; Noble, 1968). Most samples of the Warner Peak rhyolite were microcrystalline, except for AM-89-40 which was a hydrated vitrophyre (XRF prenormalized total = 96.3 wt %), and AM-89-33 which was a hydrated devitrified whole rock ignimbrite sample (XRF prenormalized total = 95.4 wt %).

Crystallization of peralkaline rhyolites causes losses of Na (8-19%), Cs (>75%), F and Cl (as large as 75-96%), and Y and REE (5 to >60%) with a decrease of Ce/Yb ratios as large as 20% (Weaver et al., 1990). Baker and Henage (1977) report gain or losses of REE and Y. Hydration causes gain of Sr and Mg, loss of Na (Weaver et al., 1990), and loss or gain of K (Macdonald and Bailey, 1973). Sample AM-89-33 has the highest Mg and Sr and the lowest Na of the peralkaline rhyolites probably resulting from the hydration of that sample. AM-89-33 and AM-89-40 also have the highest Cs concentrations found in the Warner Peak rhyolite.

The trachytic ignimbrites of the Hart Mountain trachyandesite suite (AM-89-81, AM-89-85, and AM-90-02) are compositionally distinct from the trachyte lavas (AM-89-55 and AM-89-90) erupted from the Hart Mountain volcanic complex. Compared to the lavas of similar wt % SiO_2, the ignimbrites have more K_2O, and Cs, and less Na_2O. Although these samples are not peralkaline (agpaitic indices 0.73-0.90), these compositional changes likely result from devitrification and hydration processes similar to that in peralkaline rocks.

The trachyte lavas from the Warner Peak rhyolite have less K_2O and Rb, and more Na_2O, La, Sc, and REEs than those of the Hart Mountain trachyandesite suite.

Some variations of major and trace element concentrations in rocks of the Hart Mountain volcanic complex correlate with lithology. There are systematic compositional variations with texture. Trachybasalt AM-90-23, the most primitive sample (MgO=6.48, Ni 103), is compositionally distinct and is the only sample with appreciable olivine (approximately 3 modal %). It is from the lowest exposed unit of the Hart Mountain volcanic complex (Tvc). AM-89-92, also from map unit Tvc, is a mingled lava containing abundant clasts of olivine basalt (like AM-90-23) in a trachyandesitic matrix and appears to result from the mingling of 20-25% of a trachybasalt like AM-90-23 with a trachyandesite like AM-89-74.

Major and trace element concentrations of many samples of the Warner Peak rhyolite do not vary systematically with modal mineralogy (Table 4). Pantellerites AM-90-34 and AM-90-35 have very similar compositions, but different mineralogies: AM-90-35 contains ferrohedenbergite phenocrysts and only trace amounts of amphibole; AM-90-34 has phenocrystic amphibole and only trace amounts of ferrohedenbergite in the groundmass. A similar relationship exists between comendites AM-89-14 and AM-89-93: AM-89-93 has modal amphibole, and AM-89-14 does not.

DISCUSSION

The rocks of the 26.4 Ma Hart Mountain volcanic complex are compositionally unique among suites of Tertiary volcanic rocks in the Basin and Range where suites containing peralkaline silicic rocks are rare relative to metaluminous suites (Noble and Parker, 1974). Between about 31 and 20 Ma, voluminous outpourings of metaluminous rhyolitic and dacitic ignimbrites (the "ignimbrite flareup") and subordinate lava flows characterized volcanism in the Great Basin (Stewart and Carlson, 1976; Best and Christiansen, 1991). Volcanic activity mainly occurred across central Nevada. Elsewhere in southern Oregon rocks older than the Steens Basalt consist predominantly of intermediate calc-alkaline rocks (Figure 4; Fuller, 1931; Muntzert, 1969; Wells, 1979; Thomas, 1981; Duffield and McKee, 1986; Langer, 1991).

Mildly peralkaline rhyolites are found in several other locations in the Basin and Range (Figure 20). Three of the

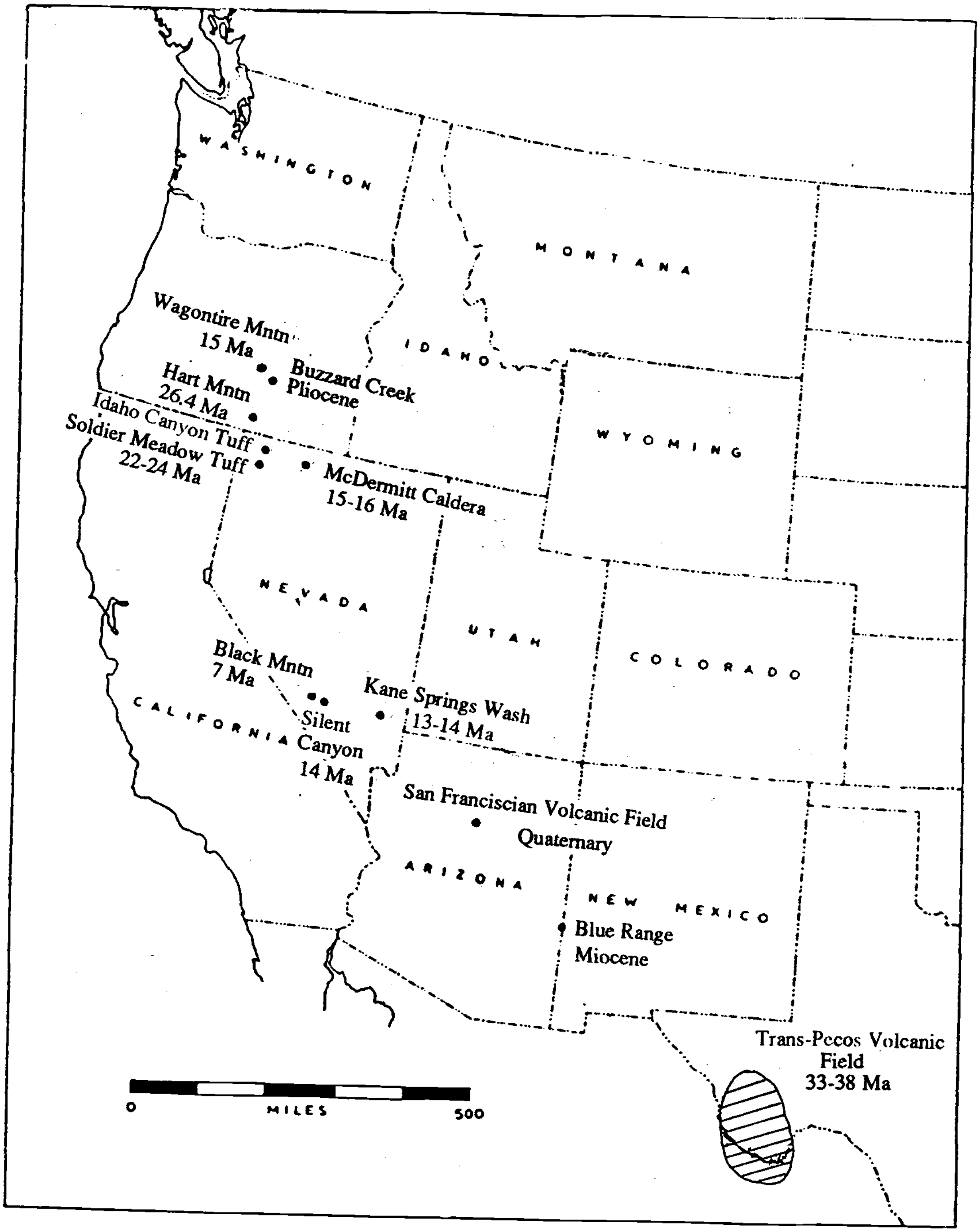
WASHINGTON
MONTANA
IDAHO
WYOMING
NEVADA
UTAH
COLORADO
CALIFORNIA
ARIZONA
NEW MEXICO
Wagontire Mntn
15 Ma
Buzzard Creek
Pliocene
Hart Mntn
26.4 Ma
Idaho Canyon Tuff
Soldier Meadow Tuff
22-24 Ma
McDermitt Caldera
15-16 Ma
Black Mntn
7 Ma
Silent Canyon
14 Ma
Kane Springs Wash
13-14 Ma
San Franciscian Volcanic Field
Quaternary
Blue Range
Miocene
Trans-Pecos Volcanic Field
33-38 Ma
0
MILES
500

Figure 20: Map of the western United States showing the locations and ages of peralkaline rhyolites found in the Basin and Range. All locations are mildly peralkaline except for Hart Mountain (after Noble and Parker, 1974).

most significant centers of peralkaline volcanism are the Kane Spring Wash caldera, southern Nevada (13-14 Ma; Novak, 1984; Novak and Mahood, 1986); McDermitt caldera, northern Nevada (15-16 Ma; Wallace et al., 1980; Conrad, 1984; Rytuba and McKee, 1984); and the Trans-Pecos volcanic field in southwest Texas (35 Ma; Parker, 1983). The peralkaline rhyolites at Hart Mountain are the most peralkaline described from the Basin and Range, and the oldest peralkaline rhyolites in the Great Basin (Noble et al., 1974; Noble and Parker, 1974). In southern Oregon, mildly peralkaline rhyolite ash flow tuffs have erupted during the late Tertiary in the Harney Basin region (Walker and Swanson, 1968a; Walker, 1970; Enlows, 1976; Greene, 1973; Streck, in progress) including occurrences at Wagontire Mountain and Buzzard Creek.

The Hart Mountain volcanic complex has characteristics intermediate between those of strongly peralkaline centers and weakly peralkaline centers (Table 12; Figures 21 and 22). Strongly peralkaline volcanic centers are typified by Pantelleria (Mahood and Baker, 1986; Civetta et al., 1984, 1988), and by Socorro Island (Bryan, 1966, 1970, 1976). Characteristics of strongly peralkaline centers include: a compositional gap between mafic and silicic endmembers; strong iron enrichment, modest negative europium anomalies, and extreme enrichments of incompatible elements in the rhyolites; and molar Na/K > 1.5. McDermitt caldera (Wallace et al., 1980; Conrad, 1984; and Rytuba and McKee, 1984) and Kane Spring Wash caldera (Novak and Mahood, 1986) are representative of mildly peralkaline centers found elsewhere in the Basin and Range, which differ in that the peralkaline rocks are high-silica rhyolites and are associated with subalkaline rhyolites.

The Hart Mountain volcanic complex more closely resembles a strongly peralkaline system: pantellerites are present (although without the characteristic modal mineral aenigmatite); the rhyolites have modest Eu negative anomalies

Table 12: Characteristics of strongly peralkaline and weakly peralkaline volcanic systems.

	Strongly peralkaline volcanic systems	Weakly peralkaline volcanic systems	Hart Mountain volcanic complex
Compositional gap (>8 wt% SiO2)	X		
Silicic Rocks			
Presence of high-Si rhyolites		X	
Presence of subalkaline rhyolites		X	
Presence of pantellerites	X		X
Extreme enrichments of incompatible elements	X		
Modest negative Eu anomalies	X		X
Fe enrichment	X		X
molar Na/K > 1.5	X		X
Mafic rocks			
High P2O5	X		X

Characteristics of strongly peralkaline volcanic systems are summarized from Pantelleria (Mahood and Baker, 1986; Civetta et al., 1984, 1988) and Socorro Island (Bryan, 1966, 1970). Characteristics of mildly peralkaline volcanic systems are taken from Kane Springs Wash caldera (Novak and Mahood, 1986) and McDermitt caldera (Rytuba and McKee, 1984; Conrad, 1984; and Wallace et al., 1980). Mahood (1984) described volcanological aspects of strongly peralkaline systems.

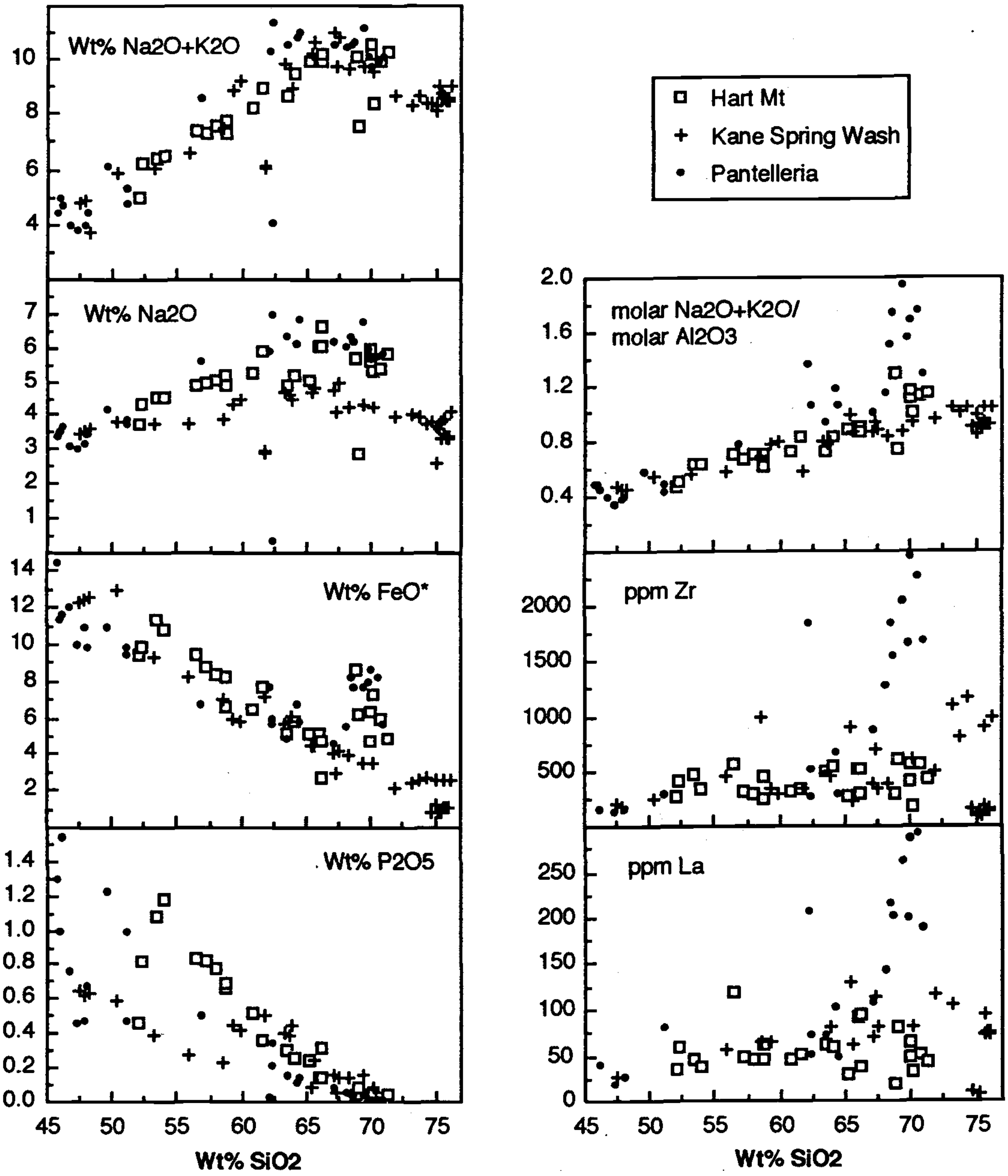

Figure 21: Selected variation diagrams demonstrating the compositional differences between rocks of the Hart Mountain volcanic complex, Kane Springs Wash caldera (weakly peralkaline), and Pantelleria (strongly peralkaline). Data from Pantelleria compiled from Civetta et al. (1984, 1988), and Mahood and Baker (1986). Data from Kane Spring Wash compiled from Novak (1984), and Novak and Mahood (1986).

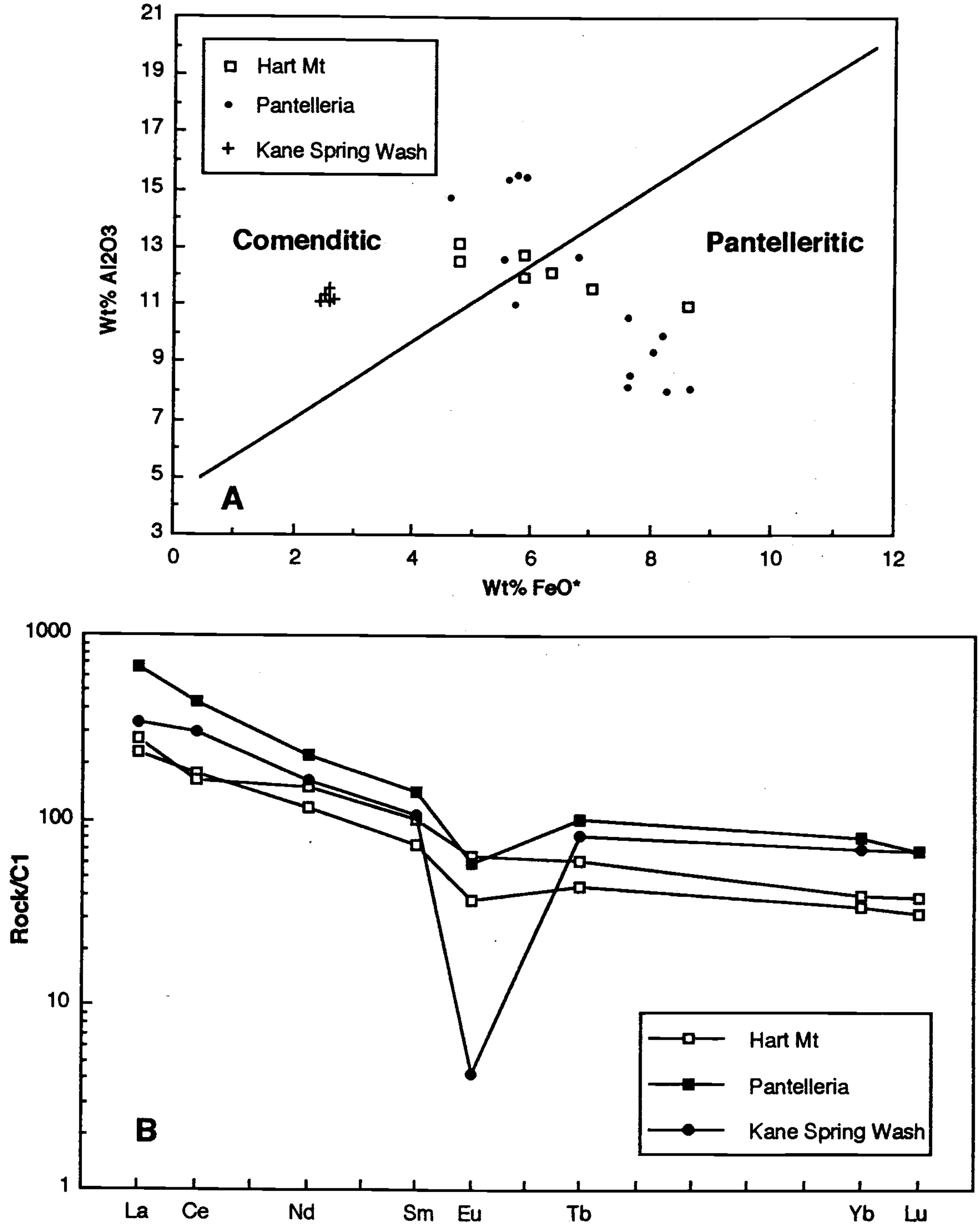

Figures 22A and B: Compositional differences between the peralkaline rhyolites of the Hart Mountain volcanic complex, Kane Springs Wash caldera, and Pantelleria. A. Weight percent Al_2O_3 versus weight percent FeO*. Classification follows LeMaitre (1989). B. REE patterns of representative peralkaline rhyolites from each suite. Data for these plots compiled from the same sources as in Figure 21.

and strong Fe enrichment and are not associated with subalkaline rhyolites; and molar Na/K is greater than 1.5. The Hart Mountain rhyolites fall within the compositional range of the Pantelleria samples on a plot of refractory oxides Al_2O_3 versus FeO* (Figure 22a).

Notable ways that the Hart Mountain volcanic complex differs from other strongly peralkaline volcanic systems include the relatively low agpaitic indices (only as high as 1.3 at Hart Mountain, but as high as 2.0 at Pantelleria), lack of a significant silica gap and of extreme enrichments of incompatible elements in the rhyolites. The low agpaitic indices and the low concentrations of REEs and some trace elements (such as Y) in the Warner Peak rhyolite relative to other pantellerites is partially explained by loss of Na, Y, and REE with crystallization in peralkaline silicic rocks (Weaver et al., 1990; Baker and Henage, 1977; Macdonald and Bailey, 1973; Noble, 1968). However, rhyolites at Hart Mountain have concentrations of Zr, which is unaffected by crystallization and hydration (Weaver et al., 1990), two to five times lower than the concentrations found at Pantelleria. Indeed, the Warner Peak rhyolites have concentrations of Zr less than those of the mildly peralkaline rhyolites at Kane Spring Wash (Figure 21).

Chapter Four: Petrogenesis of the Hart Mountain Volcanic Complex

METHODS

Crystal fractionation and mixing models were made using the program MacGPP (Geist et al., 1989). Mass balance major element crystal fractionation and mixing calculations are based on a matrix inversion procedure which determines the proportions of a set of components, which when added to or subtracted from a parent, give the best least-squares fit to a given daughter composition. Best fit solutions minimize the sum of the squares of the residuals (ΣR^2). Trace element tests of fractionation models were done using Rayleigh fractionation. Input data consist of observed parent and daughter compositions, and compositions of the fractionating phases. Output calculations yield ΣR^2, percent of fractionation, weight proportions of the phases added or subtracted, and a calculated daughter composition.

When possible, mineral compositions of fractionating phases were taken from microprobe analyses of minerals present in the parental samples. Compositions of Fe-Ti oxides, and olivine in the trachyandesite to rhyolites lack microprobe analyses and data were taken from samples of similar whole rock compositions from Pantelleria (Mahood and Baker, 1986; Mahood and Stimac, 1990), Kane Springs Wash (Novak and Mahood, 1986), and Socorro Island (Bryan, 1976). Apatite is from Deer et al. (1966).

Fits of major element models in the trachybasalt to trachyte range were very sensitive to the Fe-Ti oxide composition used in the model. A wide range of Fe-Ti oxide compositions was reported from individual samples from Pantelleria (Mahood and Baker, 1986; Mahood and Stimac, 1990). Therefore, ΣR^2 values may be artificially high or low depending whether the composition used in the particular model truly represents compositions found in rocks of the Hart Mountain volcanic complex. However, the opaque oxide composition used in a particular model did not significantly change the proportions of Fe-Ti oxide fractionating. Therefore, the effect on trace element tests of best fits should be minimal. This is especially true in trachytes to rhyolites where Fe-Ti oxides make up 1-3% of the fractionating assemblage.

PARTITION COEFFICIENTS

Partition coefficients (Kds; Table 13) used in trace element tests of the major element crystal fractionation models are from Lemarchand et al. (1987) for trachybasalts to trachytes, and from Mahood and Stimac (1990) for the trachyte to peralkaline rhyolite interval. Kds for plagioclase in the trachyte to peralkaline rhyolite models were also from Lemarchand et al. (1987). Apatite Kds for the mafic to intermediate range are from Luhr et al. (1984).

In general, partition coefficients increase with bulk SiO_2 because of increasing melt polymerization. However, in peralkaline suites, increasing peralkalinity decreases melt polymerization from trachyte to peralkaline rhyolite, and correspondingly, some partition coefficients decrease over this interval of increasing differentiation. Alkali feldspar/melt partition coefficients for Rb, Ba, Sr, and Eu decrease significantly over the interval from trachyte to pantellerite (Mahood and Stimac, 1990). The ecrease for Eu is a hundredfold. The change in the behavior of Eu from strongly compatible to an incompatible element, partially attributed to the decrease of Eu^{2+}/Eu^{3+} with melt peralkalinity, explains the small Eu anomalies characteristic of strongly peralkaline rhyolites (Mahood and Stimac, 1990).

Mahood and Stimac (1990) report partition coefficients from samples with agpaitic indices of 0.94 to 1.95. Kds used in trace element tests of crystal fractionation models used Kds from samples with agpaitic indices of 0.9-1.2 because that is the compositional range of the trachytes and peralkaline rhyolites of the Hart Mountain volcanic complex.

Table 13: Partition coefficients between mineral and listed silicate melt used in fractionation models.

	Plagioclase			Clinopyroxene				Olivine			Fe-Ti Oxides			Apatite		Alkali feldspar	
	maf.	Int.	sil.	maf.	int.	trach.	rhy.	maf.	int.	sil.	maf.	int.	sil.	maf-int.	sil.	trach.	sil.
La	0.07	0.23	0.23	0.21	0.2	0.28	0.51	0.06	0.4	0.1	0.2	0.15	0.07	21.7	27	0.071	0.004
Ce	0.08	0.20	0.20	0.2	0.5	0.48	0.81	0.06	0.6	0.1	0.1	0.15	0.07	25.8	31	0.035	0.002
Sm	0.06	0.20	0.20	0.7	0.9	1.6	1.7	0.02	0.3	0.1	0.15	0.2	0.08	31.4	38	0.0086	0.002
Eu	0.18	1.34	1.34	0.80	1.0	1.65	1.7	0.03	0.21	0.1	0.42	0.15	0.07	25.2	30	2.5	0.57
Tb	0.04	0.06	0.06	1.01	1.5	1.9	1.3	0.02	0.52	0.1	0.29	0.4	0.07	34	30	0.0035	0.002
Yb	0.03	0.2	0.20	0.9	1.0	1.4	1.3	0.02	1	0.35	---	0.4	0.05	12.3	10	0.004	0.002
Lu	---	---	0.20	---	---	1.4	1.8	---	---	0.44	---	---	0.08	---	7	0.0024	0.001
Sc	0.04	0.06	0.05	4.05	27.60	27	27	0.24	0.92	1.6	5.36	10	2.5	0.45	0.3	0.006	0.009
Zr	0.04	0.16	0.16	0.44	0.4	0.5	0.3	0.07	0.07		0.94	3.98	0.25	---	2.0	---	---
Hf	0.02	0.03	0.20	0.64	0.05	0.2	0.4	0.02	0.09	0.1	0.91	2.51	0.25	---	0.07	0.0001	---
Ta	0.03	0.03	---	0.23	0.47	0.04	0.014	0.02	0.14	0.1	2.17	2.55	2.2	0.25	0.05	0.001	0.001
Th	0.03	0.05	0.05	0.15	0.03	0.01	0.01	0.03	0.12	0.1	0.25	0.27	0.03	1.76	1.6	0.001	0.001
U	0.03	0.04	---	0.08	0.04	---	---	0.04	0.14	---	0.30	0.29	---	1.82	---	---	---
Rb	0.03	0.07	0.07	0.04	0.04	---	---	0.05	0.08	---	0.34	0.14	---	---	0.4	0.11	0.26
Sr	2	5	5.0	0.3	0.3	---	---	0.01	0.2	---	0.1	0.08	---	---	8.0	10	3.6
Ba	0.6	0.6	0.6	0.1	0.2	---	---	0.03	0.09	---	0.2	0.2	---	0.2	0.45	5.9	5.0
Co	0.08	---	---	1.55	---	---	---	6.43	---	---	8.52	---	---	---	---	---	---
Cr	0.07	---	---	1.5	---	---	---	5.0	---	---	5	---	---	---	---	---	---

Notes: Partition coefficents for the following compositional intervals: maf.=trachybasalt to basaltic trachyandesite; int.=trachyandesite to trachyte; sil.=trachyte to peralkaline rhyolite; trach.=trachyte; rhy.=peralkaline rhyolite with agpaitic index approximately 1.2. Kds for mafic and intermediate compositions are from Lemarchand et al. (1987). Silicic, trachyte and rhyolite Kds are from Mahood and Stimac (1990) except for plagioclase which is from Lemarchand et al. (1987). Mafic-intermediate Kds for apatite are from Luhr et al. (1984).

HART MOUNTAIN TRACHYANDESITE SUITE

Crystal fractionation and/or magma mixing models can account for the compositions of most of the samples erupted from the Hart Mountain volcanic complex (Figures 15 and 16). Crystal fractionation models (Table 14 and 15) were calculated for the following compositional intervals: trachybasalt to basaltic trachyandesite (AM-90-23 to AM-89-61), basaltic trachyandesite to trachyandesite (AM-89-61 to AM-89-74), trachybasalt to trachyandesite (AM-90-23 to AM-89-74 and AM-90-23 to AM-89-65), and trachyandesite to trachyte (AM-89-74 to AM-89-90). Magma mixing models (Table 16) were applied for some of the trachyandesites. Figure 23 is a summary of the proposed petrologic evolution of the Hart Mountain trachyandesite suite.

Models were considered acceptable when major element ΣR^2 values were less than 0.300 using fractionating assemblages containing petrologically reasonable mineral compositions and proportions, and when most trace elements were modeled to within 10% of the observed concentrations (which is within analytical error for most elements). Fits of certain trace elements were assigned more importance than other trace elements. For example, incompatible elements Rb and Zr do not vary linearly with each other (Figure 24): Rb should more accurately reflect differentiation because, unlike Zr, it is not sensitive to possible zircon crystallization, and because it shows less variation than Zr when plotted against other elements. Similarly, REE concentrations may be controlled by apatite fractionation. Fits of incompatible elements Th, Ta, and Ba, and compatible elements Sr and Sc were also significant in evaluating major element models.

TRACHYBASALT AND BASALTIC TRACHYANDESITES

The basaltic trachyandesites (AM-89-61, AM-89-42, and AM-90-29) can not be modeled through crystal fractionation of trachybasalt AM-90-23. AM-90-23 was selected as a parent because it is the most primitive sample collected from the

Table 14: Summary of crystal fractionation models of the petrogenesis of samples of the Hart Mountain trachyandesite suite.

Parent-	F	Plagioclase		Clinopyroxene		Olivine		Fe-Ti ox	Apat	∑R2	Rb	Rb
Daughter	%	comp	%	comp	%	comp	%	%	%		obs.	calc.
TB-TBA (23-61)	68.3	An63	20.3	Fs15	2.1	Fo85	9.2			.600	25	30
TB-TA (23-65)*	42.7	An52	32.0	Fs15	12.9	Fo78	8.4	3.8	0.3	.203	43	47
TB-TA (23-74)*	38.3	An52	32.8	Fs15	15.2	Fo78	7.8	5.3	0.6	.194	57	52
BTA-TA (61-65)	72.0	An41	11.3	Fs16	9.5	Fo53	0.6	5.1	1.4	.300	43	34
BTA-TA (61-74)	64.1	An41	13.4	Fs16	12.9	Fo53	0.2	7.5	2.0	.675	57	37
TA-TA (65-74)	88.0	An35	3.8	Fs16	4.3	---	---	3.0	0.9	.099	57	48
TA-T (74-90)	73.6	An50	17.6	Fs16	2.9	Fo40	3.4	1.6	0.9	.256	78	76
TA-T (74-90)	73.1	An50	18.1	Fs16	3.4	Fo40	3.3	1.7	0.4	.318	78	76

Notes: *designates acceptable models. TB=trachybasalt. TBA=basaltic trachyandesite, TA=trachyandesite, T=trachyte. Numbers in parenthesis are the last two digits of sample numbers of parent and daughter compositions. F=fraction of liquid remaining. An=anorthite, Or=orthoclase, Fs=ferrosilite, Fo=forsterite. Olivine compositions (Fo53 and Fo40) are from Novak and Mahood (1986) and Bryan (1976) respectively. Fe-Ti oxide compositions are from Mahood and Baker (1986) and Novak and Mahood (1986). Apatite is from Deer et al. (1966). All other mineral compositions are from microprobe analyses of parental samples. ∑R2=sum of the squares of the residuals. Rb obs. = observed Rb content (ppm) in daughter composition. Rb calc.=calculated Rb content in the daughter.

Table 15: Crystal fractionation models for the Hart Mountain trachyandesite suite.

Parent:	AM-90-23 (TB)		AM-90-23 (TB)		AM-90-23 (TB)		AM-89-61 (BTA)		AM-89-61 (BTA)	
∑R2:	0.600		0.203		0.194		0.300		0.675	
Daughter:	AM-89-61 (TBA)		AM-89-65* (TA)		AM-89-74* (TA)		AM-89-65 (TA)		AM-89-74 (TA)	
	Obs.	Calc.	Obs.	Calc.	Obs.	Calc.	Obs.	Calc.	Obs.	Calc.
SiO2	53.29	53.81	57.99	57.84	60.83	60.63	57.99	58.07	60.83	60.98
Al2O3	14.81	14.92	15.81	15.81	16.65	16.60	15.81	15.77	16.65	16.57
TiO2	2.40	2.64	1.93	2.25	1.35	1.71	1.93	1.58	1.35	0.90
FeO*	11.31	11.32	8.44	8.32	6.45	6.32	8.44	8.56	6.45	6.60
MnO	0.34	0.21	0.21	0.19	0.16	0.18	0.21	0.38	0.16	0.40
CaO	7.64	7.60	5.34	5.32	4.12	4.10	5.34	5.45	4.12	4.26
MgO	2.76	2.76	1.95	2.00	1.68	1.73	1.95	1.80	1.68	1.48
K2O	1.85	1.81	2.54	2.67	3.01	2.96	2.54	2.47	3.01	2.76
Na2O	4.53	4.26	5.01	4.82	5.24	5.24	5.01	5.27	5.24	5.70
P2O5	1.08	0.67	0.78	0.78	0.52	0.52	0.78	0.64	0.52	0.35
Sr	503	472	465	451	452	461	465	515	452	532
Rb	25	30	43	47	57	52	43	34	57	37
Ba	578	479	780	648	887	699	780	722	887	785
Th	4.2	3.8	6.0	5.7	7.6	6.2	6.0	5.4	7.6	6.0
Ta	2.2	2.2	2.6	2.9	2.7	3.0	2.6	2.6	2.7	2.7
Zr	264	264	322	367	328	391	322	328	328	350
Hf	7.2	6.7	9.3	9.1	9.1	9.6	9.3	8.8	9.1	9.3
La	37.7	33.9	48.0	46.3	43.5	45.4	48.0	34.7	43.5	32.2
Ce	81.6	73.2	101.1	98.8	94.4	95.1	101.1	70.4	94.4	63.6
Sm	10.70	9.18	12.40	11.16	10.16	10.21	12.40	7.95	10.16	6.69
Eu	3.41	2.88	3.35	3.36	2.91	3.09	3.35	2.60	2.91	2.22
Tb	1.62	1.30	1.71	1.48	1.48	1.31	1.71	1.11	1.48	0.90
Yb	3.75	3.01	4.57	3.90	4.16	3.91	4.57	3.81	4.16	3.72
Sc	19.8	27	18.3	16.0	13.2	12.9	18.3	12.5	13.2	9.7
Co	18.5	24.3	12.4	16.7	6.1	14.3	12.4	12.2	6.1	10.0
Cr	2	167	9	37	6	23				

Notes: *designates accepatable models. ° indicates 0.9% apatite fractionation. 'indicates 0.4% apatite fractionation. TB=trachybasalt. TBA=basaltic trachyandesite, TA=trachyandesite, T=trachyte.

Table 15, continued.

Parent:	AM-89-65 (TA)		AM-89-74 (TA)		AM-89-74 (TA)	
∑R2	0.099		0.256		0.318	
Sample:	AM-89-74 (TA)		AM-89-90° (T)		AM-89-90' (T)	
	Obs.	Calc.	Obs.	Calc.	Obs.	Calc.
SiO2	60.83	60.96	65.91	65.81	65.91	65.69
Al2O3	16.65	16.59	15.69	15.76	15.69	15.75
TiO2	1.35	1.36	0.69	0.76	0.69	0.74
FeO*	6.45	6.46	5.17	5.03	5.17	5.05
MnO	0.16	0.20	0.18	0.11	0.18	0.11
CaO	4.12	4.18	1.94	1.76	1.94	1.80
MgO	1.68	1.54	0.36	0.73	0.36	0.66
K2O	3.01	2.85	3.85	3.99	3.85	4.01
Na2O	5.24	5.39	6.06	5.83	6.06	5.84
P2O5	0.52	0.45	0.15	0.18	0.15	0.43
Sr	452	479	209	214	209	220
Rb	57	48	78	76	78	76
Ba	887	854	961	1050	961	1053
Th	7.6	6.6	10.7	9.9	10.7	9.9
Ta	2.7	2.7	3.5	3.4	3.5	3.4
Zr	328	348	465	393	465	394
Hf	9.1	10.0	13.6	11.7	13.6	11.7
La	43.5	43.5	49.3	43.5	49.3	49.4
Ce	94.4	88.3	99.5	89.2	99.5	103.6
Sm	10.16	10.02	10.91	9.01	10.91	10.78
Eu	2.91	2.76	2.77	2.19	2.77	2.51
Tb	1.48	1.32	1.54	1.27	1.54	1.53
Yb	4.16	4.43	5.68	4.38	5.68	4.70
Sc	13.2	14.4	8.9	10.4	8.9	9.9
Co	6.1	9.9	1.1	2.6	1.1	2.7

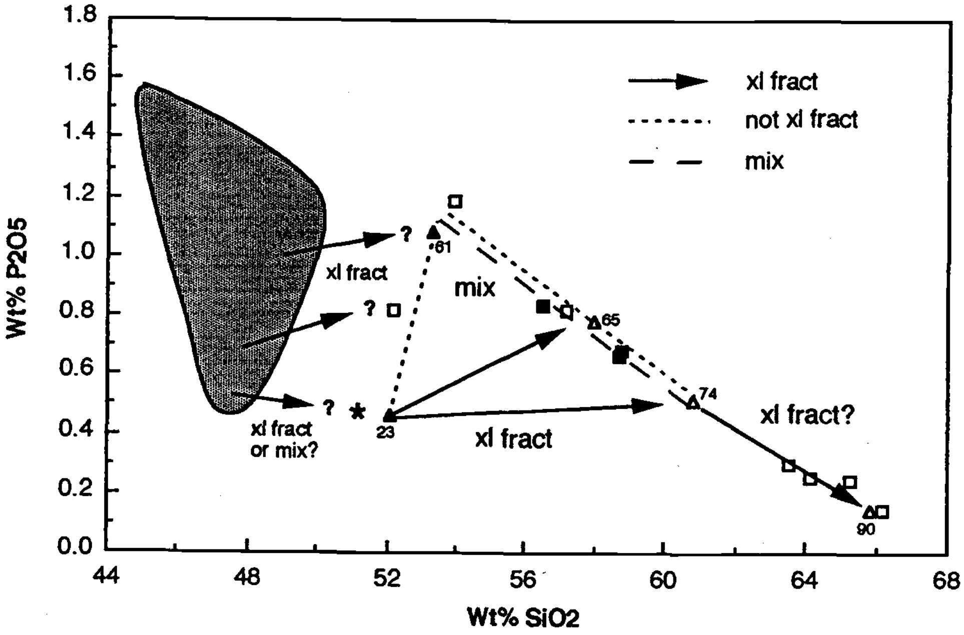

Figure 23: Summary of the proposed evolution of the Hart Mountain trachyandesite suite. The shaded area represents the composition of Pantellerian basalts (except for a sample which was visibly contaminated with alkali feldspar which is marked by a star; Mahood and Baker, 1986). Open symbols are samples with homogeneous textures, closed symbols have mingled or mixed textures and were modeled by mixing. Triangles represent endmember compositions used in fractional crystallization models. The numbers next to the triangles are the last two digits of sample numbers.

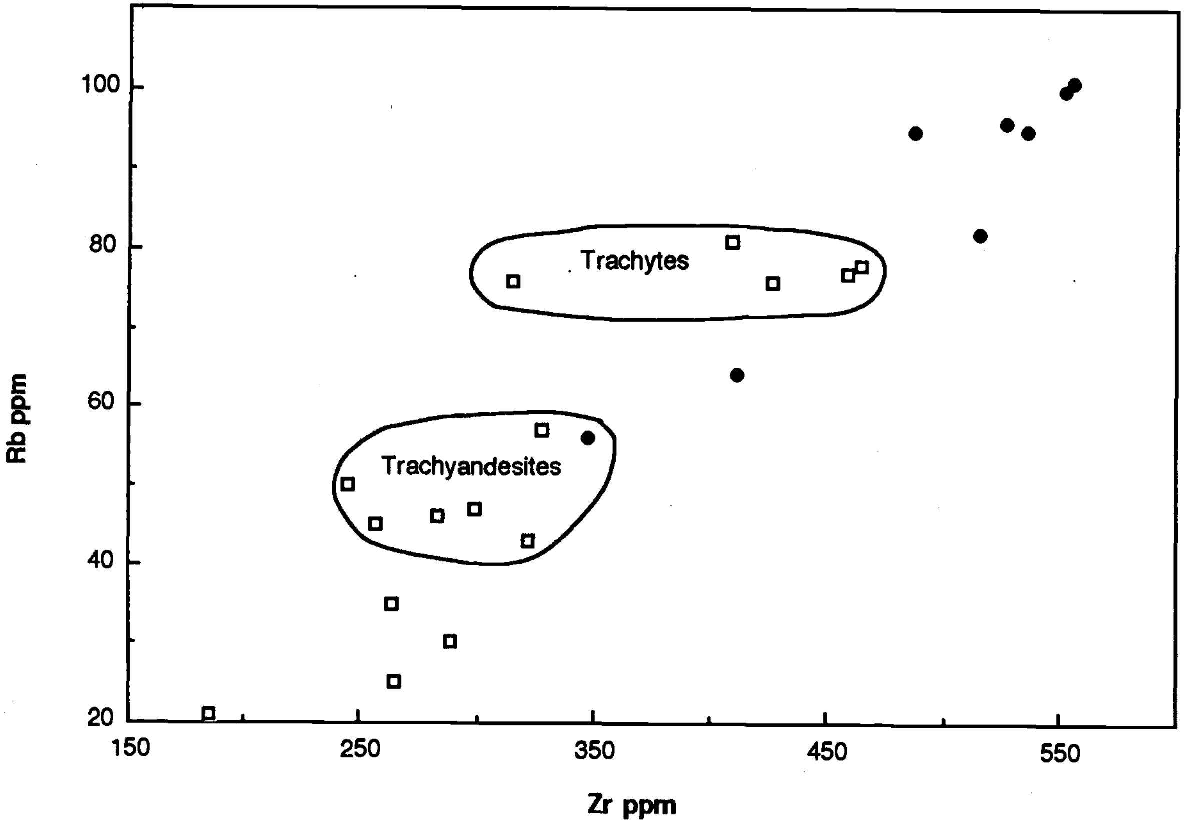

Figure 24: Plot of Rb versus Zr with fields of similar major element composition for trachytes and trachyandesites indicated.

Hart Mountain volcanic complex, and despite its relatively high SiO_2 content (52.1 wt %), it very closely resembles the alkali basalts (SiO_2 45.7-51.1 wt %) found at Pantelleria (Mahood and Baker, 1986). Its Mg# (55), MgO, Na_2O, and Sr contents are well within the range of the Pantellerian basalts (Mg# 58-45; MgO 7.0-4.3 wt %; Na_2O 3.1-4.2 wt %; Sr 763-454 ppm), although its TiO_2, FeO*, P_2O_5 and V, contents are lower (Pantelleria, TiO_2 3.6-2.6 wt %; FeO* 14.4-10.7 wt %; P2O5 1.5-0.48 wt %; V 428-281 ppm). Cr and Ni are slighter higher in AM-90-23 (Pantelleria, Cr 166-13 ppm, Ni 95-6 ppm). In fact, AM-90-23 most closely resembles a Pantellerian sample which was visibly contaminated with alkali feldspar; however, AM-90-23 did not appear to be contaminated in petrographic and handsample examination. Perhaps the compositional differences between AM-90-23 and the Pantellerian basalts arise from Fe-Ti oxides appearing on the liquidus earlier at Hart Mountain than at Pantelleria (in 1 atm experiments on Pantellerian basalts, it appears after approximately 50% crystallization; Mahood and Baker, 1986). I opted to model using a clearly comagmatic sample rather than choosing arbitrarily from Pantellerian samples, even if such compositions are potential parental magmas.

Although there is only a 1.2 wt % change in SiO_2 content between AM-90-23 and AM-89-61, MgO decreases from 6.48 to 2.79 wt % and P_2O_5 increases from 0.46 to 1.08 wt %. Major element crystal fractionation models (ΣR^2=0.600) call for 32% crystallization of plagioclase, clinopyroxene, and olivine (Tables 14 and 15). One of the most striking flaws in major element models, besides high ΣR^2 values, is the inability to drive P_2O_5 up to the observed concentrations in the basaltic trachyandesites: calculated P_2O_5 content is 0.67 wt %. If P_2O_5 is treated as a perfectly incompatible trace element over this composition interval, it would require 58% crystallization to reproduce the P_2O_5 concentration in AM-89-61. A plot of P_2O_5 versus Rb (Figure 25) shows the lack of a parental relationship clearly: crystal fractionation of AM-

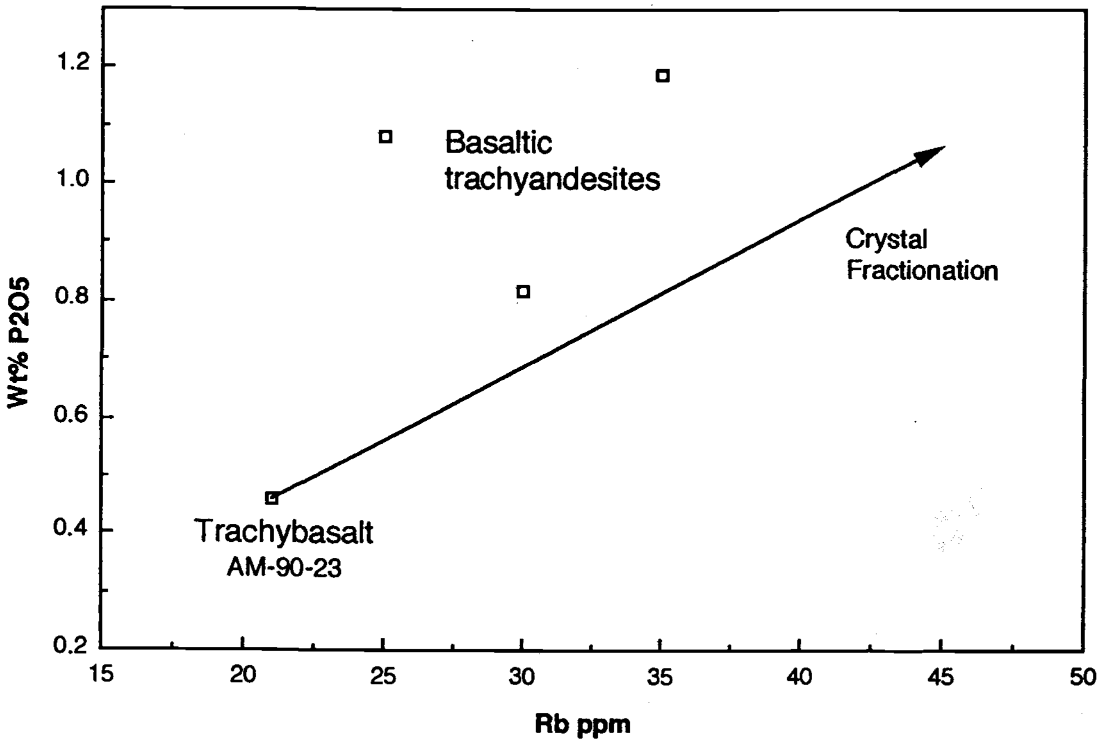

Figure 25: P_2O_5 versus Rb showing that the basaltic trachyandesites cannot be modeled by crystal fractionation of trachybasalt AM-90-23. P_2O_5 is treated as a perfectly incompatible element.

90-23 does not produce compositions within the field of observed basaltic trachyandesites. The basaltic trachyandesites of the Hart Mountain volcanic complex may have fractionated from parents with compositions within the range of the Pantellerian basalts (Figure 23).

EVOLUTION OF THE TRACHYANDESITES

Six trachyandesites were analyzed from the Hart Mountain volcanic complex. Five of these samples have very similar compositions with SiO_2 56.5 to 58.8 wt % SiO_2, and plot together on most major and many trace element variation diagrams (Figures 14 and 15), except Rb versus Zr (Figure 24). Three (AM-89-92, AM-89-60, and AM-89-42) of these samples have inhomogeneous textures (Figure 9) which suggest mixing or mingling of magmas. The other two samples (AM-89-65 and AM-89-22) and sample AM-89-74 (60.8 wt % SiO_2) do not have mingled textures and can not be modeled by simple binary mixing calculations and more likely result from crystal fractionation.

Magma Mixing

Texturally, samples AM-89-61, AM-89-42, and AM-89-92 appear to result from the mixing or mingling of magmas within the Hart Mountain volcanic complex. These samples have abundant cognate inclusions which appear to be partially incorporated into the melt. Excellent major and trace element fits of mixing models for these samples substantiate the magma mixing hypothesis (Table 16, Figure 26).

AM-89-60 and AM-89-42 were modeled as mixes of basaltic trachyandesite AM-89-61 and trachyandesite AM-89-74. Sample AM-89-92 was modeled as a mix of trachybasalt AM-90-23 and trachyandesite AM-89-74 because it contains abundant inclusions which are petrographically similar to AM-90-23. Assimilation of 5.8% plagioclase (An_{54}) was required to produce an acceptable ΣR^2 (=0.194).

Table 16: Mixing models for trachyandesites of the Hart Mountain trachyandesite suite.

Mafic endmember:	AM-89-61		AM-89-61		AM-90-23	
% in mix:	30.7		46.5		20.7	
Silicic endmember:	AM-89-74		AM-89-74		AM-89-74	
% in mix:	69.3		43.5		79.3	
∑R2	0.288		0.219		0.127	
% plag accumulation:	----		----		5.8	
Sample:	AM-89-60		AM-89-42		AM-89-92	
	Obs.	Calc.	Obs.	Calc.	Obs.	Calc.
SiO2	58.69	58.52	57.18	57.32	58.75	58.74
Al2O3	16.05	16.09	15.98	15.79	17.19	17.25
TiO2	1.62	1.67	1.86	1.84	1.53	1.36
FeO*	8.23	7.94	8.83	8.71	6.56	6.73
MnO	0.21	0.21	0.21	0.24	0.18	0.15
CaO	4.86	5.20	5.46	5.76	5.29	5.31
MgO	1.94	2.01	2.36	2.18	2.51	2.53
K2O	2.53	2.65	2.33	2.47	2.41	2.53
Na2O	5.21	5.02	4.99	4.91	4.90	4.93
P2O5	0.67	0.69	0.82	0.78	0.69	0.47
Sr	489	468	498	476	601	468
Rb	47	47	46	42	45	47
Ba	725	792	729	743	784	765
Th	6.1	6.6	6	6.0	4.8	6.2
Ta	2.5	2.6	2.3	2.5	2.3	2.4
Zr	299	308	283	298	257	282
Hf	8.4	8.5	8.0	8.2	6.7	7.8
La	40.1	41.7	39.2	40.8	38.5	37.4
Ce	85.7	90.47	84.9	88.5	82.0	81.2
Sm	10.59	10.33	10.62	10.41	9.06	8.92
Eu	3.39	3.06	3.34	3.14	2.9	2.6
Tb	1.57	1.52	1.57	1.55	1.25	1.29
Yb	4.1	4.03	4.05	3.97	3.22	3.54
Sc	16.0	15.2	16.6	16.3	14.9	14.1
Co	7.7	9.9	10.3	11.9	10.1	11.79

Note: Plagioclase added to model for sample AM-89-92 has a composition of An54.

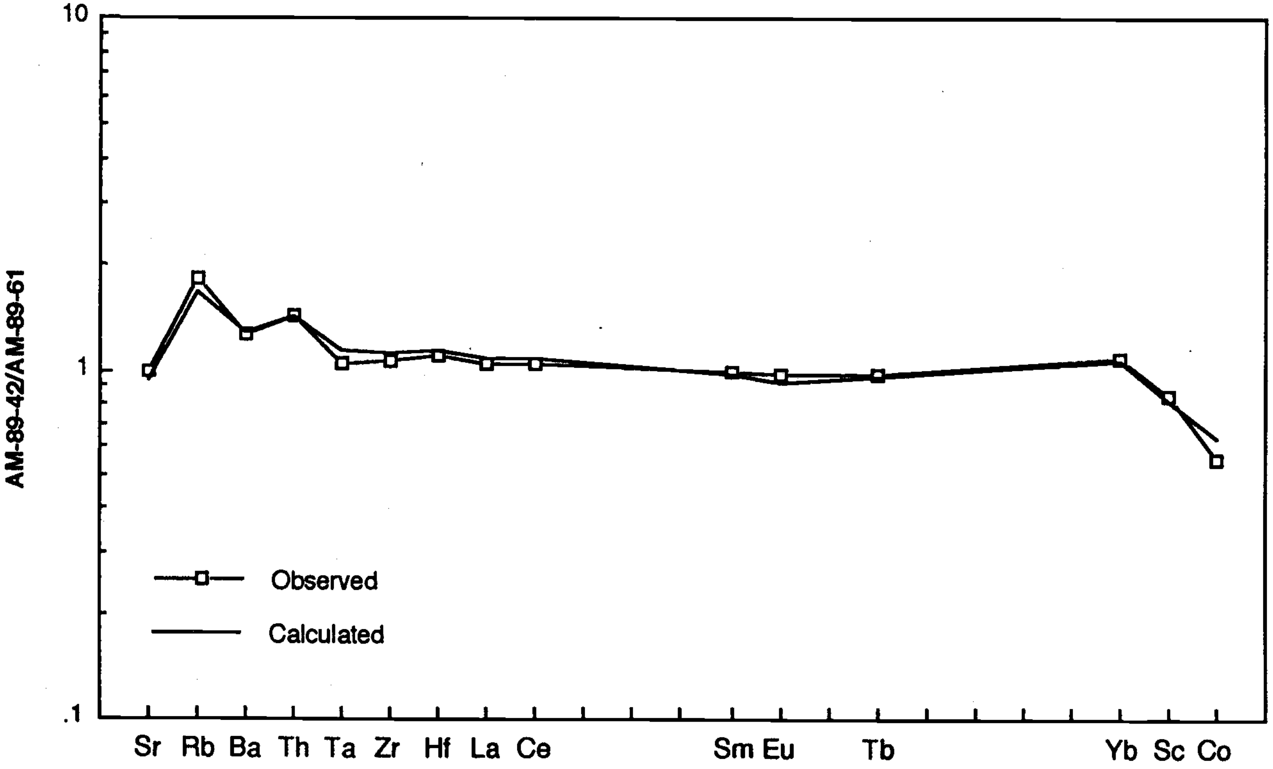

Figure 26: Calculated versus observed trace element composition of trachyandesite AM-89-42 normalized to the mafic endmember of the mixing model (AM-89-61).

Mixing models for samples AM-89-65 and AM-90-22 also yielded excellent fits for major element compositions using AM-89-61 and AM-89-74 as end members. However, REE concentrations for these two samples are higher than both endmembers of the mix, invalidating the mixing model for these samples.

Crystal fractionation

Crystal fractionation models were tested for daughter compositions AM-89-65, and AM-89-74 (Tables 14 and 15). Both a trachybasaltic (AM-90-23) and basaltic trachyandesitic (AM-89-61) composition was tested as potential parents. AM-89-61 was rejected as the parent composition because ΣR^2 values were high, fractionating assemblages contained plagioclase with low An content (An_{41}) and without sufficient olivine, and because predicted Rb concentrations were much lower than observed (for example AM-89-74 contains 57 ppm Rb, calculated is 37).

Acceptable crystal fractionation models were produced using trachybasalt AM-90-23 as parent. 57% crystallization produced AM-89-65 and 62% crystallization was required to produce AM-89-74. The fractionating assemblage which produced AM-89-65 has a higher proportion of olivine than the one for AM-89-74. Separate liquid lines of descent are required for the two daughter compositions since fractionation of AM-89-65 cannot produce AM-89-74 using an acceptable fractionating assemblages and phase compositions (Table 14).

Trace element tests of the accepted models produce good agreement between calculated and observed concentrations for most elements except Co and Cr, which are as much as 1.4 and 4.1 times higher, respectively, in the observed concentrations (Figures 27 and 28). However, the observed concentrations of these elements could be successfully

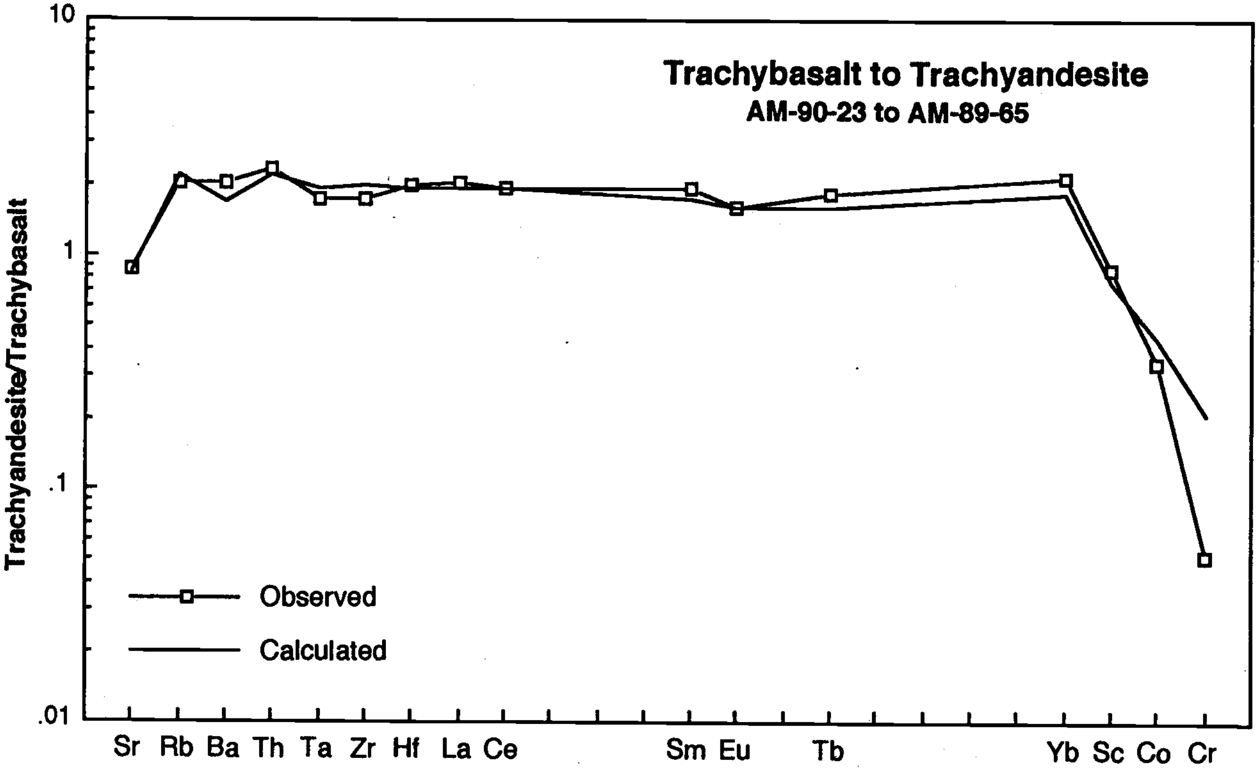

Figure 27: Calculated versus observed trace element composition of trachyandesite AM-89-65 normalized to the modeled parental trachybasalt (AM-90-23).

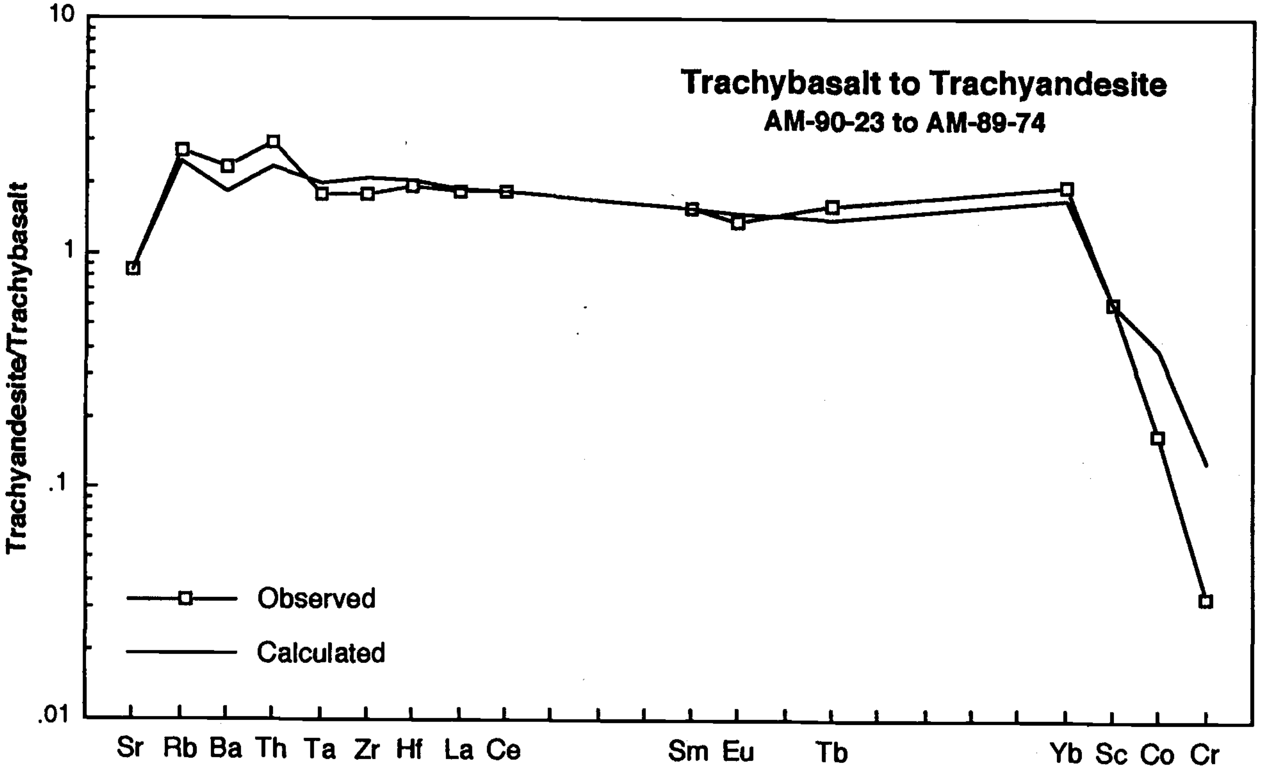

Figure 28: Calculated versus observed trace element composition of trachyandesite AM-89-74 normalized to the modeled parental trachybasalt (AM-90-23).

modeled using partition coefficients for clinopyroxene or Fe-Ti oxides within the of values given by Lemarchand et al.(1987).

FRACTIONATION OF TRACHYANDESITE TO TRACHYTE

26-27% crystallization of plagioclase >> clinopyroxene olivine > Fe-Ti oxides > apatite can model the evolution of trachyte (AM-89-90) from a trachyandesite parent (AM-89-74) (Tables 14 and 15, Figure 29). Rb, Th, Ta, Sc, Sr, and Ba concentrations are modeled very well. Calculated concentrations of Zr, Hf, and Yb are lower than observed which may indicate assimilation of zircon into the melt. REEs, with their high partition coefficients in apatite (Table 13), cannot be modeled with the amount of apatite fractionation required to produce the observed depletion in P_2O_5 from trachyandesite to trachyte.

The contribution of apatite fractionation in crystal fractionation models can be individually evaluated using F (the weight fraction of liquid remaining) and P_2O_5 concentration in the parent and daughter (Watson and Capobianco, 1981). Using an F of 0.74-0.73 from the major element model, and 0.516 wt % P_2O_5 in parent AM-89-74 and 0.108 wt % P_2O_5 in daughter AM-89-90 (Table 11), 0.9% apatite must be removed. Removal of 0.9% apatite produces REE concentrations in the daughter significantly lower than observed, but with a similar pattern (Figure 29). Reproduction of REE concentrations in AM-89-90 allows only 0.4% of apatite fractionation (Figure 29).

Watson and Capobianco (1981) emphasize that when apatite is saturated, it cannot be called upon to crystallize in any amount to conveniently model observed REE abundances. Therefore, the amount of apatite fractionation invoked in models must be controlled by parent and daughter P_2O_5 concentrations. This consideration indicates that this model is not a valid one. Either the trachytes did not evolve through crystal fractionation of trachyandesite parents, or

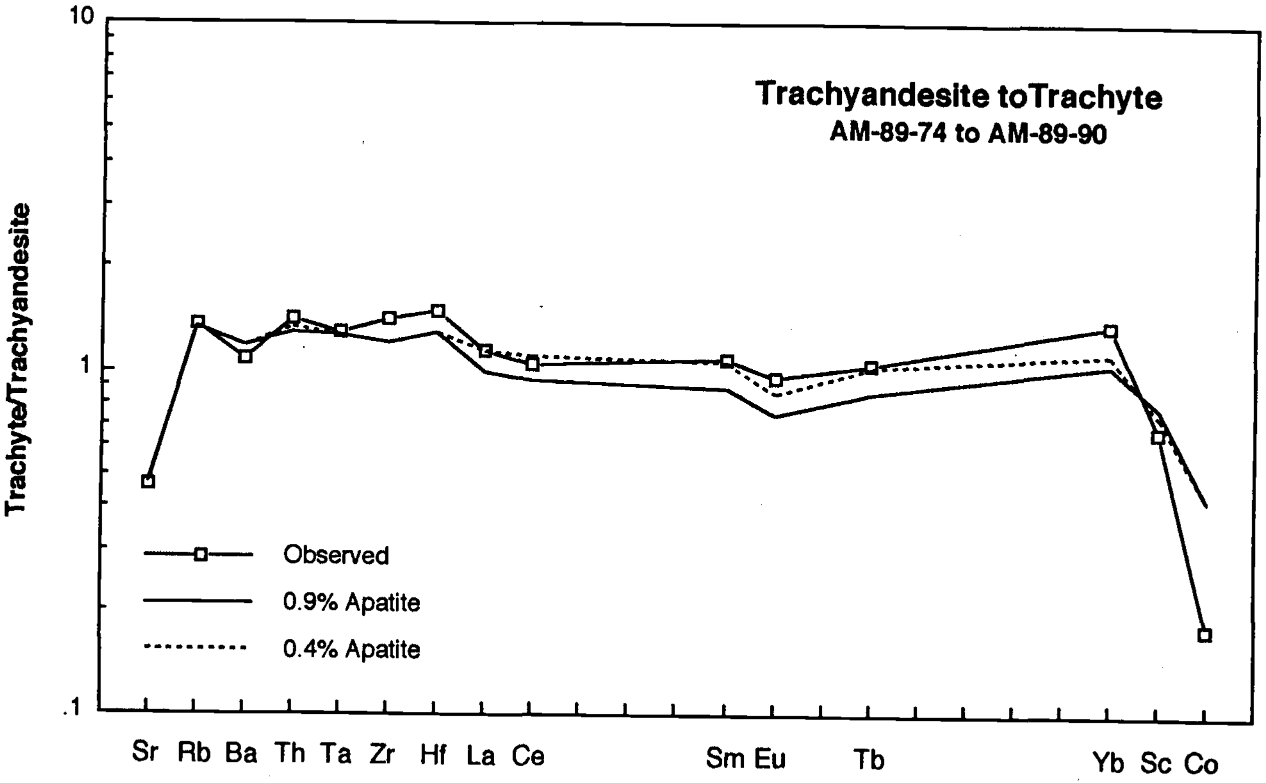

Figure 29: Calculated versus observed trace element composition of trachyte AM-89-90 normalized to the modeled parental trachyandesite (AM-89-74).

the choice of parent or daughter compositions were not valid. Both parent and daughter samples are crystal rich (10-20%) and may not represent liquid compositions.

WARNER PEAK RHYOLITE

Petrogenetic models for derivation of the Warner Peak rhyolite can only be considered qualitative because of post-emplacement compositional changes the peralkaline rhyolites have undergone with crystallization and/or devitrification. Using trachyte AM-89-90 as a parental composition, three samples of the Warner Peak rhyolite were chosen as daughter compositions for crystal fractionation models: comendite AM-89-14, and pantellerites AM-89-40 and AM-90-34. Samples AM-89-14 and AM-90-34 are devitrified and assumed to have undergone the accompanying loss of Na, and REE as documented for peralkaline rhyolites by Weaver et al. (1990). Sample AM-89-40, a hydrated vitrophyre, has lost alkalies, but most likely has retained magmatic REE concentrations.

Attempts to reconstruct magmatic major element concentrations by compensating for Na loss were done for samples AM-89-14 and AM-90-34. Weaver et al. (1990) report 8-19% Na loss from peralkaline rhyolites at Mayor Island. For Hart Mountain samples, Na losses were assumed to be a maximum of 8%. Na loss was assumed to not be higher than 8% because that would require that Na increase linearly over the trachyte to pantellerite interval on a plot of Na_2O versus SiO_2. Data from other peralkaline rhyolite volcanic centers indicate that Na concentrations decrease slightly or remain approximately the same over that interval (Novak and Mahood, 1986; Civetta et al., 1984; Figure 21). For major element crystal fractionation models both observed Na concentrations and Na concentrations adjusted for 8% Na loss were used.

ΣR^2 values on major element crystal fractionation tests increase with corrections greater than 8% Na loss. It impossible to get ΣR^2 less than one for compositions corrected for 19% Na loss. Na corrections of no more than 8% produce internally consistent major element models.

Sample AM-89-40 has lost significant K, having K_2O values of approximately 60 to 70% of the other peralkaline rhyolites. It may have also lost Na because the Na_2O concentration of AM-89-40 is well within the range of the observed concentrations found in the other peralkaline rhyolites. For major element crystal fractionation models, the observed composition of AM-89-40 was used, but K_2O was given a zero "weighting factor" in calculations of ΣR^2 values so that best fits were determined independent of K_2O concentration in the daughter.

CHOICE OF PARENT AND DAUGHTER COMPOSITIONS

Trachyte AM-89-90 was chosen as a parental composition for the peralkaline rhyolites because it is representative of the trachytes from the Hart Mountain volcanic complex. Although it is crystal rich (approximately 20%), its composition should approximate magmatic because it has a similar composition to AM-90-02, a crystal-poor vitric fiamme sample from Tib. AM-90-02 was not chosen as a parental composition because hydration has affected its concentration of alkalies. AM-89-90 is not peralkaline, but some Na loss upon crystallization cannot be excluded. Nonetheless, no attempts to correct for Na loss in AM-89-90 were made.

Trachyte AM-90-26, from the Warner Peak rhyolite, was rejected as a possible parent for the major element models based on mineralogic and major element composition considerations. The sample consists of greater than 90% feldspar indicating feldspar accumulation, and is depleted in FeO*, and MnO, and enriched in Al_2O_3, TiO_2, Na_2O, and P_2O_5 relative to the other trachytes. The low FeO* (2.64 wt %) and high Al_2O_3 (17.21 wt %), and high Na_2O/K_2O ratio (2.8) make it an unlikely candidate for a parent to the peralkaline rhyolites.

Three daughter compositions were tested because the nonsystematic variations in major and trace element composition within the peralkaline rhyolite suite indicates that different fractionating assemblages and/or liquid lines of descent are involved in their petrogenesis. Alternately, there may have been multiple parents. For example, the comendites are not intermediate in composition between the trachytes and the pantellerites. The comendites have higher SiO_2 than the pantellerites, and further crystal fractionation would only increase SiO_2 because quartz was never observed and thus was not part of the fractionating assemblage.

MAJOR ELEMENT MODELS

40-50% crystallization of plagioclase, alkali feldspar, clinopyroxene, Fe-Ti oxide, apatite, +/- olivine from trachyte AM-89-90 can adequately account for the major element compositions of the peralkaline rhyolites found at Hart Mountain (Table 17). 87-96% of the fractionating assemblages consist of plagioclase and alkali feldspar. Fe-Ti oxides, clinopyroxene (augite/ferroaugite), and apatite were essential components in each model to account for the decreases in TiO_2, MgO, and P_2O_5 respectively from trachyte to peralkaline rhyolite. Adding olivine (Fo_{25}) to the fractionation assemblage improved ΣR^2 values for comendite AM-89-14 and pantellerite AM-90-34, but not for pantellerite AM-89-40.

The Na/K ratio, and therefore the composition and proportion of the fractionating plagioclase and alkali feldspars, was critical in determining the ΣR^2 value of a given model (Table 17). Because of the uncertainties in determining the magmatic Na/K ratios of the rhyolites, less importance was placed on ΣR^2, and models with ΣR^2 as large as 1.0 were considered reasonable.

Na/K ratios in samples of the Warner Peak rhyolite are 1.8-2.0, and increase to 2.2 with corrections for 8% Na loss. Parental trachyte AM-89-90 has a Na/K ratio of 2.4.

Table 17: Crystal fractionation models of the petrogenesis of samples of the Warner Peak rhyolite.

Daughter	F	Plagioclase		Alkali feldspar		Clinopyroxene		Ol	Fe-Ti ox	Apat	ΣR2
		comp	%	comp	%	comp	%	%	%	%	
AM-90-34	54.6	An31	18.4	Or30	22.8	Fs27	1.6	0.6	1.6	0.4	.042
AM-90-34	53.5	An31	17.6	Or30	24.0	Fs35	2.4	0.6	1.6	0.3	.048
AM-90-34	54.8	An31	18.3	Or30	22.8	Fs27	2.0		2.0	0.3	.080
AM-90-34	56.6	An31	15.3	Or25	23.8	Fs27	1.4	0.6	1.6	0.4	.100
AM-90-34	56.6	An31	14.6	Or22	24.9	Fs27	1.4	0.4	1.6	0.4	.300
AM-90-34	50.0	An20	22.2	Or30	22.5	Fs27	2.5	0.4	1.9	0.5	.431
AM-90-34	52.1	An20	18.2	Or25	24.7	Fs27	2.3	0.3	1.8	0.5	.437
AM-90-34	52.1	An20	18.1	Or25	24.8	Fs27	2.6		2.0	0.5	.450
AM-90-34*	58.5	An31	20.5	Or30	17.6	Fs27	1.1	0.6	1.5	0.3	.316
AM-90-34*	58.6	An31	20.3	Or30	17.6	Fs27	1.4		1.8	0.2	.347
AM-90-34*	58.3	An31	20.0	Or30	17.8	Fs35	1.8		1.8	0.2	.378
AM-90-34*	61.3	An31	19.6	Or25	16.2	Fs27	0.6	0.6	1.4	0.3	.437
AM-90-34*	61.3	An31	19.3	Or25	16.3	Fs27	1.0		1.7	0.2	.458
AM-90-34*	63.0	An31	20.2	Or22	14.3	Fs27	0.6		1.6	0.3	.667
AM-90-34*	63.3	An31	20.7	Or22	13.6	Fs27	0.2	0.5	1.4	0.3	.669
AM-90-34*	52.7	An20	23.9	Or30	18.5	Fs27	2.2	0.3	1.8	0.5	.980
AM-89-14	56.6	An31	21.1	Or40	17.8	Fs27	1.2	1.4	1.7	0.2	.021
AM-89-14	55.8	An39	15.2	Or30	24.0	Fs27	1.6	1.3	1.8	0.3	.039
AM-89-14	55.8	An31	17.7	Or30	21.3	Fs27	1.7	1.3	1.8	0.3	.275
AM-89-14	55.1	An31	17.2	Or30	21.9	Fs35	2.3	1.3	1.8	0.4	.300
AM-89-14	58.6	An31	16.0	Or25	20.6	Fs27	1.4	1.3	1.8	0.3	.400
AM-89-14	56.1	An31	17.3	Or30	21.2	Fs27	2.6		2.6	0.2	.445
AM-89-14	60.5	An31	16.7	Or22	18.4	Fs27	1.0	1.2	1.8	0.4	.699
AM-89-14*	60.4	An39	19.5	Or40	16.4	Fs27	0.6	1.4	1.5	0.1	.108
AM-89-14*	60.7	An39	17.6	Or30	17.5	Fs27	0.9	1.4	1.6	0.2	.369
AM-89-14*	56.5	An31	20.7	Or40	18.1	Fs27	1.5	1.3	1.7	0.2	.386
AM-89-14*	65.0	An39	17.9	Or25	13.7	Fs27	0.2	1.4	1.5	0.2	.574
AM-89-14*	60.3	An31	19.9	Or30	15.3	Fs27	1.2	1.4	1.7	0.3	.878
AM-89-40	54.7	An31	16.4	Or30	26.2	Fs27	1.2		1.3	0.2	.113
AM-89-40	58.5	An31	15.0	Or25	24.7	Fs27	0.6		1.1	0.2	.193
AM-89-40	58.6	An31	14.6	Or22	25.0	Fs27	0.6		1.0	0.2	.210

Representative major element crystal fractionation models for the rhyolites using trachyte AM-89-90 as the parent. *designates daughter compositions corrected for 8% Na2O loss. F=fraction of liquid remaining. An=anorthite, Or=orthoclase, Fs=ferrosilite. Olivine (Fo25) and Fe-Ti oxide compositions are from Mahood and Stimac (1990). Apatite is from Deer et al. (1966). R2=sum of the squares of the residuals.

Fractionation of plagioclase (or calcic anorthoclase), which has molar Al greater than molar alkalies, is required to produce a peralkaline daughter composition from a nonperalkaline parent (Noble, 1968). Fractionation of alkali feldspar (anorthoclase or Na-sanidine) produces the observed and calculated Na/K ratio in the rhyolites, which is higher than the Na/K ratio produced by plagioclase fractionation alone. Models corrected for Na loss have a slightly higher proportion of plagioclase fractionation because less alkali feldspar fractionation is required to produce the Na/K ratio (Table 17), but proportions are not significantly different.

ΣR^2 values are higher in samples corrected for Na loss, but are improved by using feldspar compositions not found in the parent AM-89-90. Analyzed feldspar crystals from AM-89-90 are strongly zoned and range in composition from at least An_{31} to Or_{25} (see Table 5). Feldspar compositions with greater An (An_{39}) or Or (Or_{30-40}) content improved fits for most models. Some feldspars in AM-89-90 may have cores more calcic than the analyzed composition of An_{31} because of the strong compositional zoning. Calcic cores in feldspar in trachytes are not unreasonable: Novak and Mahood (1986) report anorthoclase phenocrysts with cores up to An_{65} in trachytes at Kane Springs Wash. However, it is more unlikely to have feldspar compositions higher than Or_{30} in fractionating assemblages because those compositions are only found in groundmass microlites of the peralkaline rhyolites.

TRACE ELEMENT TESTS

Trace element tests of major element models used two starting compositions (trachyte AM-89-90 and AM-90-26) because the trace element concentration of sample AM-89-90 may not accurately reproduce the trace element concentration of the parents to the peralkaline rhyolites at Hart Mountain. At other peralkaline volcanic systems, such as Mayor Island and Pantelleria, eruptive cycles can be recognized on the basis of Zr contents even though samples from other eruptive cycles have similar major element compositions (Houghton et al., 1992; Civetta et al., 1984). AM-89-90 is from Tv3 of the Hart Mountain trachyandesite suite, and is unlikely to be part of an eruptive cycle with the Warner Peak rhyolite. The trace element concentrations of trachyte AM-90-26 from the Warner Peak rhyolite provide a composition of an alternate parental trachyte. AM-90-26 has lower concentrations of Rb, Zr, and Th, and higher concentrations of REE than AM-89-90 (Table 11).

In general, the trace element fits are poor, especially relative to the fits of models for the Hart Mountain trachyandesite suite. Poor fits in the rhyolite suite are in keeping with the nonsystematic compositional scatter within the rhyolite suite, which in part reflects compositional changes with devitrification and/or hydration.

Variation in concentrations of the incompatible elements Rb, Zr, Hf, Ta and Th in samples of the Warner Peak rhyolite may result from variations in the amount of crystallization required to produce individual samples, or, alternately, may reflect differences in concentrations of these elements in parental compositions. Mahood and Stimac (1990) recommend using the most incompatible elements as differentiation indices.

Concentrations of compatible elements Sr and Ba, and Eu/Eu* should reflect variations in the relative proportions of plagioclase and alkali feldspar in the fractionation assemblage, compositional zonation in the fractionating feldspar, and/or changes in the partition coefficients over the fractionation interval. Feldspars may be zoned in Ba and Sr in feldspar as well (Mahood and Stimac, 1990). Because of these factors, trace element tests of major element fractional crystallization models, placed more value on the fit of incompatible elements Rb, Th, Ta, Zr, and Hf. REE concentrations were also used in tests of models for vitrophyre AM-89-40.

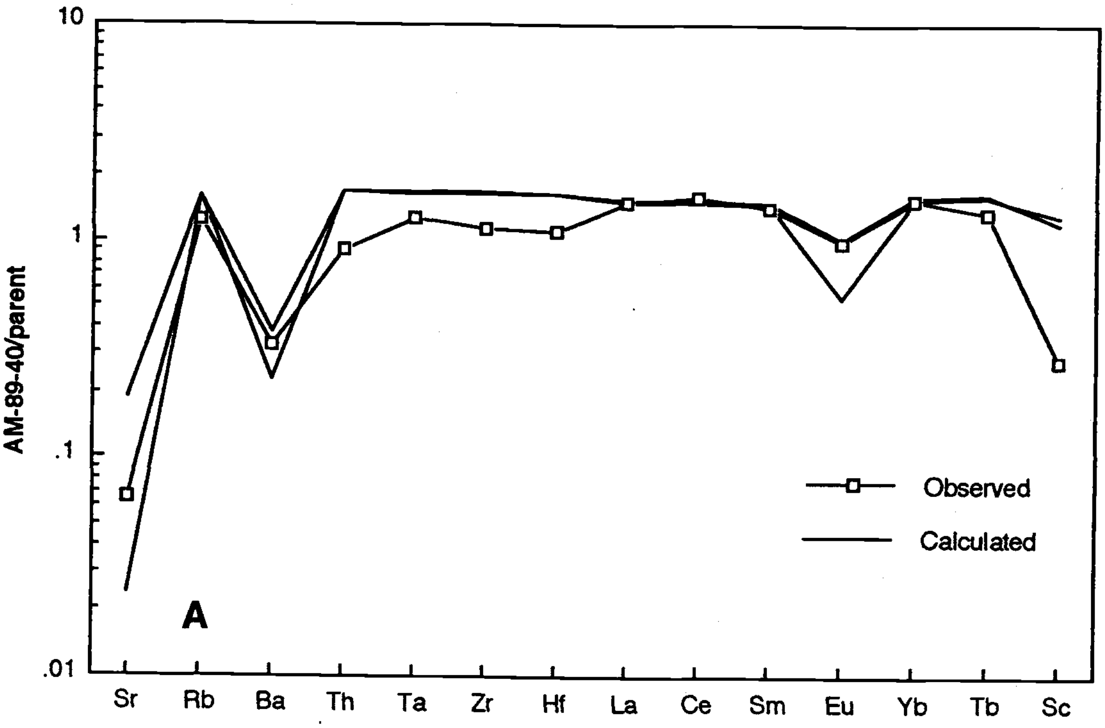

Figures 30A-C: Calculated versus observed trace element compositions of the peralkaline rhyolites normalized to the modeled parent (AM-89-90). The two calculated curves represent the range of compositions produced using Kds for trachytes and at agpaitic index of 1.2. A: AM-89-40. B: AM-90-34. C: AM-89-14.

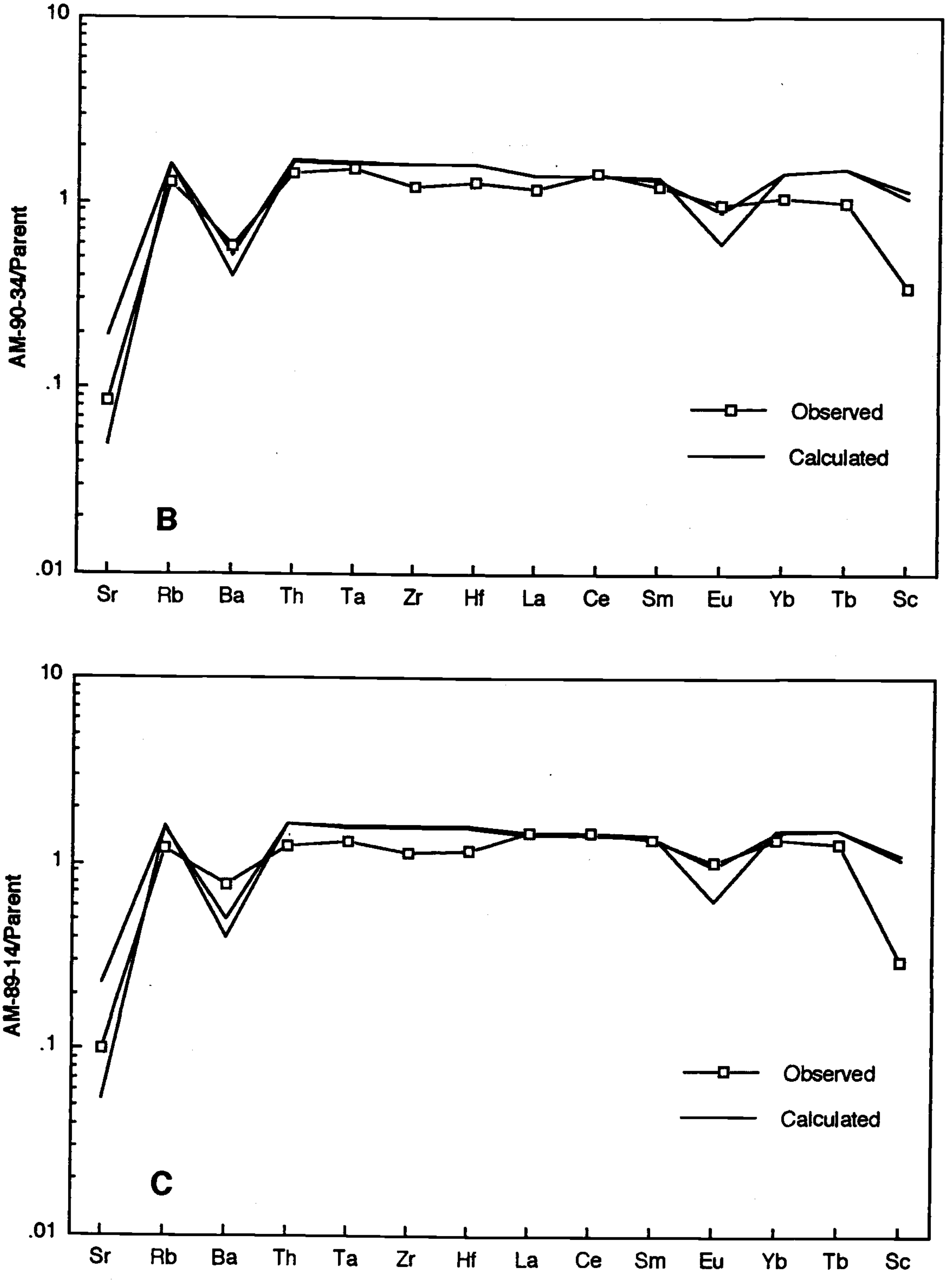

Figure 30B and C

AM-89-90 as Parent

Figure 30 shows trace element tests using AM-89-90 as the starting composition. The observed compositions of the peralkaline rhyolites have lower concentrations of incompatible elements (Rb, Th, Ta, Zr, Hf), and smaller Eu anomalies than produced by Rayleigh fractionation from AM-89-90. Compatible elements Sr and Ba can be modeled given the ranges of partition coefficients available over the composition interval from trachyte to mildly peralkaline rhyolite. Except for the negative Eu anomaly, calculated REE concentrations in vitrophyre AM-89-40 are acceptable. Using the recommended Kd for Sc (27) in pyroxene for this composition interval, Sc concentrations could not be duplicated with fractional crystallization. However, increasing the Kd to 60, which is the Kd for ferroaugite in strongly peralkaline rhyolites (Mahood and Stimac, 1990) can account for the low concentrations of Sc found in the Warner Peak rhyolite.

Using the observed concentrations of incompatible elements Rb, Zr, Th, and Ta in the peralkaline rhyolite daughters, and bulk partition coefficients of 0.1-0.2, 0.1, 0.04, and 0.1 respectively, it would take approximately 15-30% crystallization to produce samples AM-89-40, AM-90-34, and AM-89-14 from trachyte AM-89-90. Major element models call for 40-50% crystallization. In fact AM-89-90 is clearly not parental to some samples of the Warner Peak rhyolite: only 5-11% crystallization would reproduce the Rb and Zr concentrations in pantellerite AM-90-27 with AM-89-90 as the parent.

AM-90-26 as Parent

Trace element tests of crystal fractionation models (Table 14) also used trace element concentrations in AM-90-26 as a parent (Figure 31). Rb and Th contents in the peralkaline rhyolites are successfully modeled. However, calculated Zr, Ta, and Hf concentrations are still

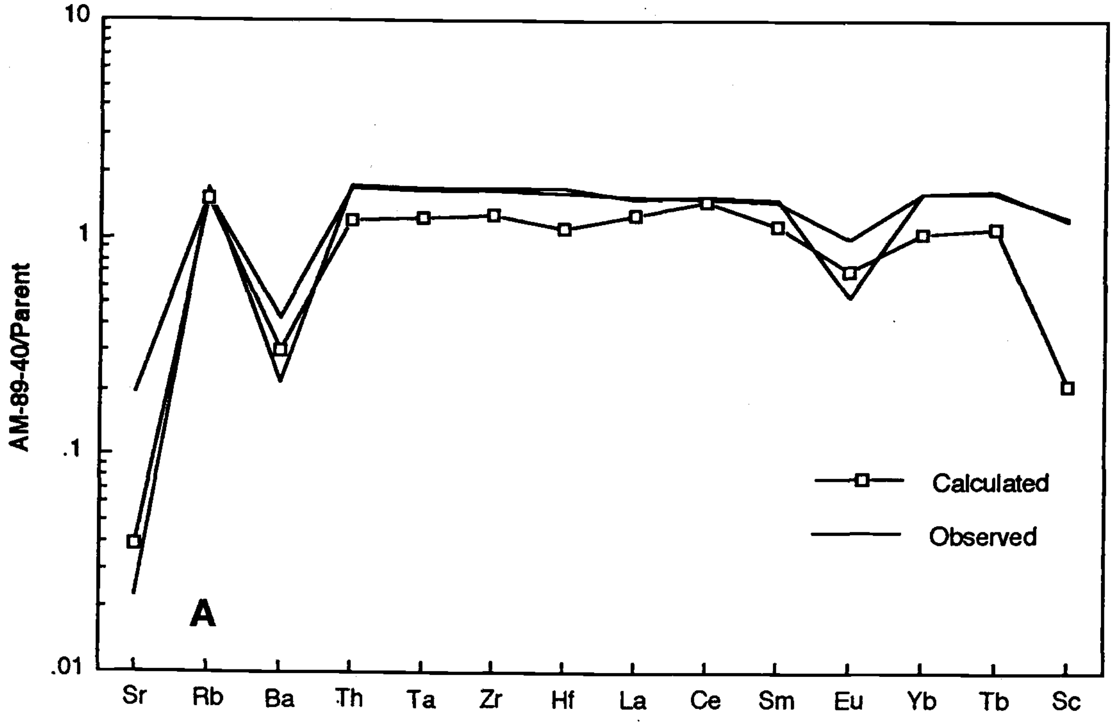

Figures 31A-C: Calculated versus observed trace element compositions of the peralkaline rhyolites normalized to the modeled parent (AM-90-26). The two calculated curves represent the range of compositions produced using Kds for trachytes and at agpaitic index of 1.2. A: AM-89-40. B: AM-90-34. C: AM-89-14.

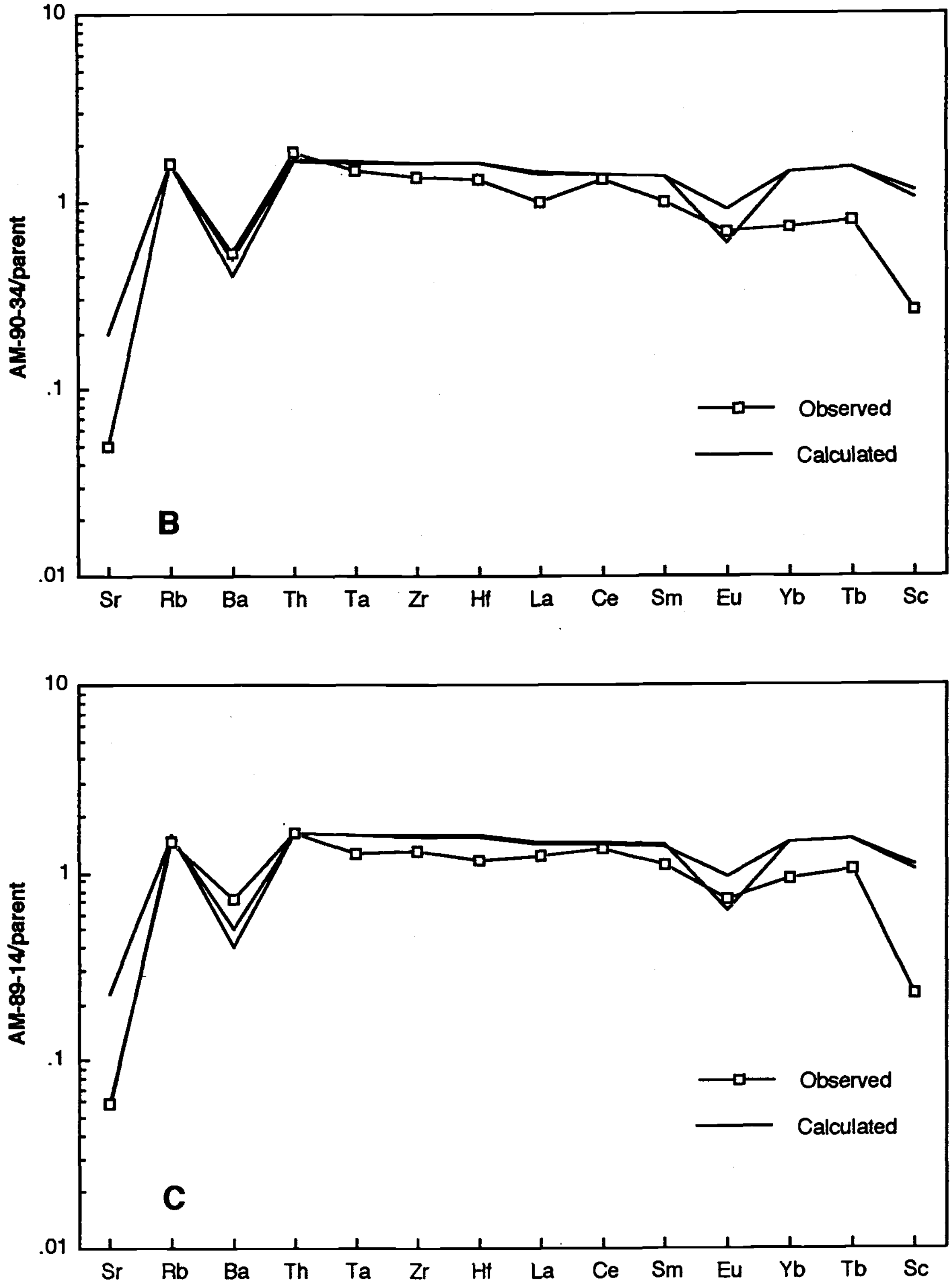

Figure 31B and C

significantly higher than observed. The low concentrations of these elements may be due to zircon fractionation. Zircon was not observed in samples from the Hart Mountain volcanic complex, but may be stable. Watson (1979) found that zircon is stable in all synthetic silicic melts which are not peralkaline (Watson, 1979). Minor amounts of zircon fractionation could have occurred before plagioclase fractionation created peralkaline melts. Because Kds for Zr and Hf in zircon are exceedingly high (1500 and 1000 respectively; Lemarchand et al., 1987), only trace amounts of zircon fractionation can account for the differences between calculated and observed concentrations for these elements.

DISCUSSION

Rocks of the Hart Mountain volcanic complex appear to result from fractional crystallization of alkali basalt parents, with some mixing of magmas within the suite to produce some of the trachyandesites. Although most elements vary systematically with differentiation, some compositional heterogeneities, e.g. P_2O_5 concentrations in the basaltic trachyandesites, indicate they did not evolve from a single parent. A range of parental magmas produced by varying degrees of partial melting (Mahood and Baker, 1986), like at Pantelleria, is required to explain these compositional differences. Heterogeneities in the rest of the suite are exemplified by the variation in Rb and Zr (Figure 24). This compositional variability perhaps results from small, or non-integrated, magma chambers, such as have been proposed at Pantelleria (Mahood and Baker, 1986).

Approximately 90% fractional crystallization is required to produce trachyte from trachybasalt in the Hart Mountain volcanic complex. This amount of fractional crystallization is consistent with other models for the derivation of trachyte from basalt (for example, 82% at Pantelleria, Civetta et al., 1988). The REE contents of the trachytes of the Hart Mountain volcanic complex are modeled very poorly due to the effect of apatite fractionation.

Models call for approximately 40-50% of trachyte to derive the peralkaline rhyolites of the Warner Peak rhyolite. Fractional crystallization of trachytic parental magmas is the most commonly proposed origin for peralkaline rhyolites (Parker, 1983; Conrad, 1984; Civetta et al., 1984; Mahood and Baker, 1986; Mahood and Hildreth, 1986; Bailey and Macdonald, 1970; Baker, 1974). Nearly all models call for at least 35-50% fractionation, and many require as much as 75% crystallization to produce peralkaline rhyolite daughters. Other models (e.g. Novak and Mahood, 1986) invoke fractional crystallization accompanied by minor amounts of crustal contamination. However, peralkaline rhyolites clearly can be produced in the absence of continental crust as evidenced by their presence on oceanic islands such as Socorro (Bryan, 1970; 1976). Noble et al. (1974) report a $^{87}Sr/^{86}Sr_i$ ratio of 0.7034 for the the Warner Peak rhyolite, which suggests that assimilation of continental crust was minimal in the evolution of the Hart Mountain volcanic complex. This is supported by the low incompatible trace element (REE, Zr, Nb) concentrations of the Warner Peak rhyolite.

The major flaw in most crystal fractionation models of peralkaline rhyolites from other volcanic centers is their inability to explain the extreme enrichments of incompatible elements. In general, the high halogen content of peralkaline rhyolites and associated volatile-complexing is used the explain the elevated trace element concentrations (Novak and Mahood, 1986; Civetta et al., 1988; Taylor et al., 1981; Gibson, 1972). At Hart Mountain, the enrichments are not extreme (Figure 21) and crystal fractionation models come close to explaining the observed concentrations. Indeed, the suite has the opposite problem in that observed concentration are lower than predicted even for some elements (Zr, Hf) immobile in hydration and devitrification.

Lowenstern and Mahood (1991) report low H_20 contents (1.4-2.1 wt%) from melt inclusions, which record pre-eruptive H_2O contents, in quartz crystals from pantellerites erupted at Pantelleria. These relatively low H_2O contents are not consistent with an origin of fractional crystallization of a basalt since water acts incompatibly. Therefore, they propose that small degrees of partial melting of amphibole-bearing alkali gabbros could produce trachytic melts. Fractional crystallization of the trachytes in shallow magma chambers would then produce peralkaline rhyolites (Lowenstern and Mahood, 1991).

Chapter Five: Summary

The Hart Mountain volcanic complex formed a shield-like volcanic edifice consisting mostly of peralkaline rhyolite lava flows, tuffs, and shallow intrusive rocks approximately 26 Ma ago. Within the last 7 Ma, Basin and Range faulting has cut through the western flank of this volcano, exposing a wide range of strongly differentiated mafic to intermediate composition rocks which are not commonly extensively exposed in other peralkaline centers. Development of shallow felsic magma chambers in peralkaline volcanic systems impedes the rise of basaltic liquids: in Quaternary peralkaline volcanoes, basalts have only erupted from flank vents (Mahood, 1984).

Crystal fractionation of multiple parents, along with some mingling of magmas, accounts for most of the compositional and textural features of rocks of the Hart Mountain volcanic complex. The large amounts of fractionation involved (approximately 90% for trachybasalt to trachyte, and 40-50% for trachyte to peralkaline rhyolite) require that a large body of alkali gabbro to syenite is present underneath the Hart Mountain volcanic complex.

Although the Hart Mountain volcanic complex has many features characteristic of strongly peralkaline volcanic system, including Fe enrichment in the rhyolites and molar Na/K greater than 1.5, in some ways it is atypical. The peralkaline rhyolites do not have extreme enrichment of incompatible elements. Mineralogic differences include the presence of plagioclase as the dominant feldspar in the trachytes and the absence of aenigmatite in the peralkaline rhyolites.

Peralkaline rhyolites are virtually always found in extensional environments, such as in continental rifts, along oceanic fracture zones and ridges, or in areas of back arc spreading (e.g., Macdonald, 1974; Smith et al., 1977; Mahood, 1984). Major peralkaline centers associated with crustal rifting include the Afar rift of Africa (Barberi et al., 1974), and some Miocene centers in the Basin and Range (for example, Kane Spring Wash, Novak and Mahood, 1986; McDermitt Caldera, Conrad, 1984; Wallace et al., 1980). Peralkaline rhyolites near convergent margin have been related to back arc spreading (Smith et al., 1977). For example, the peralkaline center Mayor Island, New Zealand is in a back arc setting approximately 100 km behind a calc-alkaline volcanic zone (Houghton et al., 1992).

Peralkaline magmas may be associated with relatively low extension rates (Mahood, 1984). They are absent among volcanic rocks associated with periods of rapid mid-Tertiary extension in the Basin and Range. The occurrence of peralkaline rhyolites in areas of low extension rates is highlighted by the presence of peralkaline volcanic centers in zones of local extension within convergent margin such as in west-central British Columbia (Bevier et al., 1979), and in the Mexican Neovolcanic Belt (La Primevera, Mahood, 1981).

Volcanism in the western United States between 50 and 17 is widely believed to result from the subduction of the Farallon plate (Christiansen and McKee, 1978; Barrash and Venkatakrishnan, 1982; Hart and Carlson, 1987). The presence of the strongly peralkaline Hart Mountain volcanic complex and the mildly peralkaline Coyote Hills implies that southern Oregon was a locus of at least local extension in the late Oligocene. (Thomas, 1981, describes the Coyote Hills as calc-alkaline despite the fact the system is strongly bimodal, and an analysis of a devitrified rhyolite with an agpaitic index of 1.00. I interpret the Coyote Hills to be a weakly peralkaline system.)

This late Oligocene extension in south-central Oregon may or may not be related to movement along the Eugene-Denio fault zone, which cuts both Hart Mountain and the Coyote Hills and was active at the time. The fact the Hart Mountain volcanic complex and the Coyote Hills did not undergo significant synvolcanic extension does not preclude an extensional environment for these volcanic centers: most Quaternary pantelleritic or trachytic shields show little evidence of normal faulting (Mahood, 1984).

Bibliography

Anders, E., and Ebihara, M., 1982, Solar system abundances of the elements: Geochimica et Cosmochimica Acta, v. 46, p. 2363-2380.

Bailey, D.K., 1974, Experimental petrology relating to oversaturated peralkaline volcanics: A review: Bulletin Volcanologique, v. 38, p. 637-652.

Bailey, D.K., Cooper, J.P., and Knight, J.L., 1974, Anhydrous melting and crystallization of peralkaline obsidians: Bulletin Volcanologique, v. 38, p. 653-665.

Bailey, D.K., and Macdonald, R., 1970, Petrochemical variations among mildly peralkaline (comendite) obsidians from the oceans and the continents: Contributions to Mineralogy and Petrology, v. 28, p. 340-351.

Baker, P.E., 1974, Peralkaline acid volcanic rocks of oceanic islands: Bulletin Volcanologique, v. 38, p. 737-754.

Baker, B.H., and Henage, L.F., 1977, Compositional changes during crystallization of some peralkaline silicic lavas of the Kenya rift valley: Journal of Volcanology and Geothermal Research, v. 2, p. 17-28.

Baksi, A.K., and York, D., and Watkins, N.D., 1967, Age of the Steens Mountain geomagnetic polarity transition: Journal of Geophysical Research, v. 72, p. 6299-6308.

Barberi, F., Santacroce, R., and Varet, J., 1974, Silicic peralkaline volcanic rocks of the Afar depression (Ethiopia): Bulletin Volcanologique, v. 38, p. 755-790.

Barrash, W., and Venkatakrishnan, R., 1982, Timing of late Cenozoic volcanic and tectonic events along the western margin on the North American Plate: Geological Society of America Bulletin, v. 93, p. 977-989.

Best, M.G., and Christiansen, E.H., 1991, Limited extension during peak Tertiary volcanism, Great Basin on Nevada and Utah: Journal of Geophysical Research, v. 96, p. 13509-13528.

Bevier, M.L., Armstrong, R.L., and Souther, J.G., 1979, Miocene peralkaline volcanism in west-central British Columbia--Its temporal and plate-tectonics setting: Geology, v. 7, p. 389-392.

Bryan, W.B., 1966, History and mechanism of eruption of soda-rhyolite and alkali basalt, Socorro Island, Mexico: Bulletin Volcanologique, v. 38, p. 755-790.

Bryan, W.B., 1970, Alkaline and peralkaline rocks of Socorro Island, Mexico, Annual Report of the Director Geophysical Lab: Carnegie Institute of Washington Year Book, v. 68, p. 194-200.

Bryan, W.B., 1976, A basalt-pantellerite association from Isla Socorro, Islas Revillagigedo, Mexico, in Volcanoes and Tectosphere, edited by A. Aoki and S. Iizuka, Tokai University Press, Tokyo, p. 75-91.

Carlson, R.W., and Hart, W.K., 1983, Geochemical study of the Steens Mountain flood basalt: Carnegie Institution of Washington Year Book 82, p. 475-481.

Carlson, R.W., and Hart, W.K., 1987, Crustal genesis on the Oregon Plateau: Journal of Geophysical Research, v. 92, p. 6191-6206.

Christiansen, R.L., and McKee, E.H., 1978, Late Cenozoic volcanic and tectonic evolution of the Great Basin and Columbia intermontaine region: Geological Society of America Memoir 152, p. 283-311.

Civetta, L., Cornette, Y, Crisci, G., Gillot, P.Y., Orsi, G., and Requejo, C.S., 1984, Geology, geochronology, and chemical evolution of the island of Pantelleria: Geological Magazine, v. 121, p. 541-562.

Civetta, L., Cornette, Y., Gillot, P.Y., and Orsi, G., 1988, The eruptive history of Pantelleria (Silicy Channel) in the last 50 ka: Bulletin Volcanologique, v. 50, p. 47-57.

Clayton, R.W., 1989, Kinematics of the northern margin of the Basin and Range, Oregon: Geological Society of America Abstracts with Programs, v. 21, no. 5, p. 66.

Conrad, W.K., 1984, The mineralogy and petrology of compositionally zoned ash flow tuffs, and related silicic volcanic rocks, from the McDermitt Caldera complex, Nevada-Oregon: Journal of Geophysical Research, v. 89, p. 8639-8664.

Couch, R., and Johnson, S., 1968, The Warner Valley earthquake sequence: DOGAMI, The Ore Bin, v. 30, p. 191-212.

Craven, G.F., 1988, Tectonic deformation of Late Pleistocene shorelines in Warner Valley, Lake County, Oregon: Geological Society of America Abstracts with programs, v. 20, n. 3, 152.

Davenport, R.E., 1971, Geology of the Ranttlesnake and older ignimbrites in the Paulina Basin and adjacent area, central Oregon: Oregon State University unpublished PhD Thesis, 132 p.

Deer, W.A., Howie, R.A., and Zussman, J., 1966, An introduction to the rock-forming minerals: Longman Group Limited, London, 528 p.

Draper, D.S., 1991, Late Cenozoic bimodal magmatism in the northern Basin and Range Province of southeastern Oregon: Journal of Volcanology and Geothermal Research, v. 47, p. 299-328.

Duffield, W.A., and McKee, E.H., 1986, Geochronology, structure, and basin-range tectonism of the Warner Range, northeastern California: Geological Society of America Bulletin, v. 94, p. 292-304.

Eaton, G.P., 1982, The Basin and Range province: Origin and tectonic significance: Annual Review Earth Planetary Science, v. 10, p. 409-440.

Enlows, H.E., 1976, Petrography of the Rattlesnake Formation at the type area, Central Oregon: Oregon Department of Geology and Mineral Industries Short Paper 25, 34 p.

Enlows, H.E., and Parker, D.J., 1972, Geochronology of the Clarno igneous activity in the Mitchell quadrangle, Wheeler county, Oregon: DOGAMI, The Ore Bin, v. 34, p. 104-110.

Feeley, T.C., and Grunder, A.L., 1991, Mantle contribution to the evolution of Middle Tertiary silicic magmatism during early stages of extension: the Egan Range volcanic complex, east-central Nevada: Contributions to Mineralogy and Petrology, v. 106, p. 154-169.

Fiebelkorn, R.B., Walker, G.W., MacLeod, N.S., McKee, E.H., Smith, J.G., 1983, Index to K-Ar determinations for the state of Oregon: Isochron/West, no. 37, p. 3-60.

Fuller, R.R., 1931, The geomorphology and volcanic sequence of Steens Mountain in southeastern Oregon: Washington University Publications in Geology, v. 3, p. 1-130.

Geist, D.J., McBirney, A.R., and Baker, B.H., 1989, MacGPP: A program package for creating and using geochemical data files, 33 p.

Gibson, I.L., 1972, The chemistry and petrogenesis of a suite of pantellerites from the Ethiopian Rift: Journal of Petrology, v. 13, p. 31-44.

Glazner, A.F., and Bartley, J.M., 1990, Contrasting Cenozoic tectonomagmatic histories of the northern and southern Basin and Range: Geological Society of America Abstracts with Programs, v. 22, n. 3, p. 25.

Greene, R.C., 1973, Petrology of the welded Tuff of Devine Canyon, southeastern Oregon: USGS Professional Paper 797, 26 p.

Gunn, B.M., and Watkins, N.D., 1970, Geochemistry of the Steens Mountain Basalts, Oregon: Geological Society of America Bulletin, v. 81, p. 1497-1516.

Harrold, J.L., 1973, Geology of the North-Central Pueblo Mountains, Harney County, Oregon: Oregon State University unpublished Masters Thesis, 133 p.

Hart, W,K., 1985, Chemical and isotopic evidence for mixing between depleted and enriched mantle, northwestern U.S.A.: Geochimica et Cosmochima Acta, v. 49, p. 131-144.

Hart, W.K., Aronson, J.L., and Mertzman, S.A., 1984, Areal distribution and age of low-K, high-alumina olivine tholeiite magmatism in the northwestern Great Basin: Geological Society of America Bulletin, v. 95, p. 186-195.

Hart, W.K., and Carlson, R.W., 1985, Distribution and geochronology of Steens Mountain-type basalts from the northwestern Great Basin: Isochron/West, no. 43, p. 5-10.

Hart, W.K., and Carlson, R.W., 1987, Tectonic controls on magma genesis and evolution in the northwestern United States: Journal of Volcanology and Geothermal Research, v. 32, p. 119-135.

Hart, W.K., Carlson, R.W., and Mosher, S.A., 1989, Petrogenesis of the Pueblo Mountains basalt, southeastern Oregon and northern Nevada: Geological Society of America Special Paper 239, p. 367-378.

Hart, W.K., and Mertzman, S.A., 1982, K-Ar ages of basalts from southcentral Oregon: Isochron/West, no. 33, p. 23-26.

Helmke, P.A., and Haskin, L.A., 1973, Rare-earth elements, Co, Sc, and Hf in the Steens Mountain basalts: Geochimica et Cosmochimica Acta, v. 37, p. 1513-1529.

Houghton, B.F., Weaver, S.D., Wilson, C.J.N., and Lanphere, M.A., 1992, Evolution of a Quaternary peralkaline volcano: Mayor Island, New Zealand: Journal of Volcanology and Geothermal Research, v. 51, p. 217-236.

Langer, V.W., 1991, Geology and petrologic evolution of the silicic to intermediate Volcanic Rocks underneath Steens Mountain Basalt, SE Oregon: Oregon State University unpublished Masters Thesis, 109 p.

Larson, E.E., 1965, The structure, stratigraphy, and paleomagnetics of the Plush area, southeastern Lake County, Oregon: University of Colorado unpublished PhD Thesis, 166 p.

Larson, E.E., and Stern, C.R., 1983, Areal extent and age of the Steens Basalt, southeastern Oregon and Northwestern Nevada: EOS, v. 64, p. 898.

Lawrence, R.D., 1976, Strike-slip faulting terminates the Basin and Range province in Oregon: Geological Society of America Bulletin, v. 87, p. 846-850.

Leake, B.E., 1978, Nomenclature of amphiboles: American Mineralogist, v. 63, p. 1023-1052.

LeBas, M.J., LeMaitre, R.W., Streckeisen, A., and Zanettin, B., 1986, A chemical classification of volcanic rocks based on the total alkali silica diagram: Journal of Petrology, v. 27, p. 745-750.

LeMaitre, R.W., ed, 1989, A Classification of Igneous Rocks and Glossary of Terms: Recommendations of the International Union of Geological Sciences Subcommission on the Systematics of Igneous Rocks: Blackwell Scientific Publications, Oxford, 193 p.

LeMarchand, F., Villemant, B., and Calas, G., 1987, Trace element distribution coefficients in alkaline series: Geochima et Cosmochimica Acta, v. 51, p. 1071-1081.

Lindsley, D.H., 1983, Pyroxene thermometry: American Mineralogist, v. 68, p. 477-493.

Lipman, P.W., Prustka, H.J., and Christiansen, R.L., 1972, Cenozoic volcanism and plate-tectonic evolution of the western United States, pt 1, Early and middle Cenozoic: Philos. Trans. Royal Society of London Ser A, v. 271, p.217-248.

Lofgren, G.E., 1974, An experimental study of plagioclase morphology: Isothermal crystallization: American Journal of Science, v. 264, p. 243-273.

Lofgren, G.E., 1980, Experimental studies on the dynamic crystallization in silicate melts, in Hargraves, R.B., Ed., Physics of Magmatic Processes: Princeton, Princeton University Press, 585 p.

Lowenstern, J.B., and Mahood, G.A., 1991, New data on magmatic H2O contents of pantellerites, with implications for petrogenesis and eruptive dynamics at Pantelleria: Bulletin Volcanology, v. 54, p. 78-83.

Luhr, J.F., Carmichael, I.S.E., and Varekamp, J.C., 1984, The 1982 eruptions of El Chichon volcano, Chiapas, Mexico: Mineralogy and petrology of the anhydrite-bearing pumices: Journal of Volcanology and Geothermal Research, v. 23, p. 69-108.

Macdonald, R., 1974, Tectonic settings and magma associations: Bulletin Volcanologique, v. 38, p. 575-593.

Macdonald, R., and Bailey, D.K., 1973, The chemistry of the peralkaline oversaturated obsidians: USGS Professional Paper, 440-N-1, p. N1-N37.

Macdonald, R., Davies, G.R., Bliss, C.M., Leat, P.T., Bailey, D.K., and Smith, R.L., 1987, Geochemistry of high-silica peralkaline rhyolites, Naivasha, Kenya Rift Valley: Journal of Petrology: v. 28, p.979-1008.

MacLeod, N.S., Walker, G.W., and McKee, E.H., 1976, Geothermal significance of eastward increase in age of upper Cenozoic rhyolitic domes in southeastern Oregon, *in* proceedings of Second Symposium on the Development and Use of Geothermal Resources, v. 1, p. 465-474.

Mahood, G.A., 1981, A summary of the geology and petrology of the Sierra La Primarera, Jalisco, Mexico: Journal of Geophysical Research, v. 86, 10137-10152.

Mahood, G.A., 1984, Calderas associated with strongly peralkaline volcanic rocks: Journal of Geophysical Research, v. 89, p. 8540-8552.

Mahood, G.A., and Baker, D.R., 1986, Experimental constraints on depths of fractionation of mildly alkalic basalts and associated felsic rocks: Pantelleria, Strait of Sicily: Contributions to Mineralogy and Petrology, v. 93, p. 251-264.

Mahood, G.A., and Baker, D.R., 1986, Experimental constraints on depths of fractionation of mildly alkalic basalts and associated felsic rocks: Pantelleria, Strait of Sicily: Contributions to Mineralogy and Petrology, v. 96, p. 251-264.

Mahood, G.A., and Hildreth, W., 1986, Geology of the peralkaline volcano at Pantelleria, Strait of Sicily: Bulletin Volcanologique, v. 48, 143-172.

Mahood, G.A., and Stimac, J.A., 1990, Trace-element partitioning in pantellerites and trachytes: Cosmochimica et Cosmochimica Acta, v. 54, p. 2257-2276.

Mankinen, E.A., Larson, E.E., Gromme, C.S., Prevot, M., and Coe, R.S., 1987, the Steens Mountain (Oregon) geomagnetic polarity transition 3. Its regional significance: Journal of Geophysical Research, v. 92, p. 8057-8076.

Mathis, A.C., 1988, Programmed cooling experiments: Morphological and compositional changes for plagioclase and olivine crystals in a basaltic melt: Honors Essay, Department of Geology, University of North Carolina, Chapel Hill, 36 p.

Minor, S.A., Plouff, D., Esparza, L.E., and Peters, T.J., 1987, Mineral resources of the High Steens and Little Blitzen Gorge Wilderness Study Areas, Harney County, Oregon: USGS Bulletin 1740-A, 21 p.

Mullen, E.D., 1978, Geology of the Greenhorn Mountains, northeastern Oregon: Oregon State University unpublished Masters Thesis, 372 p.

Muntzert, J.K., 1969, Geology and mineral deposits of the Brattain District, Lake County, Oregon: Oregon State University unpublished Masters Thesis, 70 p.

Nicholls, J., and Carmichael, J.S.E., 1969, Peralkaline acid liquids: A petrological study: Contributions to Mineralogy and Petrology, v. 20, p. 268-294.

Noble, D.C., 1968, Systematic variation of major elements in comendite and pantellerite glasses: Earth and Planetary Science Letters, v. 4, p. 167-172.

Noble, D.C., McKee, E.H., and Walker, G.W., 1974, Pantellerite from the Hart Mountain area, southeastern Oregon--Interpretation of radiometric, chemical, and isotope data: Journal Research USGS, v. 2, p. 25-29.

Noble, D.C., and Parker, D.F., 1974, Peralkaline silicic volcanic rocks of the western United States: Bulletin Volcanologique, v. 38, p. 803-827.

Noblett, J.B., 1981, Subduction-related origin of the volcanic rocks of the Eocene Clarno Formation near Cherry Creek, Oregon: Oregon Geology, v. 43, p. 91-98.

Novak, S., 1984, Eruptive history of the rhyolitic Kane Springs Wash volcanic center: Journal of Geophysical Research, v. 89, p. 8603-8615.

Novak, S.M., and Mahood, G.A., 1986, Rise and fall of a basalt-trachyte,rhyolite magma system at the Kane Springs Wash caldera, Nevada: Contributions to Mineralogy and Petrology, v. 94, p. 352-373.

Oles, K.F., and Enlows, H.E., 1972, Bedrock geology of the Mitchell quadrangle, Wheeler County, Oregon: DOGAMI Bulletin, v. 72, 61 p.

Parker, D.F., 1983, Origin of the trachyte-quartz trachyte-peralkaline rhyolite suite of the Oligocene Paisano volcano, Trans-Pecos, Texas: Geological Society of America Bulletin, v. 94, 614-629.

Peterson, N.V., and McIntyre, J.R., 1970, The reconnaissance geology and mineral resources of eastern Klamath County and western Lake County, Oregon: DOGAMI Bulletin, v. 66, 70 p.

Rogers, J.J.W., and Novitsky-Evans, J.M., 1977, The Clarno Formation of Central Oregon--Volcanism on a thin continental margin: Earth and Planetary Science Letters, v. 34, p. 56-66.

Rytuba, J.R., 1989, Volcanism, extensional tectonics, and epithermal mineralization in the northern Basin and Range Province, California, Nevada, Oregon, and Idaho: USGS Circular 1035, p. 59-61.

Rytuba, J.R., and McKee, E.H., 1984, Peralkaline ash flow tuffs and calderas of the McDermitt volcanic field, southeast Oregon and north central Nevada: Journal of Geophysical Research, v. 89, p. 8616-8628.

Rytuba, J.R., Minor, S.A., and McKee, E.H., 1981, Geology of the Whitehorse caldera and caldera-fill deposits, Malheur County, Oregon, USGS Open File Report 81-1092, 19 p.

Samson, S.D., and Alexander Jr., E.C., 1987, Calibration of the interlaboratory 40Ar/39Ar dating standard, MMhb-1: Chem. Geol. Isot. Geosci., v. 66, p. 27-34.

Smith, I.E.M., Chappell, B.W., Ward, G.K., and Freeman, R.S., 1977, Peralkaline rhyolites associated with andesitic arcs of the southwest Pacific: Earth and Planetary Science Letters, v. 37, p. 230-236.

Spear, F.S., and Kimball, K.L., 1984, RECAMP--A Fortran IV program for estimating Fe^{3+} contents in amphiboles: Computers and Geosciences, v. 10, p. 317-325.

Stewart, J.H., and Carlson, J.E., 1976, Cenozoic rocks of Nevada: Four maps and brief description of distribution, lithology, age, and centers of volcanism: Nevada Bureau of Mines Geological Map 52, scale 1:1,000,000.

Sutherland, D.S., 1974, Petrology and mineralogy of peralkaline silicic rocks: Bulletin Volcanologique, v. 38, p. 517-547.

Taylor, J.R., 1982, An Introduction to Error Analysis: University Science Books, Mill Valley, California, 270 p.

Taylor, R.P., Strong, D.F., and Fryer, B.J., 1981, Volatie control of contrasting trace element distributions in peralkaline granitic and volcanic rocks: Contributions to Mineralogy and Petrology, v. 77, p. 267-271.

Thomas, T.H., 1981, Geology and mineral deposits of the Coyote Hills Mining District, Lake County, Oregon: Oregon State University unpublished Masters Thesis, 137 p.

Thompson, G.A., 1960, Problem of late Cenozoic structure of the Basin and Ranges: Proceedings of 21st International Geological Congress, Cophenhagen, v. 18, p. 62-68.

Walker, G.W., 1961, Soda rhyolite (pantellerite?) from Lake County, Oregon: USGS Professional Paper 424-C, p. C142-C145.

Walker, G.W., 1970, Cenozoic ash-flow tuffs of Oregon: DOGAMI, The Ore Bin, v. 32, p. 97-115.

Walker, G.W., 1979, Revisions to the Cenozoic Stratigraphy of Harney Basin, Southeastern Oregon: USGS Bulletin 1475, 35 p.

Walker, G.W., and Repenning, C.A., 1965, Reconnaissance geologic map of the Adel quadrangle, Lake, Harney, and Malheur Counties, Oregon: USGS Miscellaneous Geological Investigations Map I-446, scale 1:250,000.

Walker, G.W., and Swanson, D.A., 1968a, Laminar flowage in a Pliocene soda rhyolite ash-flow tuff, Lake and Harney Counties, Oregon, in Geological Survey research 1968: USGS Profesional Paper 600-B, p. B37-B42.

Walker, G.W., and Swanson, D.A., 1968b, Summary report of the geology and mineral resources of the Poker Jim Ridge and Fort Warner areas of the Hart Mountain National Antelope Refuge, Lake County, Oregon: USGS Bulletin, 1260-M, p. M1-M16.

Wallace, A.B., Drexler, J.W., Grant, N.K., and Noble, D.C., 1980, Icelandite and aenigmatite-bearing pantellerite from the McDermitt caldera complex, Nevada-Oregon: Geology, v. 8, p. 380-384.

Watson, E.B., 1979, Zircon saturation in felsic liquids: Experimental results and applications to trace element geochemistry: Contributions to Mineralogy and Petrology, v. 70, p. 407-419.

Watson, E.B., and Capobianco, C.J., 1981, Phosphorus and the rare earth elements in felsic magmas: An assessment of the role of apatite: Geochimica et Cosmochimica Acta, v. 45, p. 2349-2358.

Weaver, S.D., Gibson, I.L., Houghton, B.F., and Wilson, C.J.N., 1990, Mobility of rare earth and other elements during crystallization of peralkaline silicic lavas: Journal of Volcanology and Geothermal Research, v. 43 p. 57-70.

Wells, R.E., 1979, Drake Peak--A structurally complex rhyolite center in southeastern Oregon: USGS Professional Paper 1124-E, p. E1-E16.

Williams, H., Turner, F.J., Gilbert, C.M., 1982, Petrography: An introduction to the study of rocks in thin sections: W.H. Freeman and Co, New York, 2nd ed., 626 p.

Appendix I: Petrographic Descriptions and Sample Locations

Sample locations and petrographic descriptions of analyzed samples are listed here. Samples are grouped according to map unit and described in ascending stratigraphic order. Locations are given with Township, Range, 1/4 section, and elevation, and are located on Plate II.

Hart Mountain trachyandesite suite

NORTH MOUNTAIN SECTION

AM-90-23, AM-89-70: Tvc. Seriate and glomeroporphyritic basalt lava flow containing 10-15% phenocrysts of plagioclase > olivine > clinopyroxene > Fe-Ti oxides in a pilotaxitic groundmass of plagioclase microlites, Fe-Ti oxides, and mafic phases. Plagioclase crystals are as large as 2.5 mm in size, and are euhedral to subhedral. Some crystals have skeletal interiors or dendritic rims. Many crystals display prominent normal zoning, and some have less pronounced oscillatory zoning. Compositions range from An_{52-81} in phenocrysts and $An_{50-67.5}$ in groundmass crystals. Subhedral clinopyroxene crystals are light tan in color, commonly have brown rims, and range in size from 0.5 to 2 mm. Compositions range from diopside ($Wo_{46}En_{45}Fs_{9}$) to augite ($Wo_{39}En_{46}Fs_{15}$). Clinopyroxene crystals may have plagioclase inclusions. Anhedral round olivine crystals are as large as 3 mm in size, and have compositions ranging from Fo_{65-85}. Olivine crystals may have plagioclase and/or opaque inclusions. Some olivine crystals are altering to calcite. Anhedral Fe-Ti oxide crystals occur as microphenocrysts in the groundmass and in glomerocrysts with clinopyroxene and olivine. The groundmass consists of 55-60% plagioclase microlites less than 0.4 mm in size, 20-25% opaques, and 15-25% mafic phases.

These samples are from a lateral lava flow to the northern-most vent complex. The two samples were collected only a few meters apart.
Location: T35S, R25E, NE 1/4 of SW 1/4 section 21, elevation 4780 feet.

AM-89-92: Tvc. Microporphyritic pilotaxitic trachyandesite containing approximately 5% vesicular cognate inclusions of seriate basalt. Microphenocrysts are subhedral plagioclase crystals approximately 0.2 mm in size (3%) with trace amounts of euhedral clinopyroxene and acicular apatite crystals. The matrix consists of 60-70% plagioclase microlites, 20-25% Fe-Ti oxides, and 10-15% mafic phases. The subrounded inclusions are as large as 3 cm in size and show partial incorporation into the matrix along the edges. Some inclusions appear to be almost completely incorporated into the matrix. The inclusions contain approximately 15% phenocrysts as large as 2 mm in size of plagioclase (An_{65} by Michel Levy) >> clinopyroxene > iddingsited olivine > Fe-Ti oxides in a cryptocrystalline groundmass. The cognate inclusions have mineralogies and textures almost identical to AM-90-23, AM-89-70.

This sample was collected from the feeder dike found in the northern-most exposed vent complex.
Location: T35S, R25E, SE 1/4 of SW 1/4 section 21, elevation 5020 feet.

AM-89-85: Tiw. Fiamme sample collected from a moderately welded fiamme and lithic-rich trachytic ignimbrite. The sample was collected from the most welded part of the flow, approximately 2-3 m above the exposed base.

Fiamme range in length from 0.5 to 30 mm. Fiamme consist mostly of red-brown obsidian displaying perlitic fracture. Rare (<1%) microphenocrysts consist of 0.5 mm subhedral to anhedral plagioclase, 0.1 mm anhedral Fe-Ti oxides, and <0.1 mm euhedral apatite.
Location: T35S, R25E, SE 1/4 of NW 1/4 section 28, elevation 4940 feet.

AM-90-29: Tvl. Porphyritic and glomeroporphyritic pilotaxitic basaltic trachyandesite lava flow containing 25-30% plagioclase laths up to 2 cm in length. Euhedral to subhedral plagioclase phenocrysts (An_{42} by Michel Levy) have undergone saussuritization along fractures. Plagioclase crystals have oscillatory zoning. Rare Fe-Ti oxides and a mafic phase which has been completely replaced by a red-brown iddingsite-like phase occur as rare (>1%) microphenocrysts less than 1 mm in size. The pilotaxitic groundmass consists of approximately 60% plagioclase microlites (<0.2 mm in length), 20% Fe-Ti oxides, 5-10% clinopyroxene (?), and 10-15% brown alteration material (replacing glass?).
Location: T36S, R25E, S 1/2 of SW 1/4 section 9, elevation 5300 feet.

AM-89-74: Tvl. Porphyritic and glomeroporphyritic basaltic trachyandesite containing 10-12% phenocrysts of plagioclase >> olivine > clinopyroxene > Fe-Ti oxides > apatite. Subhedral plagioclase phenocrysts are as large as 2 mm in size, and have compositions ranging from An_{45} to An_{50}. Subhedral to euhedral pale brown clinopyroxene phenocrysts are 2.0 to 0.2 mm in size. Subhedral olivine phenocrysts have been completely altered to iddingsite, and are less than 1 mm in size. Anhedral Fe-Ti oxides are less 0.5 mm in size and are commonly found as inclusions in plagioclase and mafic phases and commonly contain apatite inclusions. Apatite occurs as euhedral microphenocrysts and as common inclusions in the other phases. The pilotaxitic and hyalopilitic groundmass consists of approximately 55% feldspar microlites (<0.2 mm), 15-20% Fe-Ti oxides, 25-30% brown alteration

material (altered glass?), and 1-3% mafic phases. Feldspar compositions in the groundmass range from andesine ($An_{39}Ab_{57}Or_4$) to anorthoclase ($An_7Ab_{59}Or_{34}$). Pigeonite and augite are pyroxene phases in the groundmass.
Location: T35S, R25E, NE 1/4 of SW 1/4 section 21, elevation 4990 feet.

AM-89-81: Tis. Fiamme sample collected from near the base of a poorly to moderately welded, vapor-phase altered ash flow tuff. Fiamme are slightly hydrated, as long as 4 cm and contain approximately 2% euhedral to subhedral plagioclase phenocrysts as large as 3 mm. Plagioclase crystals have been altered to a slight red color.
Location: T35S, R25E, NW 1/4 of SE 1/4 section 21, elevation 5130 feet.

AM-89-75: Tis. Sample used to prepare a plagioclase separate used for K-Ar age determination. Plagioclase separate included crystals from the matrix and from the lithic inclusions. See text for sample description.
Location: T35S, R25E, SW 1/4 of NE 1/4 section 21, elevation 5130 feet.

AM-89-55: Tv2. Porphyritic and glomeroporphyritic trachyte lava flow containing approximately 15-20% phenocrysts of plagioclase >> clinopyroxene > olivine > Fe-Ti oxides. Subhedral to euhedral plagioclase phenocrysts (An_{30} by Michel Levy) are 0.2 to 2.5 mm in size, and may have inclusions of the other phases. Subhedral very pale green clinopyroxene phenocrysts are weakly pleochroic, as large as 1.5 mm in size, and may have inclusions of opaques and apatite. Euhedral to subhedral olivine(?) has been completely replaced by red-brown iddingsite, and also contain opaque and apatite inclusions. Anhedral Fe-Ti oxides are 0.1 to 0.4 mm in size, and commonly have apatite inclusions. Euhedral apatite crystals occur as microphenocrysts and as inclusions and are less than 0.1 mm in size. The pilotaxitic groundmass consists predominantly (approximately 80%) of feldspar microlites less than 0.1 mm in size, and lesser amounts of mafic phases and alteration material.
Location: T35S, R25E, NW 1/4 of SE 1/4 section 15, elevation 5200 feet.

AM-89-83: Tia. Sample collected from the densely welded vitric zone and used for microprobe analyses. See text for description.
Location: T35S, R25E, W 1/2 of SE 1/4 section 21, elevation 5400 feet.

AM-89-60: Tv3. Crystal poor (<2%) trachyandesite lava flow which shows textural disequilibrium resulting from mingling of magmas. At least two generations of plagioclase phenocrysts are present: large 1.0 to 2.2 mm sieved anhedral

crystals (An_{35} by Michel Levy) and smaller 0.1 to 1.0 mm anhedral crystals (An_{18} by Michel Levy). Subhedral weakly pleochroic clinopyroxene are less than 1.5 mm in size, and have apatite inclusions. Euhedral to subhedral olivine phenocrysts have been completely replaced by iddingsite, and have common apatite and opaque inclusions. Fe-Ti oxides are less than 0.6 mm in size. The groundmass constitute texturally distinct zones of coarser and finer grained microlites producing flow banding. Feldspar microlites define pilotaxitic texture and consist of approximately 80% of the groundmass, with the interstices between feldspars filled mostly by Fe-Ti oxides.
Location: T35S, R25E, E 1/2 of SE 1/4 section 15, elevation 5430 feet.

AM-89-61: Tv3. Hyalopilitic basaltic trachyandesite lava flow containing <1% microphenocrysts and microglomerocrysts of plagioclase, augite, olivine, and Fe-Ti oxides. Subhedral plagioclase crystals less than 1 mm in size range in composition from An_{35} to An_{50} and may have opaque inclusions. Rarely plagioclase crystals are skeletal. Light brown subhedral augite phenocrysts are as large as 0.5 mm in size. Subhedral olivine phenocrysts have been almost completely replaced by iddingsite. The groundmass consists of approximately 70% plagioclase microlites, 10% Fe-Ti oxides, 10% mafic phases, and 10% red-brown glass and alteration material. Minor alteration to calcite.
Location: T35S, R25E, E 1/2 of SE 1/4 section 15, elevation 5440 feet.

AM-89-90: Tv3. Porphyritic and glomeroporphyritic trachyte lava flow containing approximately 20% phenocrysts of plagioclase >> clinopyroxene ≈ olivine > Fe-Ti oxides. Subhedral feldspar phenocrysts are as large as 5 mm in size. Compositions range from andesine ($An_{31}Ab_{65}Or_4$) to anorthoclase ($An_4Ab_{71}Or_{25}$). Feldspar phenocrysts may have inclusions of Fe-Ti oxides, olivine, and apatite. Weakly pleochroic pale green clinopyroxene crystals range in composition from augite ($Wo_{42}En_{31}Fs_{27}$) to ferroaugite ($Wo_{42}En_{23}Fs_{35}$). Clinopyroxene phenocrysts have opaque and apatite inclusions, and may be partially altered to a red-brown iddingsite-like phase. Subhedral olivine crystals have been completely replaced by iddingsite, are up to 1 mm in size, and have apatite inclusions. The pilotaxitic groundmass consists of approximately 70% anorthoclase microlites approximately 0.1 mm in size, 10-15% Fe-Ti oxides, 5% mafic phases, and 10-15% alteration material.
Location: T35S, R25E, SW 1/4 of NE 1/4 section 28, elevation 5600 feet.

AM-90-02: Tib. Round fiamme or juvenile obsidian lithic sample collected from the trachytic gray base of a strongly zoned crystal rich ash flow tuff. Black obsidian is slightly

hydrated and appears flow banded. Contains approximately 4% euhedral feldspar phenocrysts as large as 3 mm long. Fiamme are generally less than 5 cm long.
Location: T35S, R25E, NW 1/4 of NE 1/4 section 14, elevation 5390 feet.

AM-90-22: Tv5. Crystal-poor pilotaxitic trachyandesite lava flow containing 1-2% phenocrysts and glomerocrysts of plagioclase >> Fe-Ti oxides > clinopyroxene. Subhedral, acicular plagioclase phenocrysts are as large as 2 mm in length and are An_{38} by Michel Levy. Subhedral clinopyroxene are as large as 0.5 mm and are found only in glomerocrysts. Anhedral Fe-Ti oxides are less than 0.5 mm. Accessory subhedral apatite microphenocrysts are less than 0.2 mm in size. The pilotaxitic groundmass consists of approximately 90% feldspar microlites less than 0.1 mm in size, 5-7% Fe-Ti oxides, 3-5% mafic phases and alteration material.
Location: T36S, R25E, NW 1/4 of SW 1/4 section 16, elevation 5600 feet.

AM-89-65: Tv5. Crystal poor pilotaxitic trachyandesite lava flow containing 1-2% phenocrysts and glomerocrysts of plagioclase, clinopyroxene, olivine, and Fe-Ti oxides. Euhedral to subhedral plagioclase (An_{40} by Michel Levy) may be acicular, and are as large as 2 mm in length. Colorless subhedral clinopyroxene crystals are less than 1 mm in size and are present only in glomerocrysts. Olivine phenocrysts (also present in glomerocrysts) have been replaced completely by iddingsite, and have apatite inclusions. Euhedral to subhedral Fe-Ti oxides are as large as 1 mm in size, and may have skeletal morphologies. Apatite inclusions are common in Fe-Ti oxides. Euhedral apatite crystals are also present as microphenocrysts. The pilotaxitic groundmass consists of 70-75% plagioclase microlites less than 0.1 mm in size, approximately 20% Fe-Ti oxides, and minor amounts of mafic phases and alteration material.
Location: T35S, R25E, W 1/2 of SW 1/4 section 14, elevation 5950 feet.

HART LAKE SECTION

AM-89-42: Thl. Trachyandesite lava flow containing abundant cognate inclusions which have been partially resorbed into the magma. The inclusions are coarser grained (>0.05 mm) than the matrix, have intergranular, pilotaxitic, or diabasic texture, and have irregular shapes because of partial incorporation into the matrix. Mineralogy of the coarser grained inclusions consists of andesine microlites (An_{34}), augite, olivine, Fe-Ti oxides, and apatite. The matrix contains anorthoclase ($An_{15}Ab_{61}Or_{24}$) in addition to andesine, pigeonite and augite, and Fe-Ti oxides, and does not contain apatite. 1-2% microphenocrysts (xenocrysts?) consist of anhedral sieved plagioclase (An_{30-60}), and clinopyroxene.

Plagioclase crystals may also have frittered rims. Plagioclase microphenocrysts are normally, reversely, or unzoned. The matrix consists of approximately 70% feldspar microlites, 20% mafic phases, and 10% Fe-Ti oxides.
Location: T36S, R25E, NW 1/4 of SW 1/4 section 29, elevation 5050 feet.

AM-89-43: Thl. Hyalopilitic basaltic trachyandesite lava flow containing <1% microphenocrysts of plagioclase, clinopyroxene, and Fe-Ti oxides. Subhedral plagioclase microphenocrysts (An_{48} by Michel Levy) are less than 0.5 mm in size, and rarely have sieved cores. Subhedral clinopyroxene phenocrysts are less than 0.7 mm in size, and have abundant Fe-Ti oxide inclusions. Euhedral to subhedral Fe-Ti oxide microphenocrysts are as large as 0.5 mm in size. The groundmass consists of approximately 70% plagioclase microlites less than 0.3 mm in size, 15% Fe-Ti oxides, 3-5% mafic phases, and 10% glass and alteration material.
Location: T36S, R25E, NW 1/4 of SW 1/4 section 29, elevation 5290 feet.

Warner Peak rhyolite

AM-89-33: Twpt. Light gray incipiently welded devitrified comenditic ignimbrite found near the base of the Warner Peak tuff. Sample used for whole-rock major and trace element analyses, and to prepare a feldspar separate for K-Ar age determination. See text for sample description.
Location: T35S, R25E, SE 1/4 of SE 1/4 section 33, elevation 6300 feet.

AM-90-26: Twpu. Porphyritic and glomeroporphyritic pilotaxitic lava flow containing 8-10% phenocrysts of feldspar >> Fe-Ti oxides. Subhedral to euhedral feldspar phenocrysts are less than 4 mm in size and consist mostly of plagioclase (An_{30} by Michel Levy) with <1% untwinned feldspar (sanidine or anorthoclase?). Anhedral Fe-Ti oxides are less than 0.5 mm in size and rarely have apatite inclusions. Accessary euhedral to subhedral apatite less than 0.5 mm is present as rare microphenocrysts. The light gray groundmass consists of mostly euhedral to subhedral feldspar microlites (80-85%) less than 0.1 mm in size, with minor amounts of Fe-Ti oxides and brown alteration material.
Location: T35S, R25E, NW 1/4 of NE 1/4 section 12, elevation 5530 feet.

AM-90-27: Twpu. Brecciated porphyritic pantellerite lava flow containing approximately 3% phenocrysts of alkali feldspar >> completely altered mafic phase. Subhedral feldspar crystals are less than 3 mm in size, and are generally not twinned. Some crystals display Carlsbad twinning. Phenocrysts of the altered mafic phase are subhedral and as large as 0.4 mm. The pilotaxitic groundmass

is microporphyritic with 2-4% subhedral to euhedral (and rarely skeletal) feldspar microphenocrysts 0.05 to 0.2 mm in size, and trace amounts of 0.2 mm anhedral Fe-Ti oxide microphenocrysts. The finer grained (<0.05 mm) matrix consists of 50-60% feldspar microlites, 20% green clinopyroxene, 20% brown alteration material, and trace amounts of Fe-Ti oxides.
Location: T35S, R25E, NW 1/4 of SE 1/4 section 12, elevation 5640.

AM-90-36: Twpu. Porphyritic and glomeroporphyritic black trachyte lava flow containing approximately 15% phenocrysts of plagioclase >> clinopyroxene > Fe-Ti oxides > apatite. Euhedral plagioclase phenocrysts are An_{40} by the Carlsbad-Albite method. Euhedral clinopyroxene phenocrysts display weak gray green to pink pleochroism, and are large as 1.2 mm. Subhedral to anhedral Fe-Ti oxides are less than 0.5 mm and are present as phenocrysts and as inclusions in clinopyroxene and plagioclase. Trace amounts of apatite is present as microphenocrysts and as inclusions in the other phases. The pilotaxitic groundmass consists of approximately 80% euhedral feldspar microlites less than 0.1 mm in size, 10% Fe-Ti oxides, and 5-10% brown alteration material.
Location: T36S, R25E, NE 1/4 of SW 1/4 section 16, elevation 6190 feet.

AM-90-35: Twpu. Porphyritic and glomeroporphyritic light green pantellerite lava flow containing approximately 9% phenocrysts of alkali feldspar >> green clinopyroxene > blue green amphibole (arfvedsonite). Trace amounts of pleochroic brown amphibole and Fe-Ti oxides are also present as microphenocrysts. Euhedral to subhedral feldspar phenocrysts are either untwinned or display Carlsbad twinning. Individual crystals are as large as 2.5 mm in size, and usually occur in glomerocrysts of feldspar crystals. Fe-Ti oxides are inclusions in feldspar crystals. Euhedral pyroxene crystals display weak olive green to jade green pleochroism, and are less than 0.5 mm in size. Blue to green strongly pleochroic arfvedsonite is found as anhedral phenocrysts less than 0.5 mm in size, and as replacement rims of a weakly pleochroic brown amphibole. The pilotaxitic groundmass consists predominantly (80%) of feldspar microlites less than 0.2 mm, with lesser amounts of green pyroxene, amphibole, Fe-Ti oxides, and alteration material.
Location: T36S, R25E, NW 1/4 of SE 1/4 section 16, elevation 6360 feet.

AM-90-34: Twpu. Porphyritic and glomeroporphyritic light green pantellerite lava flow containing approximately 8% phenocrysts of sanidine and anorthoclase > brown amphibole > blue green arfvedsonite > Fe-Ti oxides. Subhedral alkali feldspar phenocrysts are as large as 5 mm in size, and may have inclusions of the mafic phases. Compositions of

phenocrysts range from $Ab_{66}Or_{34}$ to $Ab_{72}Or_{28}$. Weakly pleochroic brown amphibole phenocrysts are less than 1 mm in size and have compositions between richterite and eckermanite. Anhedral strongly pleochroic green to blue arfvedsonite crystals are as large as 0.5 mm, and are replacing brown amphibole. The groundmass consists of approximately 60% feldspar microlites, 20-25% richterite-eckermanite, 15-20% arfvedsonite, with trace amounts of quartz and ferrohedenbergite.
Location: T36S, R25E, NW 1/4 of SE 1/4 section 16, elevation 6620 feet.

AM-89-14: Twpi. Porphyritic and glomeroporphyritic light green comendite intrusion containing 12-15% phenocrysts of anorthoclase >> green ferrohedenbergite >> Fe-Ti oxides. Euhedral anorthoclase phenocrysts are less than 4 mm in size and may display Carlsbad, polysynthetic Albite or Pericline, or anorthoclase grid twinning, or no twinning. Rarely do they have sieved interiors. Feldspar phenocrysts also may have inclusions of the other phases. Weakly pleochroic green ferrohedenbergite phenocrysts are less than 1 mm and may have Fe-Ti inclusions. Anhedral Fe-Ti oxide microphenocrysts are less than 0.2 mm in size. The microporphyritic pilotaxitic groundmass consists of approximately 45% feldspar microlites less than 0.2 mm in size, with minor amounts of pyroxene and Fe-Ti oxide microlites in a cryptocrystalline matrix.
Location: T35S, R25E, SE 1/4 of SE 1/4 section 22, elevation 6720 feet.

AM-89-40/41: Twpi. Porphyritic and glomeroporphyritic green comendite sill. Sample AM-89-40 (used for major and trace element analyses) was collected from the vitrophyric rim; AM-89-41 was collected from the quenched portion of the rim. Euhedral alkali feldspar phenocrysts are as large as 4.5 mm in size, and display Carlsbad, polysynthetic Albite or Pericline, or anorthoclase grid twinning. The groundmass consists of 10-15% pleochroic green clinopyroxene microlites as large as 0.4 mm in size, 5-8% euhedral feldspar microlites less than 0.2 mm in size, and trace amounts of Fe-Ti oxides in a cryptocrystalline (or vitric in AM-89-40) matrix. Groundmass feldspar microlites may be skeletal.
Location: T36S, R25E, SW 1/4 of NW 1/4 section 29, elevation 5000 feet.

AM-89-93: Twpi. Porphyritic and glomeroporphyritic comendite intrusion containing 20-25% phenocrysts of anorthoclase >> green clinopyroxene > arfvedsonite > Fe-Ti oxides in an intergranular groundmass. Euhedral to subhedral alkali feldspar phenocrysts are as large as 5 mm in size, and display Carlsbad, polysynthetic Albite or Pericline, or anorthoclase grid twinning. Feldspar phenocrysts may have inclusions of the other phases. Pleochroic green clinopyroxene phenocrysts with olive green rims are as large

as 0.5 mm, and have compositions which range between hedenbergite and ferrohedenbergite. Anhedral arfvedsonite phenocrysts are as large as 0.5 mm and have abundant inclusions of clinopyroxene and Fe-Ti oxides. Subhedral Fe-Ti oxides are less than 0.3 mm in size. The groundmass consists of approximately 80% alkali feldspar microlites less than 0.2 mm in size, 10% Fe-Ti oxides, 7% pyroxene, 3% arfvedsonite, 1-2% quartz, and trace amounts of brown amphibole.
Location: T36S, R25E, SW 1/4 of NW 1/4 section 9, elevation 4850 feet.

Appendex II: Glossary of Petrologic Terms

Agpaitic Index: The molar ratio of Na_2O+K_2O/Al_2O_3. When this ratio is greater than one, a rock is peralkaline.

Comendite: A weakly peralkaline rhyolite. Classification follows LeMaitre (1989). See Figure 22.

Mg#: Molecular 100 x $MgO/MgO+FeO$.

Pantellerite: A strongly peralkaline rhyolite. Classification follows LeMaitre (1989). See Figure 22.

REE: Rare earth elements.